Effect of a velocity gradient on the shear viscosity of a solution in the critical region

L. V. Vaĭnshteĭn, S. V. Krivokhizha,[a)] and L. L. Chaĭkov
P. N. Lebedev Physics Institute, Russian Academy of Sciences, 117924 Moscow, Russia

(Submitted 27 March 1997)
Pis'ma Zh. Éksp. Teor. Fiz. **66**, No. 1, 3–7 (10 July 1997)

An experimental study is made of the effect of a gradient of the fluid velocity on the value of the shear viscosity in a critical guaiacol–glycerin solution with a stratification region as the lower critical temperature for stratification is approached. It is shown that the interaction of concentration fluctuations with a gradient of the fluid velocity effectively decreases the measured value of the viscosity and that a theoretical description of the experimental results can be given by taking into account the breakdown of the Newtonian behavior of the viscosity near the critical temperature for stratification. © *1997 American Institute of Physics.* [S1063-7761(97)00113-3]

PACS numbers: 66.20.+d, 47.55.Hd

1. The shear viscosity of a Newtonian fluid depends on the nature of the material, the temperature, and the pressure. In cases when the viscosity becomes nonlinear or non-Newtonian it also depends on the external force or velocity gradient. Examples of such non-Newtonian fluids are suspensions, polymer solutions, and some other fluids.

More than 35 years ago, Fixman *et al.*[1,2] predicted theoretically that near the critical point for stratification a solution ceases to be a Newtonian fluid and its viscosity becomes a function of the velocity gradient ∇V and the correlation length r_c of the concentration fluctuations. Later, Oxtoby[3] developed a theory which permits quantitative analysis of such a nonlinearity of the viscosity by taking into account the interaction of the concentration or density fluctuations and the velocity gradient in a fluid flow.

Our objective in the present work is to establish experimentally a quantitative relation between the shear viscosity near the critical temperature for stratification and the velocity gradient of a flowing fluid, to compare the results with the theory of Ref. 3, and to describe the temperature dependence of the viscosity by means of the theory of critical phenomena.[4,5]

2. The dependence of the measured value of the viscosity on the correlation length r_c of concentration fluctuations and the fluid velocity gradient ∇V is calculated in the theory presented in Ref. 3. It is approximated well by the expression

$$\eta(\lambda)=\eta(0)[1-0.0175\ \ln(\lambda+0.435)-0.0146)], \tag{1}$$

where λ is a dimensionless parameter given by

$$\lambda=\eta r_c^3\nabla V_{\text{eff}}/kT. \tag{2}$$

Here η is the viscosity, k is Boltzmann's constant, T is the temperature, and ∇V_{eff} is the effective value of the fluid velocity gradient in a viscosimeter, calculated as an average over the flow.

The temperature dependence of the unperturbed viscosity $\eta(\lambda=0)$ near the stratification critical point is described by the expression[5]

$$\eta_c/\eta_B = X_\eta H(r_c q_D, r_c q_c), \tag{3}$$

where η_c and η_B are, respectively, the critical and background parts of the viscosity; X_η is the critical exponent of the viscosity; q_D and q_c are constants with dimensions of cm^{-1}; and, the function $H(r_c q_D, r_c q_c)$ has a complicated form and is presented in Ref. 5.

In the present work we investigated the viscosity of a solution with a region of stratification, viz., a guaiacol–glycerin solution containing an admixture of CCl_4 as a third component.[6] Such solutions with a stratification region possess simulataneously both upper (T_{CU}) and lower (T_{CL}) critical temperatures for stratification.[7–9] The size of the stratification region can depend on the concentration of the third component, and this region can be made to contract into a point by changing the concentration of the third component. Then the upper and lower critical points will merge into a single point, forming a double critical point. In such solutions with sufficiently small stratification regions both the upper and lower critical points influence the susceptibility and r_c, ''loosening up'' the solution and causing the concentration fluctuations to grow strongly near the critical temperature for stratification. The temperature dependence $r_c(T)$ in such solutions assumes the form[8–10]

$$r_c = r_0[(T_{CU}-T)(T_{CL}-T)/T_{CU}T_{CL}]^{-\nu}, \tag{4}$$

where generally $\nu=0.63$ and $r_0 \approx 2$ Å. It can be expected that in these solutions the theoretically predicted[3] decrease in the viscosity, as measured with a viscosimeter, due to the interaction of concentration fluctuations with the fluid velocity gradient should be especially strongly manifested because of the rapid increase in r_c as the critical temperature for stratification is approached.

3. In our experiment we investigated a guaiacol–glycerin solution with a guaiacol concentration of 48.15 wt. %. The admixutre of the third component CCl_4 amounted to 1.5 wt. % in the guaiacol. The stratification region of the solution was $T_{CU}-T_{CL}=3.38$ °C.

The viscosity was measured with a V-3 Hoeppler viscosimeter, in which a small ball rolls under the influence of gravity along a calibrated inclined tube filled with the experimental fluid. In this case, averaging ∇V over the flow in the gap between the tube and the ball gives[11]

$$\nabla V_{\text{eff}} = J_0 \frac{V_b R_t}{\Delta R^2}\frac{63}{80}\left(1-2.19\frac{\Delta R}{R_t}-4.33\frac{\Delta R^2}{R_t^2}+\ldots\right). \tag{5}$$

Here R_t is the radius of the tube, ΔR is the difference of the radii of the tube and the ball, and V_b is the velocity of the ball. A coefficient $J_0 \sim 1$ has been introduced to allow for the fact that the transverse motion of the fluid around the ball was neglected. This coefficient

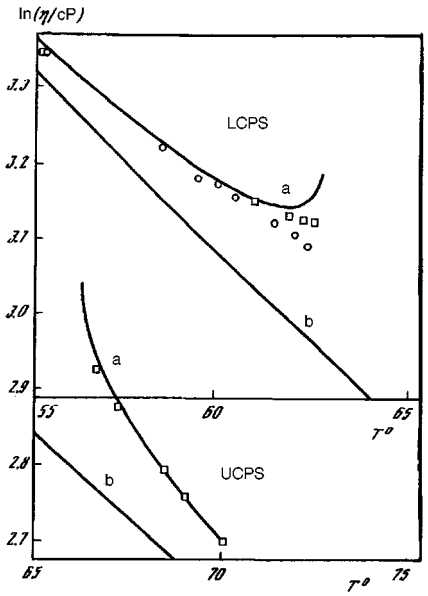

FIG. 1. Viscosity versus temperature near the upper (UCPS) and lower (LCPS) critical points for stratification of the solution. ○ — measurements performed with ball 1, □ — measurements performed with ball 2; a — viscosity with $\lambda = 0$, b — background viscosity.

was determined experimentally. The measurements were performed in a viscosimeter with a tube diameter of 1.5933 cm and two different balls: 1 — diameter 1.5557 cm and density 8.144 g/cm and 2 — diameter 1.5634 cm and density 2.225 g/cm. The first ball was used in the temperature range from 24.64 °C up to 62.22 °C and the second ball was used in the temperature range from 55.16 °C up to 92.47 °C. Both balls were used in the interval from 55 °C up to 62.22 °C near the lower critical point $T_{CL} = 62.74$ °C. Ball parameters suitable for investigating the viscosity near the upper critical point could not be found. The temperature of the viscosimeter was regulated to within 0.02 °C by a liquid thermostat. The sample temperature was measured to within 0.015 °C with a Chromel–Alumel thermocouple.

4. Figure 1 displays the results of measurements of the viscosity near the lower critical point T_{CL} of the solution, performed with the two balls indicated above. It is evident from Fig. 1 that the viscosity measured with the first ball ($\nabla V_{\text{eff}} \cong 425\ \text{s}^{-1}$) is lower than the viscosity measured with the second ball ($\nabla V_{\text{eff}} \cong 55\ \text{s}^{-1}$). This means that as the critical temperature is approached and the correlation length r_c increases, the effect of the velocity gradient on the viscosity measured with a viscosimeter increases.

5. To make a quantitative comparison of the experimental results with the theoretical predictions[3,5] we approximated our experimental data by Eq. (3) together with relations (1) and (2). The values of η_B obtained with Taman's equation

$$\eta_B = A\ \exp[B/(T - T_k)], \tag{6}$$

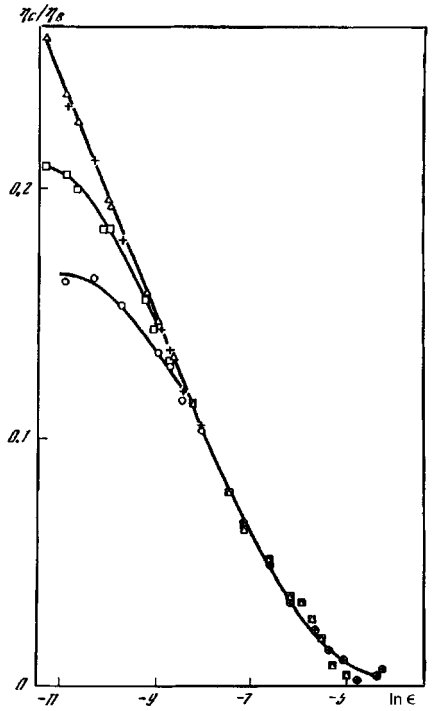

FIG. 2. η_c/η_B versus $\epsilon=[(T_{CL}-T)(T_{CU}-T)]/(T_{CU}-T_{CL})$. ○ — measurements performed with ball 1, □ — measurements performed with ball 2; measurements taking account of the interaction of ∇V and r_c: + — ball 1, △ — ball 2; solid curve — result of an approximation by Eq. (3).

where A, B, and T_k are constants, were used for the approximation. The constants A, B, and T_k in the zeroth approximation η_B^0 were determined in advance by the least-squares method using measurements of the viscosity of the solution far from the critical points. The zeroth approximation of the critical part η_c^0 of the viscosity was determined by approximating the experimental data with Eqs. (1)–(5) and then the results of viscosity measurements made outside the critical region, after η_c^0 was subtracted off, were used to make a final least-squares determination of the constants in Eq. (6). The calculations gave the following values of the constants: $A=0.0408$, $B=809.61$, and $T_k=69.667$ °C. The residual rms error in the approximation of η_B was equal to 0.34%, which corresponds to the accuracy of the experiment.

The results of the viscosity measurements were finally approximated by Eq. (3), using Eqs. (1), (2), and (5) and the least-squares method. The fit gave the values $J_0 r_c^3=3.696$ Å^3, $q_D r_0=0.0681$, $q_c r_c=0.0701$, and $X_\eta=0.0808$. Taking $r_0=2$ Å we obtain $J_0=0.0462$, $q_D^{-1}=29.39$ Å, and $q_c^{-1}=28.53$ Å.

Figure 2 displays experimental data for which the interaction of the fluid velocity gradient and the concentration fluctuations (1) and (2) is taken into account and the curve obtained by fitting expression (3). Also shown in Fig. 2 are the experimental data obtained directly from the measurements without using Eqs. (1) and (2). It is evident from

Fig. 2 that the data for which the interaction of the fluctuations and the fluid velocity gradient near the critical point are neglected deviate substantially from the curve (3) and the asymptotic straight line[5]

$$\lim_{r_c\to\infty}\frac{\eta_c}{\eta_B}=X_\eta\left[\ln(2q_0r_c)-\frac{4}{3}\right], \tag{7}$$

where $q_0^{-1}=q_D^{-1}+q_c^{-1}$. The deviation increases with ∇V_{eff}.

In our experiment, with an error of $\approx 0.33\%$, a 1% deviation of the experimental data from the curve (3) in Fig. 2 or, which is the same thing, from the straight line (7) first appears at $r_c=1050$ Å for the smaller velocity gradient ($\nabla V_{\text{eff}}\cong 55\ \text{s}^{-1}$) and at $r_c=530$ Å in the case of the larger velocity gradient ($\nabla V_{\text{eff}}\cong 425\ \text{s}^{-1}$), reaching 3% and 7% for the smaller and larger gradient, respectively. In the experimental temperature interval, for the maximum value of the ratio $\eta_c/\eta_B=20\%$ the effect (1) and (2) described above equals 30% of the total value of the critical viscosity.

In summary, if a viscosimeter in which a fluid velocity gradient $\nabla V_{\text{eff}}\approx 10-1000\ \text{s}^{-1}$ arises is used in the experiment, then the results of the viscosity measurements near the critical point cannot be described by the curve (3) or the asymptotic straight line (7) without taking account of the breakdown of the Newtonian behavior of the viscosity.

In some experimental works[12–14] systematic deviations in the behavior of the viscosity close to the critical point were described. In all of these works ∇V_{eff} was equal to $100-1000\ \text{s}^{-1}$. Oxtoby showed that all systematic deviations from Eq. (7) which were mentioned in Refs. 12–14 can be described by Eqs. (1) and (2). Taking account of this effect could eliminate the scatter in the values of the critical exponent X_η of the viscosity, which range from 0.051 to 0.070 in the works of different authors.

We thank I. L. Fabelinskiĭ for helpful remarks in a discussion of this work.

This work was supported by the Russian Fund for Fundamental Research (Project No. 96-02-16199).

[a)]e-mail: skrivokh@sci.lpi.msk.su

---

[1] W. Botch and M. Fixman, J. Chem. Phys. **36**, 3100 (1962).
[2] R. Sallavanti and M. Fixman, J. Chem. Phys. **48**, 5326 (1968).
[3] D. W. Oxtoby, J. Chem. Phys. **62**, 1463 (1975).
[4] D. W. Oxtoby and W. M. Cellbart, J. Chem. Phys. **61**, 2957 (1974).
[5] J. K. Bhattacharjee, R. A. Ferrell, R. S. Busu, and J. V. Sengers, Phys. Rev. A **24**, 1469 (1981).
[6] S. V. Krivokhizha, I. L. Fabelinskiĭ, and L. L. Chaĭkov, JETP Lett. **60**, 340 (1994).
[7] S. V. Krivokhizha, O. A. Lugovaya, I. L. Fabelinskiĭ, and L. L. Chaĭkov, Zh. Éksp. Teor. Fiz. **89**, 85 (1985) [Sov. Phys. JETP **62**, 48 (1985)].
[8] R. G. Jonston, N. A. Clark, R. Wiltzius, and D. S. Cannal, Phys. Rev. Lett. **54**, 49 (1985).
[9] C. M. Sorensen and G. A. Larsen, J. Chem. Phys. **83** 1835 (1985).
[10] S. V. Krivokhizha, O. A. Lugovaya, I. L. Fabelinskiĭ *et al.*, Zh. Éksp. Teor. Fiz. **103**, 115 (1993) [JETP **76**, 26 (1993)].
[11] S. V. Krivokhizha, O. A. Lugovaya, and L. L. Chaĭkov, Kratk. Soobshch. Fiz. **5–6**, 21 (1992).
[12] A. Stein, J. C. Allegra, and G. F. Allen, J. Chem. Phys. **55**, 4265 (1971).
[13] J. S. Allegra, A. Stein, and G. F. Allen, J. Chem. Phys. **55**, 1716 (1971).
[14] C. C. Yang and F. R. Meeks, J. Phys. Chem. **75**, 2619 (1971).

Translated by M. E. Alferieff

Brane–black hole correspondence and the asymptotic properties of the quantum spectrum

A. A. Bytsenko[a)]
State Technical University, 195251 St. Petersburg, Russia

A. E. Goncalves[b)]
Departamento de Fisica, Universidade Estadual de Londrina, 86051-970 Londrina-Parana, Brasil

S. D. Odintsov[c)]
Departamento de Fisica, Universidad del Valle, A. A. 25360 Cali, Colombia

(Submitted 30 May 1997; resubmitted 19 June 1997)
Pis'ma Zh. Éksp. Teor. Fiz. **66**, No. 1, 13–18 (10 July 1997)

The asymptotic properties of the density of quantum states for a fundamental (super)membrane are discussed in the semiclassical approach. Matching of the BPS part of the spectrum for a superstring and a supermembrane makes it possible to get stringy results via membrane calculations and vice versa. The brane–black hole correspondence (on the level of black hole states and brane microstates) is also studied.
 [S1063-7761(97)00313-2]

PACS numbers: 04.70.Dy, 11.25.Mz

1. It has been realized recently that there are very deep connections between the fundamental (super)membrane and (super)string theories. In particular, it has been shown that the BPS spectrum of states for a type IIB string on a circle is in correspondence with the BPS spectrum of a fundamental compactified supermembrane.[1,2] Remarkable progress has been made towards establishing the string–black hole correspondence relevant for the extreme black hole.[3] The entropy associated with the BPS states is then identical to the Bekenstein–Hawking entropy defined by the horizon area. The idea of string–black hole correspondence has also been formulated as the correspondence principle in Ref. 4.

2. The purpose of this work is to examine some of these questions from the fundamental-supermembrane point of view. We start from the semiclassical free energy for fundamental compactified supermembranes (which is known to be divergent) embedded in flat D-dimensional manifolds with topologies $\mathcal{M}=\mathbf{S}^1\otimes\mathbf{T}^d\otimes\mathbf{R}^{D-d-1}$ ($\mathbf{T}^d$ is the d-dimensional torus). First of all we recall that for the simplest quantum field model the free energy has the form[5,6]

$$\mathcal{F}^{(b,f)}(\beta)=-\pi^d(\det\mathcal{A})^{1/2}\int_0^\infty ds(2s)^{-(D-d+2)/2}\Xi^{(b,f)}(s,\beta)$$
$$\times\Theta\begin{bmatrix}\mathbf{g}\\ \mathbf{0}\end{bmatrix}(\mathbf{0}|\Omega)\exp\left(-\frac{sM^2}{2\pi}\right), \tag{1}$$

where

$$\Xi^{(b)}(s,\beta)=\theta_3\left(0\left|\frac{i\beta^2}{2s}\right.\right)-1,\qquad \Xi^{(f)}(s,\beta)=1-\theta_4\left(0\left|\frac{i\beta^2}{2s}\right.\right), \tag{2}$$

and $\theta_3(\nu|\tau)$ and $\theta_4(\nu|\tau)=\theta_3(\nu+\frac{1}{2}|\tau)$ are the Jacobi theta functions. Here $\mathcal{A}=\mathrm{diag}(R_1^{-2},\ldots,R_d^{-2})$ is a $d\times d$ matrix, and the global parameters R_j characterizing the nontrivial topology of $\mathcal{M}$ appear in the theory owing to the fact that the coordinates x_j $(j=1,\ldots,d)$ obey the conditions $0\leqslant x_j<2\pi R_j$. The number of topological configurations of quantum fields is equal to the number of elements in the group $H^1(\mathcal{M};\mathbf{Z}_2)$, the first cohomology group with coefficients in $\mathbf{Z}_2$. The multiplet $\mathbf{g}=(g_1,\ldots,g_d)$ defines the topological type of the field (i.e., the corresponding twist), and $g_j=0$ or 1/2, depending on the field type chosen in $\mathcal{M}$. In our case $H^1(\mathcal{M};\mathbf{Z}_2)=\mathbf{Z}_2^d$, and so the number of topological configurations of real scalars (spinors) is 2^d. We follow the notation and treatment of Ref. 7 and introduce the theta function with characteristics **a**, **b** for **a**, **b** $\in\mathbf{Z}^d$,

$$\Theta\begin{bmatrix}\mathbf{a}\\ \mathbf{b}\end{bmatrix}(\mathbf{z}|\Omega)=\sum_{\mathbf{n}\in\mathbf{Z}^d}\exp[i\pi(\mathbf{n}+\mathbf{a})\Omega(\mathbf{n}+\mathbf{a})+i2\pi(\mathbf{n}+\mathbf{a})(\mathbf{z}+\mathbf{b})]; \tag{3}$$

in this connection $\Omega=(is/2\pi^2)\mathrm{diag}(R_1^2,\ldots,R_d^2)$. The above method of calculating the free energy can be generalized to include extended objects. We shall assume that the free energy is equivalent to a sum of the free energies of quantum fields present in the modes of a membrane. The factor $\exp(-sM^2/2\pi)$ in Eq. (1) should be understood as $\mathrm{Tr}\exp(-sM^2/2\pi)$, where M is the mass operator of membrane and the trace is over an infinite set of Bose–Fermi oscillators $N_{\mathbf{n}}^{(b)}$, $N_{\mathbf{n}}^{(f)}$.

3. For the noncompactified supermembrane the reliability of the semiclassical approximation is still somewhat in question.[8] The discrete part of the supermembrane spectrum propagating in eleven-dimensional Minkowski space–time can be written in the form (see Refs. 8 and 5 for details)

$$M^2=\sum_{j=1}^{8}\sum_{\mathbf{n}\in\mathbf{Z}^2/\{\mathbf{0}\}}\omega_{\mathbf{n}}(N_{\mathbf{n}j}^{(b)}+N_{\mathbf{n}j}^{(f)}), \tag{4}$$

where

$$\omega_{\mathbf{n}}=\sqrt{(n_1\pi/a)^2+(n_2\pi/b)^2}, \tag{5}$$

and $a=\pi R_1$, $b=\pi R_2$. Thus as a result we have

$$\mathrm{Tr}\sum_{\mathbf{n}\in\mathbf{Z}^d/\{\mathbf{0}\}}\exp\left(-\frac{s}{2\pi}M^2\right)=[H_+(\Omega)H_-(\Omega)]^8, \tag{6}$$

where

$$H_\pm(\Omega)=\prod_{\mathbf{n}\in\mathbf{Z}^d/\{\mathbf{0}\}}\{1\pm\exp[-(\mathbf{n},\Omega\mathbf{n})^{1/2}]\}^{(\pm1)}, \tag{7}$$

and $\Omega=(s^2/4)\ \mathrm{diag}(a^{-2},b^{-2})$.

For generating functions $H_{\pm}(\Omega),\Omega=z\ \mathrm{diag}(1,\ldots,1),(z=t+2\pi x)$ in the half plane $\Re z>0$ there exists an asymptotic expansion uniformly in x as $t\to 0$, provided that $|\arg z|\leqslant \pi/4$ and $|x|\leqslant \frac{1}{2}$, which is given by[9]

$$H_{+}(\Omega)=\exp\{[A\Gamma(p)\zeta_{-}(1+p)z^{-p}-Z_p(0)\log 2+O(t^{c_+})]\}, \tag{8}$$

$$H_{-}(\Omega)=\exp\{[A\Gamma(p)\zeta_{+}(1+p)z^{-p}-Z_p(0)\log z+Z_p'(0)+O(t^{c_-})]\}, \tag{9}$$

where $0<c_{+},c_{-}<1$ and $Z_p(s)\equiv Z_p|^{\mathbf{g}}_{\mathbf{h}}(s)$ is the p-dimensional Epstein zeta function which has a pole with residue A. In the above equations $\zeta_{-}(s)\equiv\zeta_R(s)$ is the Riemann zeta function: $\zeta_{+}(s)=(1-2^{1-s})\zeta_{-}(s)$. The total number of quantum states can be described by the quantities $r_{\pm}(N)$ defined by

$$K_{\pm}(t)=\sum_{N=0}^{\infty} r_{\pm}(N)t^N\equiv H_{\pm}(\Omega), \tag{10}$$

where $t=\exp(-z)$, $t<1$, and N is the total quantum number. Employing the asymptotic expansion of $K_{\pm}(t)$ for $t\to 1$, which is equivalent to expansion of $H_{\pm}(\Omega,0)$ for small z, and using formulas (8) and (9), one arrives at the complete asymptotic behavior of $r_{\pm}(N)$. Thus for $N\to\infty$ one has[6,9]

$$r_{\pm}(N)=C_{\pm}(p)N^{(2Z_p(0)-p-2)/(2(1+p))}\exp\left\{\frac{1+p}{p}[A\Gamma(1+p)\zeta_{\pm}\times(1+p)]^{1/(1+p)}N^{p/(1+p)}\right\}[1+O(N^{-\kappa_{\pm}})], \tag{11}$$

$$C_{\pm}(p)=[A\Gamma(1+p)\zeta_{\pm}(1+p)]^{(1-2qZ_p(0))/(2p+2)}\frac{\exp(Z_p'(0))}{[2\pi(1+p)]^{1/2}}, \tag{12}$$

$$\kappa_{\pm}=\frac{p}{1+p}\min\left(\frac{C_{\pm}(p)}{p}-\frac{\delta}{4},\frac{1}{2}-\delta\right), \tag{13}$$

and $0<\delta<\frac{2}{3}$.

4. Let us consider the membrane excitation states with non-trivial winding number around the target space torus. In this case the spectrum of the light-cone membrane Hamiltonian is discrete.[8,5] The toroidal membrane is wrapped around the target space torus ($\mathcal{M}=\mathbf{S}^1\otimes\mathbf{T}^2\otimes\mathbf{R}^8$), and the winding number associated with this wrapping is l_1l_2. For $l_1l_2\neq 0$ a membrane is topologically protected against the usual supermembrane instabilities.[10] In the semiclassical approximation[8] the eleven-dimensional mass formula has the form ($d=2$)

$$M^2(l)=(l_1l_2R_1R_2)^2+\mathcal{H}, \tag{14}$$

where the oscillator Hamiltonian can be written as follows

$$\mathcal{H}=2\sum_{\mathbf{n}\in\mathbf{Z}^2/\{\mathbf{0}\}}(\alpha^{\dagger}_{\mathbf{n}}\alpha_{\mathbf{n}}+\omega_{\mathbf{n}}\sigma^{A\dagger}_{\mathbf{n}}\sigma^{A}_{\mathbf{n}}), \tag{15}$$

in addition one has $\omega_{\mathbf{n}}^2=\Sigma_j(l_j n_j R_j)^2$, and $A=1,\ldots,8$ are $SO(7)$ spinor indices. The two constraints for the toroidal membrane are

$$C_j=l_j k_j+\mathcal{N}_{n_j}^{(b)}+\mathcal{N}_{n_j}^{(f)}=0, \tag{16}$$

where $k_j=R_j p_j$ $(j=1,2)$; here p_j are discrete momenta. The commutation relations for the above operators can be found in Ref. 8, for example. The Fock vacuum $|0\rangle$ and the mass of a state (obtained by operating on the vacuum with creation operators) can be written as follows

$$(\text{mass})^2\sim\alpha_{n_1 n_2}^{\dagger}\ldots\alpha_{n_i n_j}^{\dagger}\sigma_{n_1 n_2}^{\dagger}\ldots\sigma_{n_i n_j}^{\dagger}|0\rangle. \tag{17}$$

As usual, the physical Hilbert space consists of all Fock space states obeying conditions (16). The quantized momenta p_1 and p_2 correspond to central charges in $N=2$ nine-dimensional supersymmetry that classify the fluctuations about the classical solution. The fact that the $M^2(l)$ is nonvanishing means that no multiplet shortening will take place, and so the vacuum must correspond to a long, massive $N=2$ multiplet with $M^2(l)=(l_1 l_2 R_1 R_2)^2$.

Let us demonstrate a correspondence between the semiclassical membrane and string results. If $R_2\to\infty$ while at the same time l_2 is increased so that the product $l_2 R_2$ is kept fixed ($l_2 R_2=1$, for example), then one dimension is shrunk while the energy is held constant and a closed string is produced. In this limit nonzero momentum p_2 is excluded, and one obtains from Eq. (14) the mass formula for a ten-dimensional superstring compactified on a circle of radius R_1. Thus the nine-dimensional mass is given by

$$M^2=l_1^2 R_1^2+\frac{k_1^2}{R_1^2}+2\sum_{j=1}^{8}\sum_{n_1\neq 0}(\alpha_{nj}^{\dagger}\alpha_{nj}+|n_1|\sigma_{nj}^{\dagger}\sigma_{nj}). \tag{18}$$

In this limit one of the constraints (16) becomes empty, while the other one yields

$$C_1=l_1 k_1+\sum_{j=1}^{8}\sum_{n_1\neq 0}(\text{sign}(n_1)\alpha_{nj}^{\dagger}\alpha_{nj}+n_1\sigma_{nj}^{\dagger}\sigma_{nj})=0. \tag{19}$$

Note that in accordance with our definitions, $\alpha_n^{\dagger}$ and $\sigma_n^{\dagger}$ create left (right)-moving states when $n_1>0$ $(n_1<0)$, while α_n and σ_n annihilate left (right)-moving states when $n_1>0$ $(n_1<0)$. The constraint (19) is equivalent to the usual condition relating left and right Hamiltonians for the string.

Let us compare the BPS part of the membrane spectrum with the BPS spectrum for a type II string. The correspondence between the spectra at the zero-mode level was established in Ref. 1. Using the constraint (19) in the mass formula (18) for free string states (note that under T-duality relating the IIA and IIB spectra, $R_1\to\alpha' R_1^{-1}$, and for the sake of simplicity here and below we assume an inverse string tension parameter α' equal to 1) we have

$$M^2=(l_1 R_1+k_1/R_1)^2. \tag{20}$$

The Kaluza–Klein mass for perturbative or (1,0) string states with $k_2=0$ (zero Ramond–Ramond charge) is given by

$$M^2_{\mathrm{IIB}}=\frac{k_1^2}{R_1^2}+l_1^2R_1^2+2(\mathcal{N}^{(b)}+\mathcal{N}^{(f)}). \tag{21}$$

For the general BPS perturbative states with the corresponding oscillating states (1,0) the masses given in formula (21) coincide with the masses of Eq. (20). The last statement is correct also for the nonperturbative type IIB string[2,11] with charges (q_1,q_2). In this case $k_1=mq_1$ and $k_2=mq_2$, with q_1, q_2 being co-prime. For the NS–NS string we have $k_2=0$, $q_1=1$, $q_2=0$, while for the R–R string, $k_1=0$, $q_1=0$, $q_2=1$ and the value of M^2_{IIB} coincides with the masses (up to a change of indices $1\rightarrow 2$) given in formula (20). Hence, for calculation of the BPS membrane Hagedorn density one can use stringy results.

If $l_2=0$ (or $l_1=0$) then the stable classical solution will be collapsed to string-like membrane wound around only one compact direction in the target space. For this classical configuration the mass formula (14) indicates the presence of massless states. The world-volume metric for this light-cone classical solution is degenerate, but the field equations are nevertheless nonsingular. It is not clear whether the semiclassical approximation can be trusted for such a configuration.[8] Indeed the equation $\omega_{n_1}=\sqrt{(n_1l_1R_1)^2}$ shows that all values of n give the same frequency ω_{n_1} in the semiclassical approximation. This infinite degeneracy will presumably be lifted when the higher-order terms in the Hamiltonian are included.

5. Let us suppose that the semiclassical approach to quantization leads to a second-quantized brane theory which can be considered as a theory of noninteracting strings. Then the Hilbert space of all multiple string states that satisfy the BPS conditions (zero branes) with a total energy momentum P has the form[12]

$$\mathcal{H}_P=\oplus_{\Sigma lN_l=N_P}\otimes_l \mathrm{Sym}^{N_l}\mathcal{H}_l, \tag{22}$$

where symbol Sym^N indicates the Nth symmetric tensor product. The exact dimension of $\mathcal{H}_P$ is determined by the character expansion formula

$$\sum_{N_P}\dim\mathcal{H}_P q^{N_P}\simeq\prod_l\left(\frac{1+q^l}{1-q^l}\right)^{\frac{1}{2}\dim\mathcal{H}_l}, \tag{23}$$

where the dimension $\mathcal{H}_l$ of the Hilbert space of single-string BPS states with momentum $k=l\hat{P}$ is given by $\dim\mathcal{H}_l=d(\frac{1}{2}l^2\hat{P})$, and $|\hat{P}|^2=|\hat{P}_L|^2-|\hat{P}_R|^2$ (see Ref. 12 for details). The asymptotic form of the generating function (23) and the dimension $\mathcal{H}_P$ can be found with the help of Eqs. (11), (12), which constitute a generalization of the Meinardus result for vector-valued functions.

Equation (23) is similar to the denominator formula of a (generalized) Kac–Moody algebra,[13] which can be written as follows

$$\sum_{\sigma\in W}(\mathrm{sgn}(\sigma))e^{\sigma(\rho)}=e^{\rho}\prod_{r>0}(1-e^r)^{\mathrm{mult}(r)}, \tag{24}$$

where ρ is the Weyl vector, the sum on the left-hand side is over all elements of the Weyl group W, the product on the right side runs over all positive roots (one has the usual

notation for the root spaces, positive roots, simple roots, and Weyl group for the Kac–Moody algebra) and each term is weighted by the root multiplicity mult(r). Equation (23) reduces to the standard superstring partition function for $\hat{P}^2=0$ (Ref. 12). The equivalent description of the second-quantized string states on the five-brane can be obtained, for example, by considering the sigma model on the target space $\Sigma_N \mathrm{Sym}^N T^4$. There is a correspondence between formula (22) and the term of order $q^{\frac{1}{2}N_p\hat{P}^2}$ in the expansion of the elliptic genus of the orbifold $\mathrm{Sym}^{N_P}T^4$ (Ref. 12). Using this correspondence, one finds that the asymptotic growth is equal that of states at level $\frac{1}{2}N_P\hat{P}^2$ in a unitary conformal field theory with a central charge proportional to N_P.

Our aim now is to compare the quantum states of a membrane and a black hole. The correspondence between the asymptotic density of states of the fundamental p-brane and the four-dimensional black hole for $p\to\infty$ was found in Ref. 14. Extreme black hole states can also be identified with the highly excited states of a fundamental string. The relevant string states are BPS states, while the string entropy is identical to the Bekenstein–Hawking entropy defined by the horizon area.[3] For calculation of the ground state degeneracy of systems with quantum numbers of certain BPS extreme black holes the D-brane method can be used. A typical 5-dimensional example has been analyzed in Refs. 15–17. Working in the type IIB string theory on $M^5\otimes \mathbf{T}^5$, one can construct a D-brane configuration such that the corresponding supergravity solutions describe 5-dimensional black holes. In addition, five-branes and one-branes are wrapped on $\mathbf{T}^5$ and the system is given by Kaluza–Klein momentum N in one of the directions. Therefore three independent charges (Q_1,Q_5,N) arise in the theory, where Q_1 and Q_5 are the electric and magnetic charges, respectively. The naive D-brane picture gives the entropy in terms of the partition function $H_{\pm}(z)$ for a gas of Q_1Q_5 species of massless quanta. For $p=1$ the integers $r_{\pm}$ in Eq. (11) represent the degeneracy of the state with momentum N. Thus for $N\to\infty$ one has

$$\log r_{\pm}(N)=\sqrt{q\zeta_{\pm}(2)N}-\frac{q+3}{4}\log N+\log C_{\pm}(1)+O(N^{-\kappa_{\pm}}), \tag{25}$$

where

$$C_{+}(1)=2^{-\frac{1}{2}}\left(\frac{q}{16}\right)^{(q+1)/2}, \quad C_{-}(1)=C_{+}(1)\left(\frac{4}{3}\right)^{(q+1)/2}. \tag{26}$$

For fixed $q=4Q_1Q_5$ the entropy is given by

$$S=[\log(r_{+}(N)r_{-}(N))]_{N\to\infty}\simeq c_1\sqrt{Q_1Q_5N}-\log N(c_2Q_1Q_5+c_3), \tag{27}$$

where c_j $(j=1,2,3)$ are some positive numbers. This expression agrees with the classical black hole entropy.

Note that for $p>1$, using the mass formula $M^2=N$, we obtain for the number of branes states of mass M to $M+dM$ (see also Ref. 14)

$$\varrho(M)dM\simeq 2C_{\pm}(p)M^{(p-1)/(p+1)}\exp[b_{\pm}(p)M^{2p/(p+1)}], \tag{28}$$

$$b_{\pm}(p)=\left(1+\frac{1}{p}\right)[A\Gamma(p+1)\zeta_{\pm}(p+1)]^{1/(p+1)}. \tag{29}$$

This result has a universal character for all p-branes.

Recently it has been pointed out that the classical result (27) is incorrect when the black hole becomes massive enough for its Schwarzschild radius to exceed any microscopic scale such as the compactification radii.[16,17] Indeed, if the charges (Q_1, Q_5, N) tend to infinity in fixed proportion $Q_1 Q_5 = Q(N)$, then the correct formula does not agree with the black hole entropy (27). If, for example, $Q(N) = N$, then for $N \to \infty$ one finds $\log[r_+(N) r_-(N)] \sim N \log N$. The naive D-brane prescription, therefore, fails to agree with U-duality, which requires symmetry among the charges (Q_1, Q_5, N).[17]

[a)]e-mail: abyts@spin.hop.stu.neva.ru
[b)]e-mail: goncalve@fisica.uel.br
[c)]e-mail: odintsov@quantum.univalle.edu.co. On leave from Tomsk Pedagogical University, 634041 Tomsk, Russia

[1] J. H. Schwarz, Phys. Lett. B **360**, 13 (1995).
[2] J. G. Russo and A. A. Tseytlin, hep-th/9611047 (1996).
[3] A. Strominger and C. Vafa, Phys. Lett. B **379**, 99 (1996); G. T. Horowitz and A. Strominger, Phys. Rev. Lett. **77**, 2368 (1996); C. V. Johnson, R. R. Khuri, and R. C. Myers, Phys. Lett. B **378**, 78 (1996).
[4] G. T. Horowitz and J. Polchinski, hep-th/9612146 (1996).
[5] A. A. Bytsenko and S. D. Odintsov, Phys. Lett. B **245**, 21 (1990); A. A. Bytsenko and S. D. Odintsov, Fortschr. Phys. **41**, 233 (1993).
[6] E. Elizalde, S. D. Odintsov, A. Romeo *et al.*, *Zeta Regularization Techniques with Applications*, World Scientific, Singapore, 1994; A. A. Bytsenko, G. Cognola, L. Vanzo, and S. Zerbini, Phys. Rep. **266**, Nos. 1, 2 (1996).
[7] D. Mumford, *Tata Lectures on Theta I, II*, Birkhäuser, 1983, 1984.
[8] M. J. Duff, T. Inami, C. N. Pope *et al.*, Nucl. Phys. B **297**, 515 (1988).
[9] A. A. Bytsenko and S. D. Odintsov, hep-th/9611151 (1996).
[10] B. de Wit, M. Lüscher, and H. Nicolai, Nucl. Phys. B **320**, 135 (1989).
[11] J. G. Russo, hep-th/9701188 (1997).
[12] R. Dijkgraaf, E. Verlinde, and H. Verlinde, hep-th/9603126 (1996).
[13] R. E. Borcherds, Invent. Math. **120**, 161 (1995); J. A. Harvey and G. Moore, Nucl. Phys. B **463**, 315 (1996).
[14] A. A. Bytsenko, K. Kirsten, and S. Zerbini, Phys. Lett. B **304**, 235 (1993); A. A. Bytsenko, K. Kirsten, and S. Zerbini, Mod. Phys. Lett. A **9**, 1569 (1994).
[15] C. Callan and J. Maldacena, Nucl. Phys. B **475**, 645 (1996).
[16] J. Maldacena and L. Susskind, Nucl. Phys. B **475**, 679 (1996).
[17] E. Halyo, A. Rajaraman, and L. Susskind, hep-th/9605112 (1996).

Published in English in the original Russian journal. Edited by Steve Torstveit.

Self-energy correction to the hyperfine splitting of the 1*s* and 2*s* states in hydrogenlike ions

V. A. Yerokhin[a)]
Institute for High Performance Computing and Data Bases, 198005 St. Petersburg, Russia

V. M. Shabaev and A. N. Artemyev
Department of Physics, St. Petersburg State University, 198904 St. Petersburg, Russia

(Submitted 20 March 1997)
Pis'ma Zh. Éksp. Teor. Fiz. **66**, No. 1, 19–22 (10 July 1997)

The one-loop self-energy correction to the hyperfine splitting of the 1*s* and 2*s* states of hydrogenlike ions is calculated for both point and finite nuclei. The results of the calculation are combined with other corrections to find the ground state hyperfine splitting in lithiumlike $^{209}Bi^{80+}$ and $^{165}Ho^{64+}$. © *1997 American Institute of Physics.* [S1063-7761(97)00413-7]

PACS numbers: 33.15.Pw, 12.20.Ds

Recent experimental investigations of the ground-state hyperfine splitting of $^{209}Bi^{82+}$ (Ref. 1) and $^{165}Ho^{66+}$ (Ref. 2) shows that the present experimental accuracy is much higher than the accuracy of the corresponding theoretical values. Measurements of the ground state hyperfine splitting of lithiumlike ions are currently planned. In this connection there is an obvious need for an accurate calculation of the QED corrections to the hyperfine splitting of the 1*s* and 2*s* states of highly charged ions.

The one-loop self-energy correction to the first-order hyperfine interaction for the ground state of hydrogenlike ions in the case of an extended nucleus was calculated in Ref. 3 over a wide interval of Z. For a point nucleus such a calculation was done in Ref. 4 for $Z=83$. In the present work we recalculate the self-energy correction for the 1*s* state and present results for the 2*s* state. The calculation was made using the full-covariant scheme based on an expansion of the Dirac–Coulomb propagator in terms of interactions with the external potential.[5,6]

The self-energy contribution to the hyperfine splitting is defined by the diagrams shown in Fig. 1, where the dotted line denotes the hyperfine interaction. The formal expressions for these diagrams can easily be derived by the two-time Green function method.[7] The diagrams in Fig. 1a are conveniently divided into irreducible and reducible parts. The reducible part is the part in which the intermediate-state energy (between the self-energy and the hyperfine interaction line) coincides with the initial-state energy. The irreducible part is the remaining one. The irreducible part is calculated in the same way as the first-order self-energy contribution. For a point nucleus the external wave function containing the hyperfine interaction line is calculated analytically by using the generalized virial relations for the Dirac–Coulomb problem.[8] For an extended nucleus a calculation of the external wave function was performed using the reduced Green function.

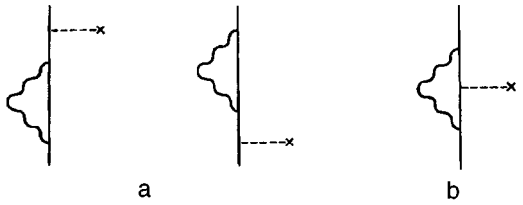

FIG. 1. Self energy-hyperfine interaction diagrams.

The reducible part is grouped with the vertex part presented in Fig. 1b. According to the Ward identity the counterterms for the vertex and the reducible parts cancel each other, and so the sum of these terms regularized in the same covariant way is ultraviolet-finite. To cancel the ultraviolet divergences we separate free propagators from the bound electron lines and calculate them in the momentum representation. The remainder is ultraviolet-finite but contains infrared divergences, which are explicitly separated out and canceled.

The calculations were carried out for both point and extended nuclei. In the latter case the model of a uniformly charged shell of radius $R=(\sqrt{15}/4)\langle r^2\rangle^{1/2}$ was used for the nuclear charge distribution. To a high precision this model is equivalent to the model of an uniformly charged sphere of radius $R=(\sqrt{5/3})\langle r^2\rangle^{1/2}$ for purposes of calculating the first-order hyperfine structure splitting. Our test calculation shows a good agreement between these models for the self-energy correction to the hyperfine splitting, too. The Green function expressed in terms of the Whittaker and Bessel functions[9] was used in the numerical calculation in the case of an extended nucleus. A part of the vertex term was calculated using the B-spline basis set method for the Dirac equation.[10]

The results of the calculation for the $1s$ state are listed in Table I. The values of the root-mean-square nuclear charge radii given in the second column of Table I are taken from Ref. 11. The quantities X listed in Table I are defined by the equation

$$\Delta E_{\rm SE}=\alpha X\Delta E_{\rm nr}, \tag{1}$$

where $\Delta E_{\rm SE}$ is the self-energy correction to the hyperfine splitting, $\Delta E_{\rm nr}$ is the nonrelativistic value of the hyperfine splitting (Fermi energy), and α is the fine-structure constant. The results of the calculation for a point nucleus are listed in the third column of

TABLE I. Self-energy correction to the hyperfine splitting of the $1s$ state in hydrogenlike ions.

Z	$\langle r^2\rangle^{1/2}$	$X_{\rm point}$	$\delta X_{\rm fin}$	$X_{\rm total}$	$F_{\rm total}$
49	4.598	−1.057	0.042	−1.015	−2.629
59	4.892	−1.496	0.096	−1.400	−3.293
67	5.190	−1.995	0.192	−1.803	−3.856
75	5.351	−2.737	0.393	−2.344	−4.470
83	5.533	−3.940	0.850	−3.090	−5.141

TABLE II. Self-energy correction to the hyperfine splitting of the $2s$ state in hydrogenlike ions.

Z	$\langle r^2\rangle^{1/2}$	X_{point}	δX_{fin}	X_{total}	F_{total}
49	4.598	−1.073	0.050	−1.023	−2.437
59	4.892	−1.605	0.107	−1.498	−3.112
67	5.190	−2.267	0.232	−2.035	−3.696
75	5.351	−3.321	0.509	−2.812	−4.347
83	5.533	−5.157	1.185	−3.972	−5.076

Table I. The finite-nuclear-size contributions and the total self-energy corrections are given in the fourth and fifth columns, respectively. The last column gives the values of the quantity F defined by the equation

$$\Delta E_{\text{SE}}=\frac{\alpha}{\pi}F\Delta E_{\text{rel}}. \tag{2}$$

Here ΔE_{rel} is the relativistic value of the first-order hyperfine splitting including the finite nuclear size correction. The quantity F is more stable than X with respect to variations of the nuclear parameters. In Table II the corresponding values for the $2s$ state of hydrogenlike ions are listed. The relative precision of the results is estimated to be not worse than 5×10^{-3}.

As is mentioned above, the self-energy correction was calculated for the $1s$ state earlier in Refs. 3 and 4. For a point nucleus with $Z=83$ the calculation of Ref. 4 gave $X=-3.8$, while the present calculation gives $X=-3.94$. This discrepancy results from the use of a noncovariant regularization procedure in Ref. 4, which, as it turns out, gives a small additional spurious term.[b)] A comparison of the present results for an extended nucleus with the previous calculation[3] reveals some discrepancy, too. For example, for $Z=83$ a value $F=5.098$ was obtained in Ref. 3, while the present calculation gives $F=5.141$ (the difference due to the discrepancy between the nuclear parameters is negligible). A detailed comparison of our calculation with that of Ref. 6 shows that this discrepancy results from a term in the vertex contribution which was omitted in Ref. 6.

Taking into account the present results for the self-energy correction and values of the other corrections (nuclear magnetization distribution, electron–electron interaction, and vacuum polarization) calculated in Ref. 12, we find that the wavelength of the hyperfine splitting transition for the $2s$ state in lithiumlike $^{209}Bi^{80+}$ and $^{165}Ho^{64+}$ is $\lambda=1.548(9)\mu$m ($\mu=4.1106(2)\mu_N$)[13] and $\lambda=4.059(13)\mu$m ($\mu=4.132(5)\mu_N$),[14,2] respectively. The uncertainty of these values is mainly due to the nuclear magnetization distribution correction.

We thank S. M. Schneider for helpful conversations. The research described in this publication was made possible in part by Grant 95-02-05571a from the Russian Fund for Fundamental Research.

[a)]e-mail: yerokhin@snoopy.phys.spbu.ru
[b)]S. M. Schneider, private communication.

[1] I. Klaft, S. Borneis, T. Engel *et al.*, Phys. Rev. Lett. **73**, 2425 (1994).
[2] J. R. Crespo Lopez-Urrutia, P. Beiersdorfer, D. Savin, and K. Widman, Phys. Rev. Lett. **77**, 826 (1996).
[3] H. Persson, S. M. Schneider, W. Greiner *et al.*, Phys. Rev. Lett. **76**, 1433 (1996).
[4] V. M. Shabaev and V. A. Yerokhin, JETP Lett. **63**, 316 (1996).
[5] N. J. Snyderman, Ann. Phys. (N.Y.) **211**, 43 (1991).
[6] S. M. Schneider, *Die Hyperfinestrukturaufspaltung von Einelektronenatomen*, Ph.D. Thesis, Frankfurt am Main, 1995 (unpublished).
[7] V. M. Shabaev, Izv. Vyssh. Uchebn. Zaved. Fiz. **33**, 43 (1990) [Sov. Phys. J. **33**, 660 (1990)]; V. M. Shabaev and I. G. Fokeeva, Phys. Rev. A **49**, 4489 (1994).
[8] V. M. Shabaev, J. Phys. B **24**, 4479 (1991).
[9] M. Gyulassy, Nucl. Phys. A **244**, 497 (1975); G. Soff and P. Mohr, Phys. Rev. A **38**, 5066 (1988).
[10] W. R. Johnson, S. A. Blundell and J. Sapirstein, Phys. Rev. A **37**, 307 (1988).
[11] G. Fricke, C. Bernhardt, K. Heilig *et al.*, At. Data Nucl. Data Tables **60**, 177 (1995); H. de Vries, C. W. de Jager, and C. de Vries, At. Data Nucl. Data Tables **36**, 495 (1987); W. R. Johnson and G. Soff, At. Data Nucl. Data Tables **33**, 405 (1985).
[12] M. B. Shabaeva and V. M. Shabaev, Phys. Rev. A **52**, 2811 (1995); V. M. Shabaev, M. B. Shabaeva, I. I. Tupitsyn *et al.*, (to be published).
[13] P. Raghavan, At. Data Nucl. Data Tables **42**, 189 (1989).
[14] G. Nachtsheim, *Präzisionsmessung der Hyperfeinstruktur-Wechselwirkung von* ^{165}Ho im Grundzustand, Ph.D. Thesis, Bonn 1980 (unpublished); L. K. Peker, Nucl. Data Sheets **50**, 137 (1987).

Published in English in the original Russian journal. Edited by Steve Torstveit.

Double ionization of atoms by multiply charged ions and a strong electromagnetic field: Effects of correlation in the continuum

L. P. Presnyakov and D. B. Uskov
P. N. Lebedev Physics Institute, Russian Academy of Sciences, 117924 Moscow, Russia

(Submitted 4 June 1997)
Pis'ma Zh. Éksp. Teor. Fiz. **66**, No. 1, 23–26 (10 July 1997)

A nonstationary theory of double ionization of two-electron atoms in collisions with multiply charged ions or by an intense electromagnetic field is developed. An approach that permits investigating both problems by a single method is formulated. A two-electron continuum wave function that takes into account the interaction of the electrons with the atomic nucleus and the external ionizer as well as with one another is obtained as a product of Coulomb waves with modified Sommerfeld parameters. The computational results obtained for the double ionization of helium atoms by multiply charged ions are in good quantitative agreement with the existing experimental data. © *1997 American Institute of Physics.* [S1063-7761(97)00513-1]

PACS numbers: 34.50.Fq

When analyzing the ionization of atoms by ion impact or by an intense electromagnetic field, the nonstationary external potential (which is comparable to or exceeds the intra-atomic potential) must be taken into account even in zeroth order, i.e., in the continuum wave functions in the final channel of the reaction. For single-electron processes, the Keldysh theory[1] makes it possible to investigate the most important characteristics of multiphoton ionization, and it can be extended to the case of ionization by multiply charged ions.[2] It is expedient to study both problems together, since they can be solved on the basis of the same approach, and in addition the existing experimental data on ion–atom collisions can greatly aid in the analysis of multiphoton ionization processes. Specifically, the theory of Ref. 1 as modified in Ref. 2 so as to go beyond the perturbation theory in calculating the transition amplitudes and probabilities gives a good quantitative description of all experimental data on the ionization of atoms[2] and the neutralization of negative ions[3] in collisions with multiply charged ions. Another correction to the theory and its modification[2] is to replace the generalized plane waves[1] by Coulomb wave functions in the field of the atomic core, taking into account the additional momentum acquired by an electron in the field of the ionizer.[4–6] This increases the ionization probability in strong fields and gives an analytically correct description of the domain of applicability of the perturbation theory (one-photon photoeffect, Coulomb–Born limit in the physics of collisions).

To analyze double ionization it is necessary to take account of, besides the points mentioned above, the interelectronic correlation in the continuum wave functions. This

problem arises even in the theory of single-ionization of atoms by electron impact. It has been shown[7] that the use of an undistorted two-particle wave function for the interelectronic repulsion gives results which are much too low. It has been proposed that an effective charge be introduced to account for the partial screening of the interelectronic repulsion in different regions of configuration space.[7] This approach gave the first quantitative description of the experimental data on the cross sections for the excitation and ionization of $H(1s)$ atoms by electrons. Systems of three particles coupled with one another by a Coulomb interaction in the continuum are now an object of intense investigations, both experimental and theoretical. The effective charge (or effective Sommerfeld parameter) of the interacting particles is found from physical considerations[8] or approximate solutions[9,10] of the Schrödinger equation. In the latter case it depends on the particle coordinates. Calculations by these methods[8–10] give good agreement with the experimental data on the differential cross sections for ionization of $H(1s)$ atoms by electrons.[8,11]

The problem solved in the present letter is a four-particle problem for the case of the interaction of atoms with ions and a three-particle problem in an external field in the case of multiphoton ionization. Using the approach of Refs. 2 and 6, we reduce the problem in both cases to a system of three particles in a nonstationary external field. This is achieved by expanding the Coulomb interaction of the electrons with the incident ion in multipoles and retaining only the dipole term. The time-dependent Schrödinger equation (in atomic units) has the form

$$i\frac{\partial\Psi}{\partial t}=\left[\sum_{j=1,2}\left(-\frac{1}{2}\nabla_{r_j}^2-\frac{Z}{r_j}-\mathbf{r}_j\cdot\mathbf{B}(t)\right)+\frac{1}{|\mathbf{r}_1-\mathbf{r}_2|}\right]\Psi(\mathbf{r}_1,\mathbf{r}_2,t). \tag{1}$$

Here r_j are the coordinates of the electrons with respect to the nucleus with charge Z of a two-electron atom and the coefficients $\mathbf{B}$ equal

$$\mathbf{B}(t)=q\mathbf{R}(t)/R^3(t) \text{ or } \mathbf{B}(t)=\mathbf{E}\cos(\omega t) \tag{2}$$

in the case of the interaction of an ion with charge q or an external field with amplitude $\mathbf{E}$ and frequency ω, respectively. The internuclear distance $\mathbf{R}(t)$ is assumed to be a given function of time. The solution is sought in the form

$$\Psi(\mathbf{r}_1,\mathbf{r}_2,t)=\exp\left[i\sum_{j=1,2}\left(\mathbf{p}_j\cdot\mathbf{r}_j-1/2\int_0^t p_j^2(\tau)d\tau\right)\right]\prod_{j=1,2}F_j(\mathbf{r}_j,\mathbf{p}_j)\Phi(\mathbf{r}_1,\mathbf{r}_2), \tag{3}$$

$$\mathbf{p}_j=\mathbf{k}_j+\mathbf{A}(t),\quad \mathbf{A}(t)=\int_0^t\mathbf{B}(\tau)d\tau,$$

$$F_j=\exp(\pi\nu_j/2)\Gamma(1+i\nu_j)F(-i\nu_j,1,-i\eta_j),\quad \nu_j=Z/p_j,\quad \eta_j=\mathbf{p}_j\cdot\mathbf{r}_j+p_jr_j. \tag{4}$$

The exponential factor in Eq. (3) is a product of two generalized plane waves.[1] The product (4) of confluent hypergeometric functions converts these plane waves into Coulomb wave functions describing the motion of each electron in the field of the atomic core and a nonstationary external field. The $\mathbf{k}_j$ are the electron momenta in the absence of an external field. Since the main time dependence is contained in the exponential cofactor (3), it can be assumed that the correlation function Φ depends on the time only parametrically; this corresponds to the perturbed stationary states approximation in the theory

of atomic collisions. We shall estimate the gradient coefficients that arise when expression (3) is substituted into Eq. (1), in the part of the configuration space where the vectors $\mathbf{p}_j$ and $\mathbf{r}_j$ are collinear, i.e., we set

$$(F_j^{-1}\nabla_{r_j}F_j)\cdot\nabla_{r_j}\Phi \approx i\nu_j(\mathbf{r}_j/r_j)\cdot\nabla_{r_j}\Phi \approx i\nu_j\mathbf{n}_j a^{-1}\cdot\nabla_{r_j}\Phi, \quad \mathbf{n}_j=\mathbf{p}_j/p_j, \tag{5}$$

where a is the characteristic size of the target atom. Here it is convenient to introduce the coordinates for the center of mass of the two electrons and the distances between the electrons. The equation for Φ separates in these coordinates. Since the equation in the center of mass coordinates contains no potentials, its solution can be set equal to a unit constant. The remaining equation acquires the form

$$\left[\nabla_{r_{12}}^2-\frac{1}{r_{12}}+i\left(\mathbf{p}_{12}+\frac{\nu_1}{a}\mathbf{n}_1-\frac{\nu_2}{a}\mathbf{n}_2\right)\cdot\nabla_{r_{12}}\right]\Phi=0, \tag{6}$$

$$\mathbf{r}_{12}=\mathbf{r}_1-\mathbf{r}_2, \quad \mathbf{p}_{12}=\mathbf{p}_1-\mathbf{p}_2\equiv\mathbf{k}_1-\mathbf{k}_2$$

and admits the exact solution

$$\Phi(\mathbf{r}_{12}=\exp(-\pi\nu/2)\Gamma(1+i\nu)F(-i\nu,1,i\eta), \quad \eta=\mathbf{d}_{12}\cdot\mathbf{r}_{12}-d_{12}r_{12}, \tag{7}$$

$$\mathbf{d}_{12}=\mathbf{k}_1-\mathbf{k}_2+(\nu_1\mathbf{n}_1-\nu_2\mathbf{n}_2)/a, \quad \nu=Z/d_{12}.$$

Equations (7) and (3) together solve the problem of the two-electron continuum wave function in the field of an atomic core and a nonstationary external field. The momenta (and the Sommerfeld parameters associated with them) in all cofactors in Eq. (3) depend explicitly on the characteristics of the external field (2). As the quantities **B** approach zero, the correlation function (7) retains its dependence on $\mathbf{k}_1$ and $\mathbf{k}_2$, the nature of which falls outside the scope of the unscreened interelectronic repulsion approximation, and can also be used in other three-particle problems.

Since double ionization is a two-step process, i.e., a sequence of single-electron processes, the two-electron probability can be represented over a wide range of values of the parameters as

$$W(\mathbf{k}_1,\mathbf{k}_2)=\int\int d\mathbf{k}_1 d\mathbf{k}_2 \frac{1}{2}\left|a_1(\mathbf{k}_1)a_2(\mathbf{k}_2)\zeta(\mathbf{k}_1,\mathbf{k}_2)+a_1(\mathbf{k}_2)a_2(\mathbf{k}_1)\zeta(\mathbf{k}_2,\mathbf{k}_1)\right|^2. \tag{8}$$

Here a_1 and a_2 are the probability amplitudes of ''independent'' single-electron ionization processes, and the factor ζ determines the interelectronic correlation effect. In previous works[2,3,6] we calculated the quantities a_1 and a_2 for the ionization of atoms by multiply charged ions without taking the correlation function (7) into account. In the general case, the function ζ appearing in Eq. (8) can be separated out as a cofactor only when the wave function of the initial (bound) state factorizes in the coordinates of both electrons. The functional properties of the correlation factor $\zeta(\mathbf{k}_1,\mathbf{k}_2)$ and the asymptotic expressions will be discussed in a separate publication. Here we give as an example the computational results for the two-electron ionization cross sections of He atoms in comparison with the published experimental data (see Fig. 1).

The main result of this letter is that the double ionization of two-electron atoms (H^- ion, He atom, and He-like ions) can be described on the basis of an approach used for solving problems in the physics of atomic collisions and multiphoton ionization. The

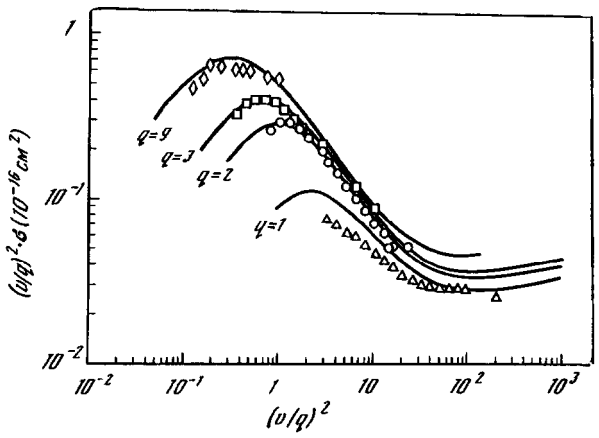

FIG. 1. Parameterized cross section for the removal of two electrons from a helium atom in collisions with multiply charged ions as a function of $(v/q)^2$, where v is the relative collision velocity in atomic units and q is the ion charge. Solid curves — computational results obtained with the proposed theory (the charges q are indicated on each curve). Experimental data: △ — $q=1$, ○ — $q=2$, □ — $q=3$, data from Refs. 12 and 13; ◇ — $q=9$, Ref. 14.

continuum wave functions obtained for the final channel explicitly take account of the ionizer (ion or electromagnetic field) as well as the electron–electron interaction. The indicated correlation is nontrivial and can be used in other problems involving the transfer of two electrons into the continuum. A comparison of the calculations with the experimental data shows that further elaboration of this approach is promising.

We are deeply grateful to V. L. Ginzburg, S. P. Goreslavskiĭ, N. B. Delon, D. A. Kirzhnits, and I. I. Sobel'man for their interest in this work and for discussions. This work was supported by the Russian Fund for Fundamental Research (Project No. 96-02-16090) and the International Science and Technical Center (Project No. 076/95).

[1] L. V. Keldysh, Zh. Éksp. Teor. Fiz. **47,** 1945 (1964) [Sov. Phys. JETP **20**, 1307 (1965)].
[2] L. P. Presnyakov and D. B. Uskov, Zh. Éksp. Teor. Fiz. **86,** 882 (1984) [Sov. Phys. JETP **59**, 515 (1984)].
[3] F. Melchert, M. Benner, S. Krudener *et al.*, Phys. Rev. Lett. **74**, 888 (1995).
[4] J. Z. Kaminski, Phys. Scr. A **42,** 417 (1990).
[5] M. H. Mittelman, Phys. Rev. A **50**, 3249 (1994).
[6] L. P. Presnyakov, H. Tawara, I. Yu. Tolstikhina, and D. B. Uskov, J. Phys. B **28,** 785 (1995).
[7] L. A. Vaĭnshteĭn, L. P. Presnyakov, and I. I. Sobel'man, Zh. Éksp. Teor. Fiz. **45,** 2015 (1964) [Sov. Phys. JETP **18**, 1383 (1964)]; L. P. Presnyakov, Zh. Éksp. Teor. Fiz. **47**, 1134 (1964) [Sov. Phys. JETP **20**, 760 (1965)].
[8] J. Berakdar and J. S. Briggs, Phys. Rev. Lett. **72**, 3799 (1994).
[9] E. O. Alt and A. M. Mukhamedzhanov, Phys. Rev. A **47**, 2004 (1993).
[10] J. Berakdar, Phys. Rev. A **53**, 3214 (1996).
[11] S. Jones, D. H. Madison, and D. A. Konovalov, Phys. Rev. A **55**, 444 (1997).
[12] H. Knudsen, L. Andersen, P. Hvelplund *et al.*, J. Phys. B **17**, 3545 (1984).
[13] M. B. Shah and H. B. Gilbody, J. Phys. B **18**, 899 (1984).
[14] J. L. Shinpaugh, J. M. Sanders, J. M. Hall *et al.*, Phys. Rev. A **45**, 2922 (1992).

Translated by M. E. Alferieff

Destruction and appearance of surface metallization in the system K/Si(111)7×7

G. V. Benemanskaya and D. V. Daĭneka
A. F. Ioffe Physicotechnical Institute, Russian Academy of Sciences, 194021 St. Petersburg, Russia

G. É. Frank-Kamenetskaya
St. Petersburg Technological Institute, 198013 St. Petersburg, Russia

(Submitted 24 April 1997)
Pis'ma Zh. Éksp. Teor. Fiz. **66**, No. 1, 27–30 (10 July 1997)

Qualitative changes are observed in the character of the surface electronic structure accompanying the adsorption of potassium on a Si(111) 7×7 surface. The metallic conductivity of the Si(111)7×7 surface is destroyed at the very early stages of adsorption. A new band induced by the adsorption of potassium is observed below the Fermi level. It is found that the K/Si(111)7×7 interface is semiconducting right up to saturating coverage. A surface transition from an insulating into a metallic state, accompanied by pinning of the Fermi level, is observed in the region of saturating coverage. Metallic conductivity arises in the adsorbed potassium layer as a result of the development of an induced surface band at the Fermi level. © *1997 American Institute of Physics.* [S1063-7761(97)00613-6]

PACS numbers: 73.20.At, 73.25.+i

Research on the electronic structure of different silicon surfaces covered with alkali-metal atoms is driven by the development of nanostructure technology, which at present is based mainly on silicon. Fundamental problems include the character of the electronic structure upon the formation of a metal–semiconductor interface and the nature of the adsorption bond. The most important questions in the first problem are the mechanisms leading to the appearance of metallic interfacial conductivity. Theoretical investigations have shown that interfacial metallization with submonolayer adsorption can be of two types: It can arise due to the realization of conductivity either in the top quasi-two-dimensional layer of the substrate or in the adsorbed metal layer.[1,2]

Investigations have shown[3–5] that the electronic structure of a Si(111)7×7 reconstructed surface possesses three filled surface states S_1, S_2, and S_3. One of these states, S_1, crosses the Fermi level and thereby gives a metallic type of electronic surface structure. The dangling bonds of the so-called ''adatoms'' of the substrate in the generally accepted dimer–adatom model (the dimer–adatom stacking fault model) are responsible for this.[6] The Si(111)7×7 surface is unique from the standpoint of investigations of the local properties in the presence of an interaction with adsorbed metal atoms.[7] Furthermore, for this reconstruction a search can be made for metal–insulator and insulator–metal type surface transitions. The electronic structure of the K/Si(111)7×7 system has

been investigated by photoemission spectroscopy.[8–10] It has been shown that at the very early stages of adsorption the metallization of the substrate is destroyed, and a shift and modification of the characteristic surface states S_1 and S_2 are also observed. However, in investigations of the spectra near the Fermi level the methods are too insensitive to observe a number of important processes, including the development of the electronic structure of the interface near saturating coverage.

We have investiged the surface photoemission for the system K/Si(111)7×7, making a simultaneous determination of both the ionization energy and the work function. We found that the metallic conductivity of the Si(111)7×7 surface is destroyed at a low, submonolayer coverage $\Theta<0.4\Theta_{\text{sat}}$. At $\Theta\sim0.5\Theta_{\text{sat}}$ a band induced by potassium adsorption was observed in the spectrum of the surface states near E_F. The development of this band stops at Θ_{sat}. It was established that, all the way up to saturating coverage, an energy gap is present in the K/Si(111)7×7 spectrum and the interface is of a semiconducting character. An insulator–metal type surface transition was observed to occur near saturating coverage. Pinning of the Fermi level $\Delta E\sim0.15$ eV relative to the valence-band top (VBT) in the bulk is observed at the same time.

The investigations were performed *in situ* under ultrahigh vacuum conditions ($P<2\times10^{-10}$ torr) at room temperature. A clean Si(111)7×7 surface (p-type sample, $\rho=10\ \Omega/\text{cm}$) was obtained by the well-known annealing procedure.[11] A standard source of atomically pure potassium was employed. The investigations were conducted by the threshold photoemission spectroscopy method with excitation by *s*- and *p*-polarized light. The angle of incidence of the light was equal to 45°. The method is based on selective excitation of photoemission from the bulk and from filled surface states; this makes it possible to study the energy spectrum of the surface bands and the position of the VBT (the ionization energy) and to ascertain the presence of a finite density of states at the Fermi level.[12,13] The experimental photoemission spectra $I_s(h\nu)$ and $I_p(h\nu)$ obtained with excitation by *s*- and *p*-polarized light, respectively, were investigated in the submonolayer adsorption regime.

Figure 1 displays the change in the thresholds $h\nu_s$ and $h\nu_p$ of the photoemission spectra $I_s(h\nu)$ and $I_p(h\nu)$, respectively, as a function of the K deposition time. It is evident that there is a pronounced difference in the behavior of the thresholds in the course of adsorption. The threshold $h\nu_s$ determines the energy position of the VBT relative to the vacuum level, i.e., it is the ionization energy ϕ.[14] It is evident from Fig. 1 (curve *1*) that the adsorption of potassium on the Si(111)7×7 surface sharply decreases ϕ to ~1.75 eV at a deposition time of ~1500 s. A further increase of coverage does not change ϕ, i.e., ϕ reaches saturation. Following Refs. 8–10, we shall define the potassium coverage corresponding to saturation as the saturating coverage and we shall designate it as Θ_{sat}.

Figure 1 (curve *2*) displays the surface photoemission threshold $h\nu_p$ as a function of submonolayer coverage. The value of $h\nu_p$ was obtained by approximating the spectrum $I_p(h\nu)$ in the energy range where there is no photoemission from the bulk and so the $I_p(h\nu)$ spectrum is formed only as a result of emission from a surface band. In this case, the threshold $h\nu_p$ is determined either by the position of the edge of the surface band of filled states in the presence of a semiconductor gap or by the position of the Fermi level in the case of metallization.[15] Three fundamentally different coverage intervals with a

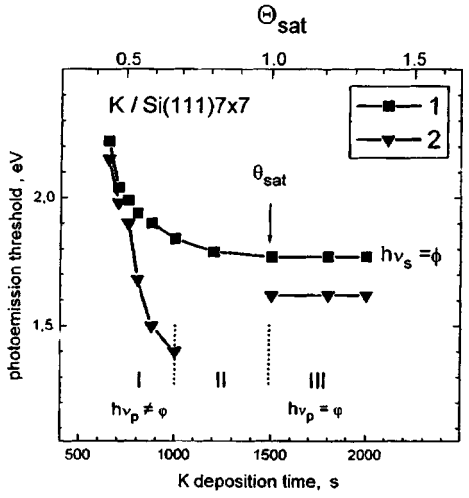

FIG. 1. Variation of the photoemission thresholds $h\nu_s$ (curve *1*) and $h\nu_p$ (curve *2*) for *s*- and *p*-polarized excitation, respectively, as a function of the potassium deposition time.

qualitatively different character of the variation of $h\nu_p$ were observed.

It was established that in the interval I there is no local density of surface states at E_F. For coverage near $0.4\Theta_{\text{sat}}$ the difference of the thresholds is small, $h\nu_s - h\nu_p \sim 0.02$ eV. This indicates that the edge of the surface band lies between E_F and the VBT but close to the VBT. Therefore, the destruction of the metallic conductivity of the Si(111) 7×7 surface, i.e., a metal–insulator transition, occurs at submonolayer coverage, less than $0.4\Theta_{\text{sat}}$. One can see that as the coverage increases to $0.7\Theta_{\text{sat}}$ the difference between the thresholds increases, reaching a maximum value of 0.45 eV. Therefore a substantial shift of the band edge in the direction of E_F is observed. However, the surface band does not cross E_F. This attests to the presence of an energy gap in the spectrum of surface states of the system K/Si(111)7×7.

In the interval II, signal instability makes it impossible to determine the position of the threshold $h\nu_p$ unequivocally. For this reason, it is impossible to establish the position of the surface-band edge in this range of coverage. For coverage ranging from $0.7\Theta_{\text{sat}}$ up to Θ_{sat} we were not able to determine whether the K/Si(111)7×7 interface is metallic or semiconducting.

In the interval III, analysis of the spectra $I_p(h\nu)$ near threshold shows that the induced surface band crosses the Fermi level. This attests to metallization of the interface.In this case, the threshold $h\nu_p$ determines the work function. Thus a transition to metallic conductivity, i.e., an insulator–metal transition, has been observed in the system K/Si(111)7×7 near saturating coverage. Further formation of the interface for $\Theta > \Theta_{\text{sat}}$ does not change the type of conductivity or the position of E_F with respect to the VBT, i.e., pinning of the Fermi level at 0.15 ± 0.01 eV occurs in the metallization process.

Figure 2 displays the surface photoemission spectra $I_p(h\nu)/I_s(h\nu)$ of the K/Si(111)

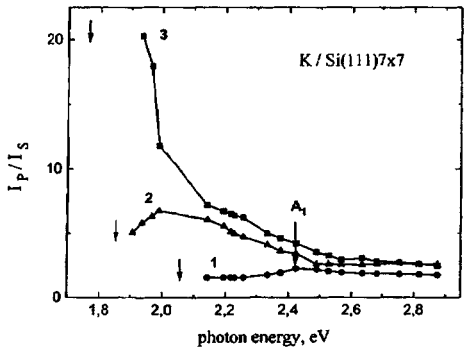

FIG. 2. Surface photoemission spectra I_p/I_s for the K/Si(111)7×7 system at different potassium coverage: Curve *1* — $\Theta = 0.5\Theta_{sat}$; *2* — $\Theta = 0.7\Theta_{sat}$; *3* — $\Theta = \Theta_{sat}$.

7×7 system for different potassium coverages. The spectra reflect the local density of surface states near the VBT.

For low coverage $\Theta \leqslant 0.5\Theta_{sat}$ a band with a maximum at $h\nu \sim 2.45$ eV, 0.45–0.50 eV below the VBT, is observed in the spectrum. The energy position and evolution of the band indicate that it is similar to the band A_1 in Ref. 10. It was shown that the band A_1 is a result of the evolution of the characteristic surface states S_1 and S_2 at the very early stages of potassium adsorption, which destroys the metallic conductivity of the Si(111) 7×7 surface. We observed that as the submonolayer K coverage increases, the density of states increases markedly and a new band induced by the adsorption of K and possessing a much lower binding energy (~ 0.2 eV) is formed. The development of the K band stops at coverage close to Θ_{sat}.

In summary, the destruction of metallic conductivity of the Si(111)7×7 surface occurs at the very early stages of K adsorption. Then, at coverages close to saturating, adsorption gives rise to interfacial metallization of a nature that is determined by the formation of a new induced K band. Therefore, two surface transitions exist in the Si(111)7×7 system: a metal–insulator transition at the very early stages of adsorption, and an insulator–metal transition in the region of saturating potassium coverage. This behavior of the K/Si(111)7×7 system can be explained from the standpoint of local interactions of adsorbed atoms with the substrate. As K is adsorbed on the Si(111)7×7 surface, in the region of low submonolayer coverage the K atoms interact with the dangling bonds of the substrate. In the process, charge becomes localized and is partially transferred from the substrate to the K atoms, which destroys the metallic conductivity of the Si(111)7×7 surface. The adsorption bond in this case is predominantly covalent. As a result, for less than saturating coverage the K/Si(111)7×7 interface is semiconducting. Near saturating coverage, in the region of an insulator–metal surface transition, the density of K atoms increases to such an extent that the direct overlapping of the valence electronic states of the K atoms becomes possible, leading to interfacial metallization. Therefore metallic conductivity is realized in the adsorbed potassium layer.

This work is supported by the Ministry of Science of the Russian Federation (grant

No. 96-2.28) as part of the program No. 012, ''Surface Atomic Structures.''

[1] J. M. Lopez-Sancho, M. C. Refolio, M. P. Lopez-Sanco, and J. Rubio, J. Vac. Sci. Technol. A **11**, 2483 (1993).
[2] J. M. Lopez-Sancho, M. C. Refolio, M. P. Lopez-Sanco, and J. Rubio, Surf. Sci. Lett. **285**, L491 (1993).
[3] F. J. Himpsel, D. E. Eastman, P. Heiman *et al.*, Phys. Rev. B **24**, 1120 (1981).
[4] J. E. Demuth, B. N. I. Persson, and A. I. Schell-Sorokin, Phys. Rev. Lett. **51**, 2214 (1983).
[5] R. J. Hamers, R. M. Tromp, and J. E. Demuth, Phys. Rev. Lett. **56**, 1972 (1986).
[6] K. Takayanagi, Y. Tanishiro, M. Takahashi *et al.*, J. Vac. Sci. Technol. A **3**, 1502 (1985).
[7] K. D. Brommer, M. Galvan, A. DalPino *et al.*, Surf. Sci. **314**, 57 (1994).
[8] K. O. Magnusson and B. Reihl, Phys. Rev. B **41**, 12071 (1990).
[9] B. Reihl, R. Dudde, and L. S. O. Wiklund, Appl. Surf. Sci. **56–58**, 123 (1992).
[10] H. H. Weitering, J. Chen, N. J. DiNardo, and E. W. Plummer, Phys. Rev. B **48**, 8119 (1993).
[11] A. Ishizaki and Y. Shiraki, J. Electrochem. Soc. **133**, 666 (1986).
[12] G. V. Benemanskaya, M. N. Lapushkin, and M. I. Urbakh, Zh. Eksp. Teor. Fiz. **102**, 1664 (1992) [Sov. Phys. JETP **75**, 899 (1992)].
[13] A. Libsch, G. V. Benemanskaja, and M. N. Lapushkin, Surf. Sci. **302**, 1303 (1994).
[14] G. V. Benemanskaya, G. E. Frank-Kamenetskaya, and M. N. Lapushkin, Surf. Sci. **331–333**, 552 (1995).
[15] G. V. Benemanskaya, D. V. Daineka, and G. E. Frank-Kamenetskaya, Surf. Rev. Lett. (1997), in press.

Translated by M. E. Alferieff

Soliton–antisoliton collisions during phase transitions in thin films of oxygen-containing polymers

E. S. Shikhovtseva and O. A. Ponomarev[a)]
Institute of the Physics of Molecules and Crystals, Ufim Science Center of the Russian Academy of Sciences, 450065 Ufa, Russia

(Submitted 5 May 1997)
Pis'ma Zh. Éksp. Teor. Fiz. **66**, No. 1, 31–36 (10 July 1997)

The dynamics of the soliton–antisoliton interaction is investigated for a system described by a perturbed sine–Gordon equation. The conditions under which a stable high-conductivity channel (soliton–antisoliton scattering without annihilation) is formed are obtained for different structures of the polymer molecule and different kinds of external perturbations. © *1997 American Institute of Physics.*
[S1063-7761(97)00713-0]

PACS numbers: 73.61.Ph, 68.55.Nq

It has now been established experimentally that the transition of thin films of some oxygen-containing polymers to a high-conductivity state[1–4] is due to the formation of thin conducting channels. A possible mechanism of the formation of such channels is proposed in Ref. 5, where it is attributed to solitonic propagation of a conducting state along a polymer molecule by means of the breaking of C–O bonds between carbon in the main molecule and oxygen in a side group and the rotation of the side group. This approach yields a stable channel even with allowance for the radiative energy losses accompanying the soliton motion and intermolecular hops of the soliton excitation.[6] Single-soliton solutions are sufficient to describe the insulator–metal transitions induced by external influences concentrated at the surface (for example, an ultralow uniaxial pressure $\sim 10^2$ Pa)[5,6] or the effect on channel formation of an external perturbation uniformly distributed over the thickness of the film (for example, a strong ac electric field with intensity $\sim 10^5 - 10^6$ V/cm).[7] However, there exist external perturbations that give rise to a rotation of a side group in an internal (not at the film boundary) fragment of the molecule. In this case a motion of excitations toward each other, specifically, soliton–antisoliton collisions, are possible. Irradiation of a film with an electron beam is an example of such an external perturbation.[8,9] Furthermore, two-soliton solutions must always be considered when describing the effect of the film boundary on channel formation. For example, when an excitation reaches the end of a channel, reflection of a soliton by the film surface and propagation of an antisoliton in the negative direction are possible. The case when reflection of an antisoliton by the boundary does not occur is also described on the basis of a doublet solution, if it is assumed that annihilation of a soliton with a virtual antisoliton occurs at the boundary, and so the soliton vanishes there. In this letter we investigate the effect of soliton–antisoliton collisions on channel formation and examine how

the character of the scattering is influenced by the energy degeneracy of the ground state of the side group, the radiative losses, and the initial conditions for the appearance of excitations.

To obtain a doublet solution we employ the Hamiltonian[6] of a quasi-one-dimensional polymer molecule with side groups:

$$H=\sum \epsilon_n a_{i,n}^{+}a_{i,n}+\frac{J_1}{2}\sum (\sin^2\varphi_{i,n}+\sin^2\varphi_{i,n+g})(a_{i,n}^{+}a_{i,n+g}+a_{i,n+g}^{+}a_{i,n})$$

$$+J_2\sum \sin^2(\varphi_{i,n+g}-\varphi_{i,n})(a_{i,n}^{+}a_{i,n+2g}+a_{i,n+2g}^{+}a_{i,n})+\sum_{i\neq j} J_{i,j}a_{i,n}^{+}a_{j,n}$$

$$+\sum \frac{(M_{i,n}^{z})^2}{2I}+\frac{U}{2}\sum (1-\cos(4\varphi_{i,n}))+\frac{A}{2}\sum (1-\cos(2\varphi_{i,n})). \qquad (1)$$

Here $a_{i,n}^{+}$ and $a_{i,n}$ are operators creating and annihilating an electron with energy ϵ_n in the nth fragment of the ith polymer strand; $\varphi_{i,n}$ is the rotation angle of the side molecule; J_1, J_2, and J_{ij} are exchange interaction parameters, described in greater detail in Ref. 6; $M_{i,n}^{z}$ is the angular momentum operator of the side group; and, I is the moment of inertia of the side molecule for rotation by an angle $\varphi_{i,n}$. The quantities U and A determine the dependence of the energy of the side molecule on its position relative to the main chain.

The value of the angle $\varphi_{i,n}$ along the chain characterizes the conductivity of the polymer molecule. A fragment of the polymer molecule is transferred from an insulating state ($\varphi_{i,n}=0$) into a conducting state ($\varphi_{i,n}=\pi/2$) by a rotation of the side group. Introducing, following Ref. 6, the radiative losses σ_1 accompanying the interaction of the side group and the main chain of its polymer molecule and the radiative losses σ_2 accompanying the interaction with neighboring molecules, we have the equation of motion for $\varphi_{i,n}$[6]:

$$\frac{d^2y}{dt_1^2}=-\sin(y)+\frac{d^2y}{dx_1^2}+\epsilon\cdot\sin(y/2)-\sigma_1(y)\left|\frac{dy}{dt_1}\right|-\sigma_2\frac{dy}{dt_1}. \qquad (2)$$

Here

$$y=4\varphi_{i,n},\quad t_1=2t(U/I)^{1/2},\quad x_1=x(2U/\beta)^{1/2},$$

$$\epsilon=-(A+\alpha)/U,\quad \sigma_1(y)=\sigma_{10}\sin(y/2),$$

$$\alpha=(J_1/2)\langle a_{i,n}^{+}a_{i,n+g}+a_{i,n+g}^{+}a_{i,n}\rangle,\quad \beta=(J_2/2)\langle a_{i,n}^{+}a_{i,n+2g}+a_{i,n+2g}^{+}a_{i,n}\rangle.$$

Analysis of the positive solutions of Eq. (2) shows[6] that as a result of the energy degeneracy of the ground state and intramolecular friction, the soliton ($y(x\to-\infty)=0$, $y(x\to+\infty)=2\pi$) is accelerated in the positive direction and the antisoliton ($y(x\to-\infty)=2\pi$, $y(x\to+\infty)=0$) is accelerated in the negative direction. The reverse is true for the negative solutions. Introducing the explicit function $\sigma_1(y)$ makes it possible to describe multisoliton (specifically, doublet) solutions. For single-soliton solutions, this gives only a renormalization of the coefficient of friction σ_1. The radiative losses due to the interaction with neighboring polymer molecules cause deceleration of any excitation in both directions.

To change the soliton–antisoliton scattering dynamics, we employ a slowly time-varying doublet solution of the perturbed sine-Gordon equation[10]

$$y=-4\arctan(\sinh\,(T)/u\,\cosh(\psi)),\quad T=\left[\int_0^{t_1}u(t')dt'+x_0(t_1)\right](1-u^2)^{(1/2)},$$

$$\psi=x_1(1-u^2)^{(-1/2)}. \tag{3}$$

Before a collision the solution (3) represents a soliton ($y(x\to-\infty)=0$, $y(x\to+\infty)=2\pi$) moving from left to right with velocity u and an antisoliton ($y(x\to-\infty)=2\pi$, $y(x\to+\infty)=0$) moving from right to left with velocity u. If the solitons do not annihilate on colliding, then after the solitons pass through each other a soliton ($y(x\to-\infty)=-2\pi$, $y(x\to+\infty)=0$) moving from left to right with velocity u and an antisoliton ($y(x\to-\infty)=0$, $y(x\to+\infty)=-2\pi$) moving from right to left with velocity u are obtained. Here $T(t_1)$ is the distance between the soliton and antisoliton. In the present representation $T<0$ before the collision, $T>0$ after the collision, and the scattering occurs at $T=0$.

On the basis of the perturbation theory developed in Ref. 10 for sine-Gordon equations, we write a system of equations for the parameters $u(T_1)$ and $T(t_2)$ appearing in solution (3):

$$\frac{du}{dt_1}=\frac{\cosh(T)(1-u^2)u^2FL}{\sinh^2(T)+u^2}-\frac{\pi\sigma_{10}}{4}u(1-u^2)\sinh\,(T)\cosh^2(T)N,$$

$$\frac{dT}{dt_1}=\frac{u}{\sqrt{1-u^2}}-\left\{8uF\left[\frac{2L}{\sinh^2(T)+u^2}M+\frac{1}{(1-u^2)\sqrt{\sinh^2(T)+u^2}}\ln\left|\frac{\sqrt{\sinh^2(T)+u^2}+\sinh(T)}{u}\right|\right]\right.$$

$$\left.-32\sigma_{10}\sinh(T)\cosh(T)[\pi MN-\sinh\,(T)Ju^5(1-u^2)^{-1}]\right\}K^{-1}. \tag{4}$$

Here

$$F=\frac{\epsilon}{2}\sinh(T)\sqrt{1-u^2}-\sigma_2u\,\cosh(T),\quad N=\frac{4u^2+\sinh^2(T)}{(u^2+\sinh(T))^{5/2}},$$

$$M=\left(\frac{Tu^2\cosh(T)}{1-u^2}-\sinh(T)\right),\quad J=\int_{-\infty}^{\infty}\frac{\cosh^2(\psi)\sinh(\psi)\psi d\psi}{(u^2\cosh^2(\psi)+\sinh^2(\psi))^3},$$

$$L=\frac{1}{u^2}+\frac{1}{2\sinh(T)\sqrt{\sinh^2(T)+u^2}}\ln\left|\frac{\sqrt{\sinh^2(T)+u^2}+\sinh(T)}{\sqrt{\sinh^2(T)+u^2}-\sinh\,(T)}\right|,$$

$$K=\frac{d}{du}\left\{\frac{16u^3\cosh^2(T)L}{\sqrt{1-u^2}(\sinh^2(T)+u^2)}\right\}.$$

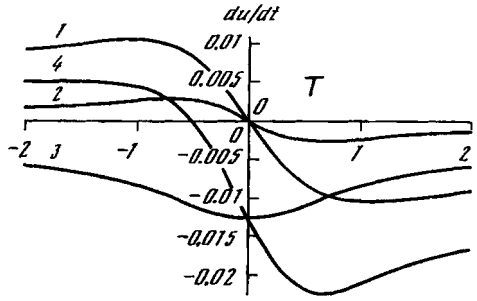

FIG. 1. Variation of the soliton and antisoliton velocities near the scattering region $T=0$ in the ''scattering without annihilation'' regime. Curve *1* describes the contribution of the energy degeneracy of the ground state of the side group, *2* — contribution of radiative losses due to intermolecular friction, *3* — contribution of intermolecular friction, *4* — resultant curve.

The character of the interaction at short distances between the soliton and antisoliton that solve Eq. (2) can be seen by examining the change in the soliton and antisoliton velocities near the scattering region $T=0$ (Fig. 1). The solution of the system (4) in the ''scattering without annihilation'' regime shows that the velocity u in the scattering region varies quite smoothly (see Fig. 2). Therefore, a qualitative picture of the variation of the velocity with time can be obtained from the first equation in system (4) under the assumption that $u=u_m$, where u_m is the average velocity with which the excitation

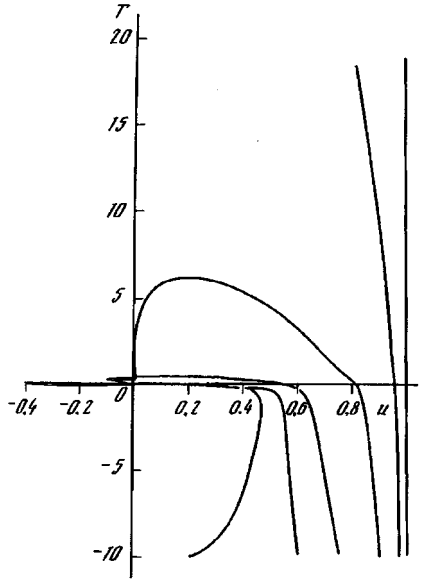

FIG. 2. Phase diagrams of the doublet solution for $\epsilon=-0.1$, $\sigma_{10}=0.01$, and $\sigma_2=0.09$ and different initial velocities $u_0=u(T_0)=0.2$, 0.6, 0.75, 0.9, 0.97, and 1.0. $T_0=-10$.

passes through the point $T=0$. The larger u_m, the smoother are the functions $du(T)/dt$. Figure 1 displays curves for $\epsilon=-0.2$, $\sigma_{10}=0.01$, $\sigma_2=0.03$, and $u_m=0.9$. It is evident from Fig. 1 that as the soliton and antisoliton approach each other ($T<0$) their velocities increase, and as they recede from each other after scattering ($T>0$) their velocities decrease, i.e., attraction occurs. But in contrast to the interaction of excitations which are solutions of the simple sine-Gordon equation, which also attract each other (at large separations the attraction potential is estimated as $\exp(-kT)$ (Ref. 11)), in the case at hand the interaction is more complicated. The resulting function $du(T)/dt$ is not symmetric about the point $T=0$. For values of ϵ and σ_{10} which are sufficiently small compared with σ_2, the resulting function $du(T)/dt$ can lie completely in the negative region, and before colliding the soliton and antisoliton repel each other. Figure 1 describes scattering without annihilation. If the doublet solution (3) is destroyed in a collision, then u^2 becomes negative and instead of the solution (3) a breather forms near $T=0$.

The solutions of system (4) for $u(t_1)$ and $T(t_1)$ completely determine the evolution of the doublet solution (3). For every ratio of σ_{10}, σ_2, and ϵ there exists a definite initial threshold velocity below which the doublet solution breaks down. It is obvious that the value of the threshold velocity decreases when intramolecular friction predominates over energy losses due to the interaction with neighboring molecules and $|\epsilon|$ is large ($\epsilon<0$ for all polymers in which the side-group position with lowest energy corresponds to the insulator state of the corresponding molecular fragment). In the case of a collision without annihilation the channel closes for only a short time (the transit time for a double soliton along a channel, which is obtained from the solution of system (4) as the time required for T to change from T_0 to $T=T_0+h$, where h is the length of the channel) and is restored after scattering. Scattering with annihilation destroys the conducting channel. Annihilation can occur without oscillations near $T=0$ (these are the curves in Fig. 2 that correspond to the initial velocities $u_0=0.2$ and 0.6) or after oscillations near $T=0$ ($u_0=0.75$). But these two cases are equivalent from the standpoint of the destruction of the conducting channel. For phase diagrams with $u_0=0.9$, 0.97, and 1.0 in Fig. 2 a collision without annihilation occurs at the point $T=0$, and the conducting channel is restored. It should be noted, however, that the double-soliton solution of Eq. (2) is less stable than the single-soliton solution. The change of the sign of the soliton and antisoliton at the moment of scattering has the effect that the acceleration is replaced by deceleration and the solution decays even after a collision at $T=0$ (the curve for $u_0=0.9$). Only the solution with $u_0=1.0$, for which $du/dt=0$, is absolutely stable. The small precollision increase in the velocity on the curve with $u_0=0.2$ is explained by the fact that for $\sigma_2>\sigma_p$ the motions of the soliton and antisoliton tend toward the equilibrium velocities $u_{s,a}=\pm[1+4(\sigma_p-\sigma_2)^2/\epsilon^2]^{-1/2}$ ($\sigma_p=\sigma_{10}\pi/4$ is the renormalized coefficient of friction; the factor $\pi/4$ appears as a result of $\sigma_1=$ const being replaced by $\sigma_1(y)$).[6] In the present example, even if the initial state made it possible to buildup to an equilibrium velocity, $|u_{s,a}|$ is still less than the threshold velocity u_* for soliton–antisoliton pair annihilation (u_* is determined by the ratio of σ_{10}, σ_2, and ϵ; annihilation occurs for $u(T=0)<u_*$). In principle, however, it is possible to have motion of soliton and antisoliton toward each other with very low initial velocities and large initial distances T_0 such that collisions will occur without destruction of the channel for $|u_{s,a}|>u_*$.

In order to use these solutions to explain experiments in which a film is irradiated

with an electron beam, the following should be noted. When a film is irradiated with a monochromatic electron beam with energy E_0, the side group obtains an excitation energy qE_0, where q is the transfer coefficient. At the same time, the energy E_s and velocity u of a soliton (antisoliton) are related as $E_s=8(1-u^2)^{1/2}$. Therefore, the soliton and antisoliton are created with the same velocities (which is necessary for scattering) and their initial velocities are determined in terms of the energy of the electron beam: $qE_0=8(1-u^2)^{-1/2}$. Channel selection occurs with respect to T_0 and u_0. The experimentally observed[9] vanishing of weakly luminescing channels and the relation between the delay time of channel formation and destruction and the beam energy are explained.[8] Another required refinement is related with the soliton–antisoliton collisions in a composite channel. One would think that an intermolecular hop of one of the excitations destroys the doublet solution, since in this case the soliton and antisoliton velocities do not change synchronously. But analysis shows (see the system (4) and Fig. 2 of Ref. 6) that the velocity relaxes quite rapidly and the doublet solution can be preserved by introducing an additional delay time. However, if an intermolecular hop of one excitation occurs with a short soliton–antisoliton distance and the time up to a collision is too short for relaxation, then the soliton and antisoliton meet with different velocities. Therefore, they do not interact and channel destruction does not occur.

In summary, we have obtained a doublet solution of the perturbed sine–Gordon equation describing a quasi-one-dimensional polymer molecule with a side group with an energy-degenerate ground state. We have investigated the conditions for soliton–antisoliton scattering without destruction and for scattering with annihilation of a soliton–soliton pair, i.e., regimes in which the conducting channel is preserved and destroyed.

[a)]e-mail: igor@physics.bash.ru

[1] N. S. Enikolopyan, L. N. Grigorov, and S. G. Smirnova, JETP Lett. **49**, 371 (1989).
[2] O. V. Demicheva, S. G. Smirnova, V. M. Andreev, and L. N. Grigorov, Vyskomolekulyarnye Soedineniya **32**(B), 3 (1990).
[3] V. N. Arkhangorodskiĭ, E. G. Guk, A. M. El'yashevich *et al.*, Dokl. Akad. Nauk SSSR **309**, 603 (1989) [Sov. Phys. Dokl. **34**, 1016 (1989)].
[4] A. N. Lachinov, A. Yu. Zherebov, and V. M. Ḳornilov, JETP Lett. **52**, 103 (1990).
[5] O. A. Ponomarev and E. S. Shikhovtseva, Zh. Éksp. Teor. Fiz. **107**, 637 (1995) [JETP **80**, 346 (1995)].
[6] E. S. Shikhovtseva and O. A. Ponomarev, JETP Lett. **64**, 509 (1995).
[7] E. S. Shikhovtseva and O. A. Ponomarev, Physica A **231**, 484 (1995).
[8] V. M. Kornilov and A. N. Lachinov, JETP Lett. **61**, 520 (1995).
[9] V. M. Kornilov and A. N. Lachinov, Pis'ma Zh. Tekh. Fiz. **20**(14), 13 (1994) [Tech. Phys. Lett. **20**, 567 (1994)].
[10] D. W. McLayghlin and A. C. Scott, Phys. Rev. A **18**, 1652 (1978).
[11] R. Rajaraman, Phys. Rev. D **15**, 2866 (1977).

Translated by M. E. Alferieff

Isotope effect in the vibrational spectra of water measured in experiments with a scanning tunneling microscope

M. V. Grishin, F. I. Dalidchik, S. A. Kovalevskiĭ, N. N. Kolchenko, and B. R. Shub

N. N. Semenov Institute of Chemical Physics, Russian Academy of Sciences, 117977 Moscow, Russia

(Submitted 17 April 1997; resubmitted 20 May 1997)
Pis'ma Zh. Éksp. Teor. Fiz. **66**, No. 1, 37–39 (10 July 1997)

The vibrational frequencies of adsorbed H_2O and D_2O molecules are measured under high-vacuum conditions by in-cavity scanning tunneling spectroscopy. An isotope effect is observed. © *1997 American Institute of Physics.* [S1063-7761(97)00813-5]

PACS numbers: 33.20.Tp

The fundamental processes of heterogeneous catalysis — adsorption and desorption, surface migration, and chemical reactions — have been investigated for many years by many methods (optical and corpuscular, beam and kinetic). These methods have a common drawback: They give only averaged information pertaining to macroscopic ensembles of particles. This is inadequate for constructing the physical foundations of heterogeneous catalysis. Under real conditions, many different heterogeneous complexes with different structures and properties coexist on the surface of a catalyst.[1] Qualitatively new information, structural and dynamic, obtained with a spatial resolution of the order of atomic dimensions is required. This can be done only by methods which employ a scanning tunneling microscope (STM).

The possibilities of the standard methods of scanning tunneling microscopy (and spectroscopy) in the solution of problems of heterogeneous catalysis, including adsorption, have been described, for example, in the reviews cited as Refs. 2–4. These methods are based on elastic electron tunneling processes, whose probabilities are determined by the spatial and energy distributions of the electron density of the surface and tip. The lack of reliable information about the geometry and electronic structure of the tip and the difficulty of solving inverse problems in the theory of STM substantially limit the analytical possibilities of the well-known STM methods (especially for systems which do not exhibit spatial symmetry). The problem of identifying the particles observed in a STM is central in modern ''atomic-resolution'' chemistry.[2–4] Here, new approaches which make it possible to study with the aid of a STM the effects of inelastic electron tunneling accompanied by the excitation of the vibrational degrees of freedom of the adsorbed particles, are required. In macroscopic systems (metal–insulator–metal junctions) these effects are well known[5] and are widely used for studying the adsorption of molecules on metal oxides. Inelastic tunneling effects have still not been observed in experiments with a STM, though estimates show that under resonance tunneling conditions vibrational transitions of adsorbed particles can substantially change the current and conductivity of

STM nanocontacts (by up to 10%).[6] The difficulties of searching for systems with optimal inelastic resonance tunneling conditions, a theory of which has been constructed in Ref. 7 ($|E_F - E^0| \leqslant \Gamma$, $\Gamma \leqslant \omega$, $\alpha > 1$, E_F is the Fermi level, E^0 is the energy of the resonance level, Γ is the reciprocal of the lifetime of a resonant electronic–vibrational complex, ω is the vibrational frequency, and α is the electronic–vibrational coupling parameter), can be overcome by using a STM operating in the field-emission mode.[8,9] For voltages such that $eV > \phi$ ($\phi \sim 5$ eV is the work function) an electronic nanocavity, in which the adsorbed particle under investigation may be located, forms in the tunneling gap.[10] Electron transitions from the tip into the cavity and from the cavity into the sample change the force field in which the adsorbed particle vibrates and induce transitions (including multiquantum transitions), which are manifested experimentally as resonance features of the STM currents (and conductivities). In Ref. 11, electronic–vibrational series of field-emission resonances corresponding to vibrational transitions of TiO_2 were observed by the ''in-cavity scanning tunneling spectroscopy'' method in air.

This letter reports the results of high-vacuum experiments in which these methods were used to measure the vibrational frequencies of H_2O and D_2O molecules adsorbed on a naturally oxidized titanium surface. The isotope effect, which the results presented below demonstrate, leaves no doubt that the observed resonance maxima correspond to vibrational transitions of water.

The experiments were performed on an Omicron STM by scanning a platinum tip over a titanium surface oxidized in air and placed in a high vacuum ($\sim 10^{-9}$ torr). The procedure for performing the spectroscopic and topographic measurements is described in Ref. 11. The procedure for preparing the surfaces for the measurements included heating a sample (to 550 K) and holding it in a high vacuum, followed by exposure to water vapor at pressure $P \sim 10^{-6}$ torr. After the sample was heated for 2 h and held for a long time in a high vacuum, the current–voltage characteristics which we measured for most points of the surface contained only weakly expressed series of resonances with vibrational frequencies corresponding to titanium oxide (see Fig. 1, curve a). Subsequent exposure to water vapor ($T \approx 300$ K) produced large changes in the spectra. At many points of the surface, the spectra obtained 100 s after exposure possessed the form displayed in Fig. 1 (curve b, negative tip). Resonance maxima corresponding to single-quantum ($\omega_1 \approx e(V_3 - V_1) \approx 0.5$ eV, $\omega_2 \approx e(V_2 - V_1) \approx 0.2$ eV), two-quantum ($\omega_3 \approx e(V_5 - V_1) \approx 2\omega_1$), and combination ($\omega_4 \approx e(V_4 - V_1) \approx \omega_1 + \omega_2$) vibrational transitions (n enumerates the resonances presented in the figure and V_n are the corresponding values of the voltage) are clearly seen in this figure. The small maxima between the first and second (and also third and fourth) resonances in the curve b apparently correspond to vibrations of the TiO bond ($\omega \approx 0.1$ eV). Our measured values of the frequencies ω_1 and ω_2 are close to the known (from IR experiments) values of the frequencies of stretching and deformation vibrations of H_2O molecules ($\omega_1^{IR} = 0.46$ eV, $\omega_2^{IR} = 0.20$ eV) adsorbed on a titanium oxide surface.[12] The regions where type-b spectra were observed possessed an island structure with islands ranging in size from 10 to 50 nm (which is characteristic for adsorption of water on polycrystalline surfaces). It is natural to assume that these islands are formed by adsorbed water molecules. Similar spectra (see Fig. 1, curve c) with frequencies $\omega_1(D_2O) \approx 0.35$ eV and $\omega_2(D_2O) \approx 0.15$ eV were obtained in control experiments with deuterated water (D_2O). To within an accuracy of the order of 10%,

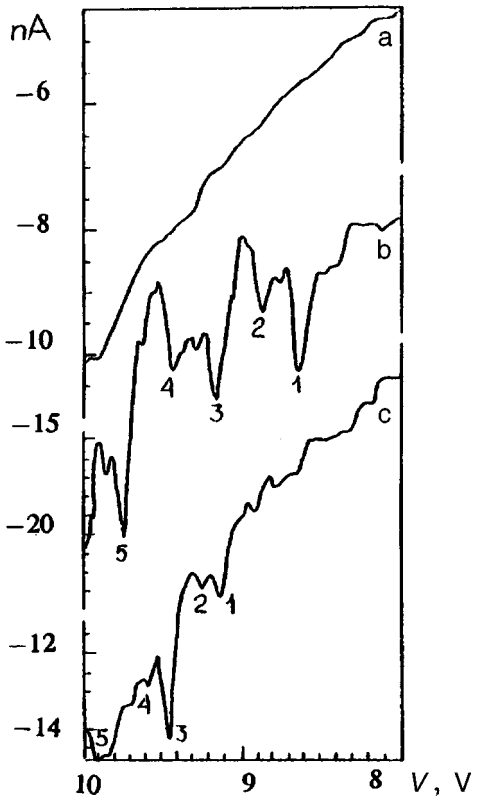

FIG. 1. Vibrational series of STM field-emission resonances for water molecules adsorbed on a naturally oxidized titanium surface (curve b — H_2O molecules, curve c — D_2O molecules). Curve a — current–voltage characteristic of the STM scanning a titanium surface with no water molecules.

these frequencies correspond to the expected isotope effect ($\omega(H_2O)/\omega(D_2O) \approx \sqrt{2}$).

This work was supported by the Russian Fund for Fundamental Research (Project No. 96-03-34129).

[1] O. V. Krylov and B. R. Shub, *Nonequilibrium Processes in Catalysis* [in Russian], Khimiya, Moscow, 1990.
[2] H.-J. Günterrodt and R.Wiesendanger (Eds.), *Scanning Tunnelling Microscopy I*, Springer Series in Surface Science, Vol. 20, Springer-Verlag, New York, 1992; *Scanning Tunnelling Microscopy* II, Springer Series in Surface Science, Vol. 28, Springer-Verlag, New York, 1992.
[3] Ph. Avoris, J. Chem. Phys. **94**, 2246 (1990).
[4] R. J. Hamers, Annu. Rev. Phys. Chem. **40**, 531 (1989).
[5] J. Lambe and R. C. Jaklevic, *Tunnelling Phenomena in Solids*, Plenum Press, New York, 1969.
[6] B. N. J. Persson and A. Baratoff, Phys. Rev. Lett. **59**, 339 (1987).
[7] F. I. Dalidchik, Zh. Éksp. Teor. Fiz. **87**, 1384 (1984) [Sov. Phys. JETP **60**, 795 (1984)].
[8] F. I. Dalidchik, M. V. Grishin, N. N. Kolchenko, and S. A. Kovalevskii, in *Abstracts of the 43rd International Field Emission Symposium*, Moscow, Russia, July 14-19, 1996, abstract P-25.
[9] F. I. Dalidchik, M. V. Grishin, S. A. Kovalevskii, and N. N. Kolchenko, Surf. Sci. (1997), in press.
[10] R. C. Becker, I. A. Golovchenko, and B. S. Swartzentruller, Phys. Rev. Lett. **55**, 987 (1985).

[11] F. I. Dalidchik, M. V. Grishin, S. A. Kovalevskiĭ, and N. N. Kolchenko, JETP Lett. **65**, 325 (1997).
[12] V. F. Kiselev and O. V. Krylov, *Adsorption Processes on Semiconductor and Dielectric Surfaces* [in Russian], Nauka, Moscow, 1978.

Translated by M. E. Alferieff

Dynamic conductivity of interacting electrons in open mesoscopic structures

V. A. Sablikov[a)] and B. S. Shchamkhalova
Institute of Radio Engineering and Electronics, Russian Academy of Sciences, 141120 Fryazino, Moscow Region, Russia

(Submitted 22 May 1997)
Pis'ma Zh. Éksp. Teor. Fiz. **66**, No. 1, 40–44 (10 July 1997)

It is shown that in one-dimensional mesoscopic structures the electron–electron interaction leads to qualitatively new effects in the dynamic conductivity which are best manifested in the frequency dependence of the impedance. Interelectronic repulsion increases the resistance and narrows the resonance dips of the resistance at transit frequencies. Interelectronic attraction gives rise to resonance peaks of the resistance against a high-conductivity background. These effects are due to the reflection of bosonic excitations of a Luttinger liquid from the boundaries of a quantum channel with current-lead electrodes and to resonances of these excitations over the length of the channel. © *1997 American Institute of Physics.* [S1063-7761(97)00913-X]

PACS numbers: 73.23.Ps

1. It is now generally recognized that the electron–electron interaction plays a fundamentally important role in electron transport in mesoscopic structures. It is sufficient to mention the Coulomb blockade arising in low-conductivity (compared with e^2/h) nanostructures. This letter is devoted to mesoscopic systems with high conductivity (of the order of e^2/h). Examples of such systems are a quantum wire connecting two electronic reservoirs under ballistic electron transport conditions, quantum point contacts, and edge states in the quantum Hall effect. In these systems (called open[1]) a Coulomb blockade is not observed but the electron–electron interaction is also very important. It leads to a strong correlation in the motion of the electrons, as a result of which the idea of a Fermi liquid becomes invalid. In this case the behavior of one-dimensional systems is described in the Luttinger liquid approximation[2,3] with acoustic-type bosonic elementary excitations. The velocity of these excitations is determined by the parameter K, which depends on the interaction; specifically, $v=v_F/K$, where v_F is the Fermi velocity. In the absence of interaction $K=1$; if the interaction is repulsive, then $K<1$; and, in the case of interelectronic attraction $K>1$. It has been shown in a number of works (see, for example, Refs. 4 and 5) that in the Luttinger-liquid model the interelectronic interaction should lead to a renormalization of the conductivity: The conductivity for a single state equals Ke^2/h. However, an experiment[6] performed on quantum wires in GaAs does not support this conclusion. The conflict was resolved in Refs. 7–9. The point is that the linear conductivity of a quantum wire in the ballistic electron transport regime is determined by contacts with the current-lead electrodes.[7] The interelectronic interaction does not play a large role in the regions serving as electrodes to the wire. Since there is no scattering

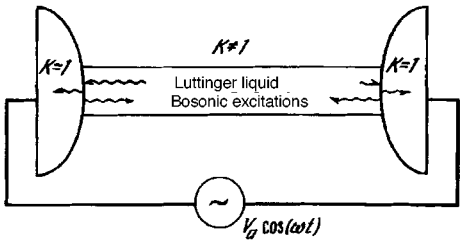

FIG. 1. Mesoscopic structure with a quantum wire. The wavy lines depict the propagation of bosonic excitations generated by an ac electric field.

inside the wire, the momentum flux in it is conserved. Therefore the electron–electron interaction does not change the conductivity much, which raises the question of whether or not it is possible to observe a Luttinger liquid in these mesoscopic systems.

We wish to call attention to the fact that the conclusion drawn above concerns only the steady-state conductivity in a linear regime. In a nonstationary regime, the current response measured in an external (with respect to the mesoscopic system under study) circuit depends on the charge distribution inside this system.[1] Therefore, the dynamic current response of a mesoscopic structure with a quantum wire is largely determined by electron transport in the quantum wire, and features characteristic of a Luttinger liquid should be manifested in it. To study these features, this letter examines the dynamic conductivity of an open mesoscopic system in the Luttinger-liquid model.

2. Let us consider a mesoscopic system in the form of a quantum channel connecting two electron reservoirs to which a low-amplitude ac voltage is applied (Fig. 1). The electrons in the high-conductivity reservoirs can be regarded as free, while in the quantum channel the electron–electron interaction is important. Following the approach of Refs. 7–9, we shall consider the entire system to be a nonuniform Luttinger liquid. In the reservoirs ($x<-L/2$ and $x>L/2$) one has $K=1$ and $v=v_{F0}$, while in the channel ($-L/2<x<L/2$) $K\neq 1$ and $v=v_F/K$.

The approach based on the Luttinger-liquid model permits describing low-energy excitations in a one-dimensional gas of interacting electrons by means of a bosonic phase field $\Phi(x,t)$.[2,3] To clarify the characteristic features of the dynamic conductivity which are associated with the electron–electron interaction, we shall employ the simplest variant of the theory, in which the electron–electron interaction is considered to be short-ranged, transfer processes are neglected, and spin effects are ignored. These assumptions are justified for a one-dimensional electron gas in semiconductor nanostructures. In this case, the bosonized Hamiltonian of the interacting electrons has the form

$$H_0=\frac{1}{8\pi}\int_{-L/2}^{L/2}dx\ v\left[\frac{1}{K}\left(\frac{\partial\Phi}{\partial x}\right)^2+K\pi^2\Pi^2\right],$$

where Π is the generalized momentum conjugate to Φ. The interaction parameter K can be estimated as

$$K=(1+U/2\varepsilon_F)^{-1/2},$$

where U is the interaction potential for neighboring electrons and ε_F is the Fermi energy.

The charge density $\rho(x,t)$ and the electronic current $j(x,t)$ are expressed in terms of $\Phi(x,t)$ as

$$\rho(x,t)=-\frac{e}{2\pi}\frac{\partial\Phi}{\partial x},\quad j(x,t)=\frac{e}{2\pi}\frac{\partial\Phi}{\partial t}. \tag{1}$$

The equation of motion for the bosonic field $\Phi(x,t)$ in the presence of an external electric field $E(x,t)$ has the form

$$\frac{\partial}{\partial t}\left(\frac{1}{Kv}\frac{\partial\Phi}{\partial t}\right)-\frac{\partial}{\partial x}\left(\frac{v}{K}\frac{\partial\Phi}{\partial x}\right)=2eE(x,t). \tag{2}$$

The field $\Phi(x,t)$ and $(v/K)(\partial\Phi(x,t)/\partial x)$ must be continuous at the limits $x=\pm L/2$.

3. To solve Eq. (2), we assume that there is no field $E(x,t)$ in the electrodes and that $E(x,t)=E(x)\exp(-i\omega t)$ in the channel. The field $E(x)$ in the channel is determined by the charge induced on the surfaces of the current-lead electrodes (assuming ideal conductors) and in the channel by the external voltage source. If the electrodes are massive formations (compared with the size of the channel), then the surface charges dominate and the field $E(x)$ produced by them is determined by the geometry of the electrodes. Equation (2) can be solved for any function $E(x)$, but for concreteness we shall present below the results for the case when $E(x)=$ const, which corresponds to a plane–parallel electrode geometry in a region of the order of L in size.[b)]

Inside the quantum channel $(-L/2<x<L/2)$ the solution has the form

$$\langle\Phi(x,t)\rangle=\frac{2evKE}{\omega^2}\left[-1+\frac{K\cos(qx)}{K\cos(qL/2)-i\sin(qL/2)}\right]e^{-i\omega t}, \tag{3}$$

where $q=\omega/v$. Outside the channel

$$\langle\Phi(x,t)\rangle=i\frac{2evKE}{\omega^2}\frac{\sin(qL/2)}{K\cos(qL/2)-i\sin(qL/2)}e^{i[q_0(\mp x-L/2)-\omega t]}, \tag{4}$$

where $q_0=\omega/v_{F0}$, the upper sign corresponds to $x<-L/2$, and the lower sign corresponds to $x>L/2$.

The current in the external circuit, from which the conductivity is determined, is the sum of the current flowing through the channel

$$j=\frac{1}{V_a}\int_{-L/2}^{L/2}dx\;E(x)\langle j(x,t)\rangle \tag{5}$$

and the displacement current through the interelectrode capacitance. In what follows we shall consider only the conductivity due to the channel.

Using Eqs. (5), (3), and (1), we find the admittance

$$Y(\omega)=\frac{2e^2K}{hqL}\left[i+\frac{1-r}{qL}\frac{1-e^{iqL}}{1-re^{iqL}}\right],$$

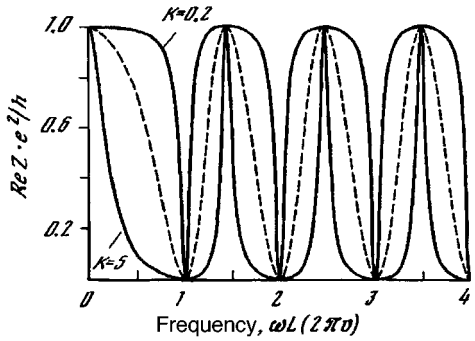

FIG. 2. Frequency dependence of ReZ for a repulsive electron–electron interaction ($K=0.2$), for an attractive interelectronic attraction ($K=5$), and in the absence of an interaction (dashed line).

where $r=(1-K)/(1+K)$ is the reflection coefficient for bosonic excitations at the contacts of the channel with the electrodes at the points $x=\pm L/2$.

In the limit $\omega\to 0$, the admittance approaches the interaction-independent value $Y_0=e^2/h$; this corresponds to Refs. 7–9. However, the electron–electron interaction becomes important in the dynamic regime. It is especially strongly manifested in the frequency dependence of the impedance $Z(\omega)=1/Y(\omega)$.

The frequency dependence of the real part of the impedance is shown in Fig. 2 for three values of the interaction parameter K. In the absence of an electron–electron interaction ($K=1$), the result is identical to the calculation performed in Ref. 10 by means of a direct solution of the single-electron Schrödinger equation.

In all cases ReZ is oscillatory, vanishing at the resonance frequencies $\omega_n=2\pi nv/L$ ($n=1, 2, \ldots$) determined by the time of flight of the electrons through the channel with the interaction-renormalized velocity $v=v_F/K$. We call attention to the fact that in Fig. 2 the normalization of the frequency depends on K, i.e., it is different for different curves and is chosen so that the dimensionless resonance frequencies would coincide. This representation of the plots shows well the effect of the electron–electron interaction on the frequency dependence of ReZ. Interelectronic repulsion increases the resistance and narrows the resonances at which the resistance decreases. Conversely, interelectronic attraction decreases the resistance and broadens the resonances, causing resistance peaks to appear at the frequencies $\sim 2\pi(n+1/2)v/L$. It is interesting that the value of ReZ at these frequencies does not depend on the interaction and equals h/e^2.

The influence of the electron–electron interaction on the frequency dependence of the impedance is due to the reflection of bosonic excitations, generated by the electric field in the channel, from the channel–electrode boundaries. Charge waves appear in the channel under the action of an ac electric field. They also exist in the absence of an electron–electron interaction,[10] but in this case bosonic excitations are not reflected from the boundaries. The interaction of the electrons (more accurately speaking, the spatial nonuniformity of the interaction parameter K) leads to a reflection of the waves of the bosonic field from the boundaries and interference of the waves in the quantum channel,

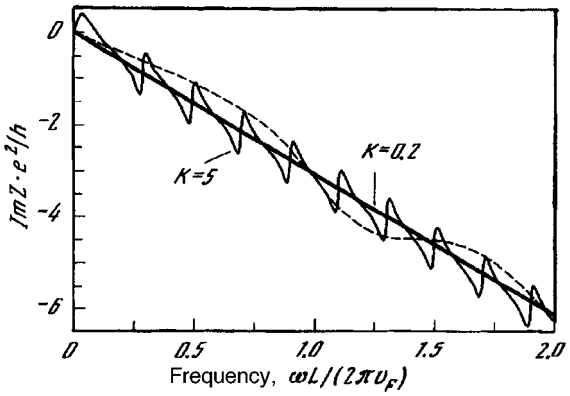

FIG. 3. Frequency dependence of ImZ for a repulsive electron–electron interaction ($K=0.2$), for an attractive interelectronic attraction ($K=5$), and in the absence of an interaction (dashed curve). The frequency is normalized to the time of flight of electrons with the Fermi velocity, which is the same for all curves.

as a result of which the charge density and current change. The charge density in the channel equals

$$\langle \rho(x,t) \rangle = \frac{eKE}{\pi\omega} \frac{K \sin(qx)}{K \cos(qL/2) - i \sin(qL/2)} e^{-i\omega t}. \tag{6}$$

As one can see from this expression, an interelectronic repulsion ($K<1$) decreases ρ and the current, while an interelectronic attraction produces the opposite effect.

Under resonance conditions an integral number of charge waves fit into the channel. As one can see from Eqs. (3) and (4), in this case $\Phi(x,t)$ and the charge density are concentrated only in the channel, and $\Phi=0$ outside the channel. The electron transport current through the boundary of the channel with the contacts equals zero. The charge density is redistributed in time only inside the channel, and since dissipation in the channel was neglected in our calculation, ReY and ReZ vanish under resonance conditions.

With the exception of a small region of low frequencies where Im$Z>0$ for $K>1$, the imaginary part of the impedance is practically always negative. The frequency dependences of ImZ for different cases of the electron–electron interaction are shown in Fig. 3.

A negative sign of ImZ signifies that the current lags the applied voltage in phase and that the reactive component of the impedance is inductive. It is interesting that in the case of a repulsive interaction ImZ is approximately proportional to the frequency, so that the effective inductance is frequency-independent:

$$L_{\text{eff}} = hL/2e^2 v_F .$$

The phase delay of the current is evidently due to the lag of the electron transport in the channel.

Mesoscopic structures with quantum wires in semiconductors are of interest for the experimental investigation of the electron–electron interaction, since ε_F and correspondingly the interaction parameter K can be measured with a field-effect electrode. Variations of K can be observed in the frequency dependences of the impedance.

This work was supported by the Russian Fund for Fundamental Research (Grant No. 96-02-18276) and the Interdisciplinary Science and Technology Program ''Physics of Solid-State Nanostructures'' (Grant No. 97-1054).

[a)]e-mail: vas199@ire216.msk.su

[b)]The question of the effect of a nonuniformity of the field on the dynamic conductivity of noninteracting electrodes was studied in Ref. 10.

[1]M. Büttiker and T. Christen, in *Quantum Transport in Semiconductor Submicron Structures*, edited by B. Kramer, NATO ASI Series, **326**, 263 (1996).
[2]F. D. M. Haldane, J. Phys. C **14**, 2585 (1981).
[3]J. Voit, Rep. Prog. Phys. **58**, 977 (1995).
[4]W. Apel and T. M. Rice, Phys. Rev. B **26**, 7063 (1982).
[5]C. L. Kane and M. P. A. Fisher, Phys. Rev. B **45**, 15 233 (1992).
[6]S. Tarucha, T. Honda, and T. Saku, Solid State Commun. **94**, 413 (1995).
[7]D. I. Maslov and M. Stone, Phys. Rev. B **52**, R5539 (1995).
[8]V. V. Ponomarenko, Phys. Rev. B **52**, R8666 (1995).
[9]I. Safi and H. J. Schulz, Phys. Rev. B **52**, R17040 (1995).
[10]V. A. Sablikov and E. V. Chenskiĭ, JETP Lett. **60**, 410 (1994).

Translated by M. E. Alferieff

Splitting of transverse optical phonon modes localized in GaAs quantum wires on a faceted (311)A surface

V. A. Volodin,[a)] M. D. Efremov, V. Ya. Prints, V. V. Preobrazhenskiĭ, B. R. Semyagin, and A. O. Govorov

Institute of Semiconductor Physics, Siberian Branch of the Russian Academy of Sciences, 630090 Novosibirsk, Russia

(Submitted 27 May 1997)
Pis'ma Zh. Éksp. Teor. Fiz. **66**, No. 1, 45–48 (10 July 1997)

The energy splitting of fundamental localized transverse optical (TO1) phonon modes in GaAs/AlAs superlattices and quantum wires grown by molecular-beam epitaxy on a faceted (311)A GaAs surface is observed by Raman spectroscopy. The form of the Raman scattering tensor makes it possible to observe the TO_x and TO_y modes separately, using different scattering geometries (the y and x axes are the directions of displacement of the atoms and are directed parallel and transverse to the facets on the (311)A surface). Enhancement of the splitting of the $TO1_x$ and $TO1_y$ modes is observed as the average thickness of the GaAs layers is decreased from 21 to 8.5 Å. The splitting is probably due to the effect of the corrugation of the GaAs/AlAs (311)A heterointerface on the properties of localized phonon modes. © *1997 American Institute of Physics.* [S1063-7761(97)01013-5]

PACS numbers: 73.61.Ey, 73.20.Dx, 63.22.+m

A topical problem in modern solid-state physics is the production and study of nanometer-size one- and zero-dimensional quantum objects (quantum wires and dots). On account of the limitations of modern lithography there is great interest in using the properties of self-organizing systems to obtain nanometer objects with reproducible shape and size in a planar direction. For this, the faceting of high-index GaAs surfaces is a promising direction. Faceting of a (311)A GaAs surface (appearance on it of a periodic array of microfacets in the (233) direction with period 32 Å in the (011) direction) was observed[1–3] at the beginning of the 1990s and has been confirmed by many authors.[4–8] According to the data obtained by different authors, the microfacets are 10.2 Å (Refs. 1–3) or 3.4 Å (Refs. 5 and 6) high. This letter focuses mainly on the properties of transverse optical phonons in thin GaAs layers with a corrugated heterointerface and in a periodic array of phonon-isolated GaAs quantum wires. Analysis of the frequencies of localized optical phonons can supplement existing published data on the structure of microfacets on a (311)A GaAs surface. The production of a periodic array of quantum wires by joining of microfacets during heteroepitaxial growth of ultrathin layers by molecular beam epitaxy presupposes the appearance of anisotropy of the properties of the electronic and phonon subsystems in this system. The characteristic features of the electronic spectrum and carrier transport in such structures have been studied both theoretically and experimentally. Specifically, conductivity anisotropy in directions parallel and

transverse to the facets, which persists all the way up to a temperature of 500 K, has been observed in them.[9] The properties of phonons in superlattices on a (311)A surface were investigated in Refs. 10–13. However, a detailed investigation was performed mainly for relatively thick GaAs and AlAs layers (16 and more monolayers),[10–12] while the strongest manifestation of the anisotropy of phonon properties should occur in the case when the thicknesses of the layers are comparable to the height of the microfacets. In the present work we attempted to use the polarization of transverse phonons in directions parallel and transverse to quantum wires to observe the splitting of these modes in the case of an additional planar symmetry due to the formation of an array of quantum wires.

The experimental structures were grown by molecular beam epitaxy on semi-insulating GaAs (311)A substrates. The lateral superlattices consisted of periodically repeating thickness-modulated (corrugated) GaAs and AlAs layers. The modulation period corresponds to the period of the microfacets (32 Å) and the modulation amplitude corresponds to the depth of the microfacets. The average thickness of the AlAs layers for all samples was equal to 27 Å. The average thicknesses d_{GaAs} of the GaAs layers in a series of five samples was equal to 21, 18, 15, 11.3, and 8.5 Å. It should be noted that for the last two samples the average thickness of the GaAs layers is almost the same or even less than the height of the microfacets of the GaAs/AlAs heterointerface in one of the models (10.2 Å),[1–3] i.e., in this case the facets of neighboring AlAs layers probably touched during the growth process and GaAs formed not a continuous corrugated layer but rather a periodic array of isolated quantum wires. Each lateral superlattice contained 75 periods and was covered with a protective GaAs layer. The experimental structures are described in greater detail in Ref. 13. The Raman scattering spectra (RSS) were recorded in a quasi-backscattering geometry at room temperature using a spectrometer based on a DFS-52 double monochromator and an argon laser operating in the 488 nm mode.

The RSS tensors for transverse optical phonons with different polarization in the case of backscattering from the (311) surface have the form[12]

$$\mathrm{TO}_x - \frac{1}{\sqrt{2}}\begin{pmatrix} 0 & -d & d \\ -d & 0 & 0 \\ d & 0 & 0 \end{pmatrix}, \quad \mathrm{TO}_y - \frac{1}{\sqrt{2}}\begin{pmatrix} 0 & 3d & 3d \\ 3d & 0 & -2d \\ 3d & -2d & 0 \end{pmatrix}.$$

The TO_x and TO_y modes correspond to phonon polarization with the atoms undergoing displacements in the X $(00\overline{1})$ and Y $(\overline{2}\,\overline{2}3)$ directions, i.e., transverse and parallel to the facets, respectively; the Z axis is directed along the (311) direction. According to the symmetry selection rules, the Raman scattering intensity is proportional to the squared product of the polarization vector of the incident light, the RSS tensor, and the polarization vector of the scattered light. The incident or scattered light was polarized along the vectors $x-(1/\sqrt{2})\,(00\overline{1})$ and $y-(1/\sqrt{22})\,(\overline{2}\,\overline{2}3)$. Therefore, in the $Z(YY)\overline{Z}$ geometry (the axes outside the parentheses indicate the direction of the momentum and the axes enclosed in parentheses the direction of the polarization of the incident and scattered photon) the Raman-scattering intensity in the TO_y mode is proportional to $(54/11\sqrt{22})^2 d^2$ and scattering in the TO_x mode is forbidden, and in the $Z(YX)\overline{Z}$ geometry the Raman scattering intensity in the TO_x mode is proportional to $(2/11)d^2$ and scattering in the TO_y mode is forbidden,[12] i.e., these two different modes are observed in

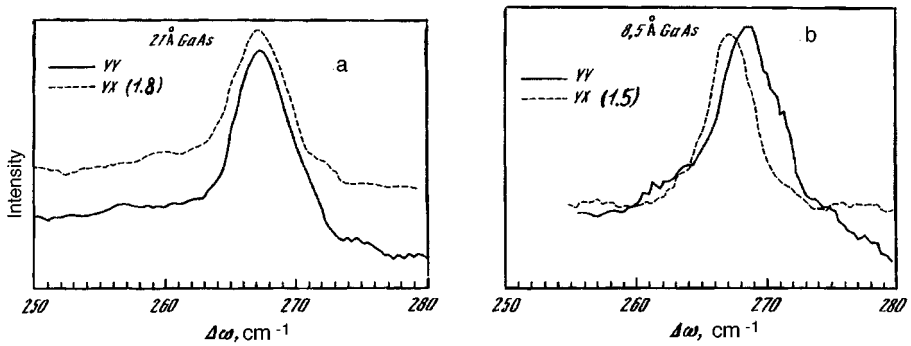

FIG. 1. Raman scattering spectra in the geometries $Z(YY)\overline{Z}$ (solid line) and $Z(YX)\overline{Z}$ (dashed line) for samples with $d_{\mathrm{GaAs}}=21$ Å (a) and 8.5 Å (b).

two different geometries and they can therefore be resolved, to a high degree of accuracy, according to the position of the corresponding Raman peaks in the spectrum.

Figure 1 displays the spectra of Raman scattering by transverse optical modes localized in GaAs for samples with adjacent GaAs layers 21 and 8.5 Å thick in different scattering geometries. It is clearly seen that there is almost no splitting of the fundamental localized $\mathrm{TO1}_y$ and $\mathrm{TO1}_x$ modes for the sample with $d_{\mathrm{GaAs}}=21$ Å (Fig. 1a), while a large splitting of these modes is observed for the sample with $d_{\mathrm{GaAs}}=8.5$ Å (Fig. 1b). It should also be noted that the intensities of the peaks due to Raman scattering by the TO_y and TO_x modes differ by a factor of 1.8 for superlattices with $d_{\mathrm{GaAs}}=21$ Å. This ratio decreases as the GaAs layers decrease in thickness and equals 1.5 for a superlattice with ultrathin GaAs layers ($d_{\mathrm{GaAs}}=8.5$ Å), while for bulk GaAs these peaks should differ in intensity by approximately a factor of 6, as was in fact observed for Raman scattering from a GaAs (311)A substrate. Apparently, the change in the ratio of the Raman scattering intensities for the TO_y and TO_x modes for lateral superlattices is due to a change in the ratio of the total projections of the polarizable GaAs bonds in directions parallel and transverse to the facets as a result of modulation of the thickness of the layer along one of the directions — (001).

The position of each peak corresponding to Raman scattering by different fundamental localized transverse optical modes was determined by approximating the experimental spectra by a Gaussian curve and minimizing the standard deviation. The corresponding vibrational frequency was determined to an accuracy of approximately 0.2 cm^{-1}. The data on the frequency splitting of the TO1 modes with different polarization are displayed in Fig. 2 for all experimental samples. One can see that the splitting of the two different TO1 modes increases with decreasing average thickness of the GaAs layers, the frequency of the $\mathrm{TO1}_y$ mode (in which the atoms vibrate in a direction along the quantum wires) being higher than that of the $\mathrm{TO1}_x$ mode (in which the atoms move in a direction transverse to the quantum wires). This effect is probably due to the corrugation of the heterointerface and not to the mixing of the TO modes with longitudinal modes as a result of the low symmetry of the (311) direction, since in this case, according to

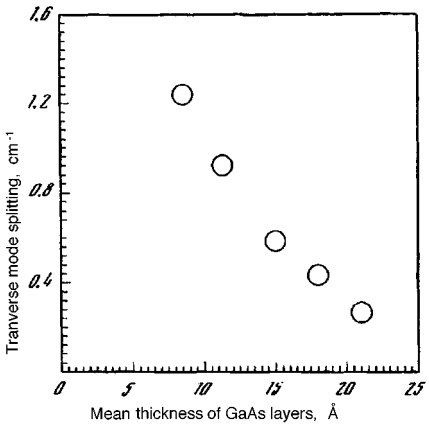

FIG. 2. Frequency splitting of the $TO1_y$ (the atoms move in a direction parallel to the microfacets) and $TO1_x$ (the atoms move in a direction transverse to the microfacets) modes as a function of the mean thickness of the corrugated GaAs layers in a lateral superlattice.

calculations neglecting the corrugation, this effect is present only for modes with wave vectors approximately at the center of the Brillouin zone.[11] The increase in the splitting of the TO_x and TO_y modes with decreasing average thickness of the GaAs layers (Fig. 2) is apparently due to the appearance of separate GaAs quantum wires in the case of thin GaAs layers (rather than corrugated layers as in the case of relatively thick GaAs layers in lateral superlattices) and, correspondingly, the localization of optical phonons in the additional (lateral) direction. Although in this direction the GaAs wires lie very close to one another, the optical phonon modes should be localized in them, since the penetration depth of the optical phonons from GaAs in AlAs equals only one monolayer.[14,15]

It should be underscored that the observed frequency splitting of the TO_y and TO_x modes enables us to assert that virtually the entire Raman scattering signal comes from the lateral superlattice and not from the GaAs substrate, since for long-wavelength vibrations allowed in Raman scattering from bulk GaAs these modes are degenerate, and splitting of the transverse modes in bulk GaAs was not observed in the experiment. The splitting of these modes was also confirmed in an experiment on Raman scattering by samples with the protective GaAs layer removed and also in the case of specially prepared membranes, with the GaAs substrate removed by selective etching and the Raman scattering signal from the lateral superlattice recorded on the AlAs buffer-layer side.

This work was supported by the Russian Fund for Fundamental Research (Project No. 97-02-18422). We are also grateful to the Scientific Council of the Institute of Semiconductor Physics of the Siberian Branch of the Russian Academy of Sciences for supporting of these investigations by awarding V. A. Volodin a stipend for young scientists.

[a)]e-mail: volodin@isp.nsc.ru

[1] R. Notzel, N. N. Ledentsov, L. Dawerits *et al.*, Phys. Rev. Lett. **67**, 3812 (1991).
[2] R. Notzel, N. N. Ledentsov, L. Dawerits *et al.*, Phys. Rev. B **45**, 3507 (1992).
[3] R. Notzel, N. N. Ledentsov, L. Dawerits, and K. Ploog, Surf. Sci. **267**, 209 (1992).
[4] M. V. Belousov, V. L. Berkovits, A. O. Gusev *et al.*, Fiz. Tverd. Tela (St. Petersburg) **36**, 1098 (1994) [Phys. Solid State **36**, 596 (1994)].
[5] M. Wassermeier, J. Sudijono, M. D. Johnson *et al.*, J. Cryst. Growth **150**, 425 (1995).
[6] M. Wassermeier, J. Sudijono, M. D. Johnson *et al.*, Phys. Rev. B **51**, 14721 (1995).
[7] Paulo V. Santos, A. Cantarero, M. Cardona *et al.*, Phys. Rev. B **52**, 1970 (1995).
[8] Z. V. Popovic, M. B. Vukmirovic, Y. S. Raptis *et al.*, Phys. Rev. B **52**, 5789 (1995).
[9] V. Ya. Prints, I. A. Panaev, V. V. Preobrazhenskiĭ, and B. R. Semyagin, JETP Lett. **60**, 217 (1994).
[10] M. V. Belousov, V. Yu. Davydov, I. É. Kozin *et al.*, JETP Lett. **57**, 120 (1993).
[11] Z. V. Popovic, M. Cardona, R. Notzel *et al.*, Phys. Rev. B **49**, 7577 (1994).
[12] A. J. Shields, Z. V. Popovic, M. Cardona *et al.*, Phys. Rev. B **49**, 7584 (1994).
[13] V. A. Volodin, M. D. Efremov, V. Ya. Prints *et al.*, JETP Lett. **63**, 994 (1996).
[14] M. Cardona, Superlattices Microstruct. **5**, 27 (1989).
[15] C. Colvard, T. A. Gant, M. V. Klein *et al.*, Phys. Rev. B **31**, 2080 (1985).

Translated by M. E. Alferieff

Transport-current-induced unidirectional decrease of spin-wave absorption in a magnet–superconductor structure

Yu. V. Gulyaev, Yu. F. Ogrin, N. I. Polzikova,[a] and A. O. Raevskiĭ
Institute of Radio Engineering and Electronics, Russian Academy of Sciences, 103907 Moscow, Russia

(Submitted 28 May 1997)
Pis'ma Zh. Éksp. Teor. Fiz. **66**, No. 1, 49–52 (10 July 1997)

The effect of a current on spin-wave propagation in a magnet–superconductor layered structure is investigated experimentally. The phenomenon of nonreciprocal ''brightening'' of the structure is observed. It is shown that this phenomenon is due to the motion of hypervortices of magnetic flux in a Josephson medium. © *1997 American Institute of Physics.* [S1063-7761(97)01113-X]

PACS numbers: 74.70.Ad, 75.30.Ds

The electrodynamic properties of superconductors in the field of a traveling wave are different from those in a uniform electromagnetic field. For example, in Refs. 1 and 2 it was shown that for a uniform superconducting film the complex high-frequency conductivity contains a contribution from the motion of Abrikosov vortices, which arises due to both an ac current, induced by the traveling wave, and a dc transport current. Those papers analyzed the absorption and intensification of a traveling spin wave (SW) propagating in a layered magnet–superconductor structure in a direction perpendicular to the transport current. However, this question has not been studied experimentally.

In the present work we have investigated experimentally the effect of the magnitude and direction of the transport current on the change in the absorption of a spin wave. A theoretical interpretation of the results is proposed in terms of a model involving the motion of hypervortices of magnetic flux in a Josephson medium.

The experimental structure consisted of an yttrium iron garnet (YIG) film and an high-T_c superconductor film on suitable substrates. An epitaxial doped YIG film with thickness $d=32$ μm and saturation magnetization $4\pi M_0=475$ G at 77 K was used. Wire transducers, 20 μm in diameter, were placed on the YIG film to excite and receive SWs. The $YBa_2Cu_3O_{7-x}$ films, prepared by cathodic sputtering, had thicknesses $b=1\times10^3$–1.5×10^3 Å. The electrical parameters of the film were measured by the four-probe method. The temperature dependence of the resistivity of the films was of a metallic character and close to linear with characteristic values $\rho_{300}\approx180$ $\mu\Omega$/cm and $\rho_{100}\approx45$ $\mu\Omega$/cm. The superconducting transition in the films occurred at $T_C\approx88$ K. The critical current density at 77 K was equal to 10^5 A/cm^2. The high-T_c superconducting film was clamped to the YIG film between the transducers. A magnetic field of 1.2 kOe was directed normal to the film planes. In this geometry, forward volume SWs, the lower limit of whose spectrum was equal to 22 GHz, were excited. A dc transport current was passed perpendicular to the direction of wave propagation. The size of the film in the direction

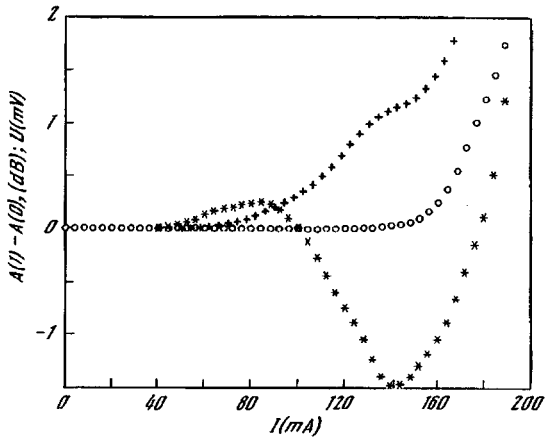

FIG. 1. Current–voltage characteristic $U(I)$ of the structure ($\circ$) and the change $A(I)-A(0)$ in the absorption of a spin wave in the case when **q** and **v** are parallel ($+$) and antiparallel ($*$).

of current flow was equal to $L=1$ cm and the size in the direction of wave propagation was equal to $l=0.5$ cm.

The current–voltage (IV) characteristic $U(I)$ of the structure was measured at temperature $T=77$ K. The absorption coefficient for the wave was determined according to the magnitude of the peaks in the amplitude–frequency characteristics $A(I)$ of the structure, which were measured with different transport currents simultaneously with the IV characteristic. The quantity $A(I)$ corresponds to the minimum total losses, consisting of purely magnetic losses in the YIG film, losses resulting from the conductivity of the high-T_c superconducting film, and conversion losses.

Figure 1 displays the IV characteristics of the film and a curve of the variation of the damping $\Delta A(I)=A(I)-A(0)$. One can see that a region of ''brightening,'' where the damping of the wave is less than in the absence of a current, is present in the range from 100 mA to 180 mA. When the direction of propagation of the wave is reversed, the damping increases monotonically. A similar change in the behavior of the damping of SWs was observed with a fixed direction of the wave vector **q** but with a change in the direction of the transport current or magnetic field. When the directions of any two vectors of the triplet **(H,I,q)** were reversed at the same time, the form of the curves did not change. This shows that the observed nonreciprocity of absorption is due to the dynamics of magnetic flux vortices in the superconductor. The electromagnetic field of a SW produces an alternating density of vortices, which moves with velocity $\mathbf{v}\propto\mathbf{I}\times\mathbf{H}$ under the action of the transport current. In the geometry of the experiment, v is either parallel or antiparallel to the phase velocity $v_{\rm ph}=\omega/q$ of the SW; this results in nonreciprocity of absorption.

Since the magnitude H_0 of the field corresponds to the region of a mixed state of the high-T_c superconducting film, it would be natural to assume that the effect is due to the motion of Abrikosov vortices. However, because of the high viscosity, their velocity is found to be $\leqslant 10^2$ cm/s, which is much lower than $v_{\rm ph}=10^7$ cm/s. The penetration of the

magnetic field into the high-T_c superconducting film, which consists mainly of a system of superconducting granules connected by Josephson junctions, can occur not only in the form of Abrikosov vortices but also in the form of Josephson vortices and hypervortices.[3,4] These vortices do not possess a normal-phase core, and for this reason their velocity can be much higher than that of Abrikosov vortices. The existence of hypervortices has been confirmed, for example, by experiments on the characteristic radiation from bridge structures.[5]

Let us examine the contribution of hypervortices to SW absorption. The change in the damping of the wave $\Delta A(I) = -4.3[q''(I) - q''(0)]l$ is determined by the imaginary part of the wave number $q = q' + iq''$, which is related with the frequency ω of the wave by the relations[6]

$$q''(\omega') = \frac{\text{Im } \omega(q')}{\partial \omega'(q')/\partial q'}, \quad \omega' = \text{Re } \omega(q'), \quad \omega(q) \cong \omega_H + \omega_m \frac{qd}{2} \frac{1+\chi}{2+\chi}. \tag{1}$$

Here $\omega_H = \omega_{H0} - \omega_m$, $\omega_{H0} = \gamma H_0$, $\omega_m = 4\pi\gamma M_0$, γ is the gyromagnetic ratio, $\chi = b/q\lambda^2$, $\lambda = [q^2 + \tilde{\lambda}^{-2}]^{-1/2}$ is the complex penetration depth of the electromagnetic field of the wave into the conducting medium, $\tilde{\lambda} = [i \times 4\pi\omega\sigma/c^2]^{-1/2}$, and $\sigma = \sigma' + i\sigma''$ is the effective high-frequency conductivity. The parameter χ equals the ratio of the wavelength to the effective electromagnetic screening length λ^2/b of the thin film. The relations presented above hold for the weakly damped ($q'' \ll q'$) lowest mode of the forward volume SW in the approximations $q\lambda \ll 1$, $qd \ll 1$, and $b/\lambda \ll 1$, which hold under the conditions of the experiment. We obtain an expression for the penetration depth of the field in the film on the basis of the equations of electrodynamics of a Josephson medium[7–10] and a self-consistent description of the motion of the vortices:[11]

$$\tilde{\lambda} = \left(\frac{\lambda_j^2 \cdot f(I) \cdot \mu + [\lambda_C^{-2} - 2i\lambda_F^{-2} \cdot (1 - v/v_{\text{ph}})]^{-1}}{1 - 2i\lambda_J^2/\lambda_{Nb}^2} \right)^{1/2}, \tag{2}$$

$$\lambda_J = \left(\frac{c\Phi_0}{8\pi^2 j_C(\delta + 2\lambda_L)} \right)^{1/2}, \quad \lambda_F = \left(\frac{c^2}{2\pi\sigma_F\omega} \right)^{1/2},$$

$$\lambda_{Nb} = (c^2/2\pi\sigma_{Nb}\omega)^{1/2},$$

where λ_J is the Josephson penetration depth, Φ_0 is the magnetic flux quantum, λ_L is the London penetration depth, δ is the average thickness of an intergranular interlayer, $\mu \leqslant 1$ is the effective magnetic permeability of the medium, j_C is the critical current density of the contact, λ_C is the Campbell penetration depth determined by the pinning of vortices in a Josephson medium, λ_F is the penetration depth determined by the conductivity σ_F of the viscous flow of the vortices, λ_{Nb} is the skin-layer depth, σ_{Nb} is the normal conductivity of the intergranular interlayers, and $f(I) = (1 - I^2/I_C^2)^{-1/2}$. The velocity of the hypervortices is $v = v_F\Theta(I - I_{CF})$, where I_{CF} is the critical vortex-pinning current, $\Theta(x)$ is a step function, $v_F \cong \pi c_0 \sqrt{\beta} I/4I_C$, c_0 is the Swihart velocity, and β is the McCumber–Stewart parameter.[12] Since $c_0 \cong v_{\text{ph}} \cong 10^8$ cm/s, we obtain $v/v_{\text{ph}} \leqslant 1$ for $I_{CF} < I < I_C$.

Figure 2 displays the variation of the damping of a wave as a function of $x = I/I_C$ for different values of λ_J and for $v/v_{\text{ph}} = -0.3x$, $1/\sigma_{Nb} = 38.5$ $\mu\Omega$/cm, and $1/\sigma_F = 23$

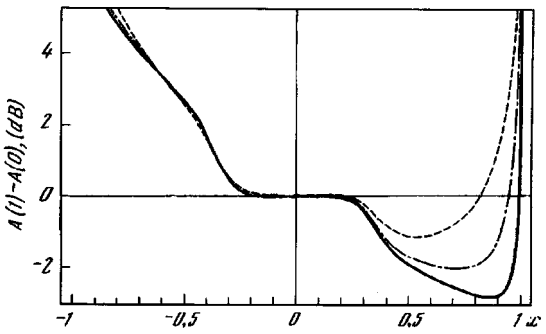

FIG. 2. Contribution of the motion of hypervortices to the absorption of a spin wave: Solid curve — $\lambda_J = 1.26\times10^{-4}$ cm; dot-dashed curve — $\lambda_J = 1.79\times10^{-4}$ cm; dashed curve — $\lambda_J = 2.53\times10^{-4}$ cm.

$\mu\Omega$/cm. In the calculation, $\Theta(x)$ was replaced by a ''smeared'' step; physically, this signifies averaging over the distribution of the pinning currents of different granules. The presence of the factor $(1-v/v_{\rm ph})$ in Eq. (2) results, for antiparallel velocities, in an effective increase of the conductivity σ_F of the vortices; this gives a monotonic decrease of absorption with increasing x. At the same time, as $x^2\to1$ the absorption should grow without bound as a result of an effective increase in the Josephson depth λ_J. The competition between these effects results in a minimum in the total absorption for $I\leqslant I_C$, which gives the observed ''brightening'' of the structure. When the velocities are parallel, the conductivity of the vortices effectively decreases and the total absorption can increase monotonically. Therefore the observed nonreciprocity of absorption is satisfactorily explained by the motion of hypervortices.

We thank I. M. Kotelyanskiĭ for providing the high-T_c superconducting films.

This work was supported by the Russian Fund for Fundamental Research (Project No. 95-02-05465a) and the Ministry of Science and Technologies (Grant No. 94-002).

[a)]e-mail: polz@mail.cplire.ru

[1] A. F. Popkov, Pis'ma Zh. Tekh. Fiz. **15**(5), 9 (1989) [Sov. Tech. Phys. Lett. **15**, 166 (1989)].
[2] N. I. Polzikova and A. O. Raevskii, J. Adv. Sci. **4**, 197 (1992).
[3] É. B. Sonin, JETP Lett. **47**, 496 (1988).
[4] M. Tinkham and C. J. Lobb, in *Solid State Physics*, Vol. 42, edited by H. Ehrenreich and D. Turnbull, New York (1989), p. 91.
[5] L. É. Amatuni, A. A. Akhtumyan, R. B. Aĭapetyan *et al.*, JETP Lett. **50**, 385 (1989).
[6] N. I. Polzikova and A. O. Raevskii, J. Magn. Magn. Mater. **146**, 351 (1995).
[7] T. L. Hylton, A. Kapitulnik, M. R. Beasley *et al.*, Appl. Phys. Lett. **53**, 1343 (1988).
[8] É. B. Sonin and A. K. Tagantsev, Zh. Éksp. Teor. Fiz. **95**, 994 (1989) [Sov. Phys. JETP **68**, 572 (1989)].
[9] C. Attanasio, L. Maritato, and R. Vaglio, Phys. Rev. B **43**, 6128 (1991).
[10] J. Halbritter, J. Supercond. **8**, 691 (1995).
[11] M. W. Coffey and J. R. Clemm, Phys. Rev. B **45**, 9872 (1992).
[12] K. K. Likharev, *Dynamics of Josephson Junctions and Circuits*, Gordon and Breach, Philadelphia, 1986 [Russian original, Nauka, Moscow, 1985].

Translated by M. E. Alferieff

Concerning the two magnetic correlation lengths above T_c in an Invar iron–nickel alloy

S. V. Grigor'ev,[a] S. A. Klimko, S. V. Maleev, A. I. Okorokov, and V. V. Runov
St. Petersburg Institute of Nuclear Physics, Russian Academy of Sciences, 188350 Gatchina, St. Petersburg, Russia

R. Kampmann and H. Eckerlebe
GKSS Forschungszentrum, 21502 Geesthacht, Germany

(Submitted 2 June 1997)
Pis'ma Zh. Éksp. Teor. Fiz. **66**, No. 1, 53–57 (10 July 1997)

The magnetic phase transition in the Invar alloy $Fe_{70}Ni_{30}$ is investigated by means of small-angle neutron scattering over a wide range of momentum transfer. This method was used to measure two magnetic correlation lengths R_{c1} and R_{c2} which coexist in the alloy above the phase transition temperature T_c. The critical correlations with correlation length R_{c1} are described well by an Ornstein–Zernicke expression, and the critical correlations with the second correlation length, an order of magnitude larger than R_{c2}, are described well by a squared Ornstein–Zernicke expression. The temperature dependences obtained for the correlation lengths R_{c1} and R_{c2} satisfy the power law $R_c \sim ((T-T_c)/T_c)^{-\nu}$ with critical exponents $\nu_1 = 0.65 \pm 0.05$ and $\nu_2 = 1.3 \pm 0.1$ for the shorter and longer scales, respectively. © *1997 American Institute of Physics.* [S1063-7761(97)01213-4]

PACS numbers: 75.30.Kz, 75.50.Bb

The coexistence of two length scales of critical fluctuations near a phase transition is observed in a number of systems: $SrTiO_3$ (Refs. 1 and 2), Ho (Ref. 3), $RbCaF_3$ (Ref. 4), $KMnF_3$ (Ref. 5), Tb (Ref. 6), and UPd_2Al_3 (Ref. 7). Investigations of the structural and magnetic phase transitions by x-ray and neutron diffraction methods have shown that a narrow peak, superposed on an existing wide peak due to the ordinary critical scattering, appears in the dependence of the scattering intensity on the momentum transfer above the transition temperature T_c. The appearance of a narrow peak in this temperature range indicates the existence of a second, longer scale together with the ordinary characteristic scale of the critical fluctuations. The appearance of a narrow component in the critical scattering was established with the aid of high-resolution x-ray systems.[1] Later it was shown that it is spatially localized within a 0.2 mm thick layer near the surface of the crystal[6] and that its characteristic parameters depend strongly on the method used to work the surface.[7] The ordinary fluctuations are uniformly distributed over the entire volume of the sample. At the same time, experiments with $RbCaF_3$ (Ref. 4) and $KMnF_3$ (Ref. 5), which undergo a first-order phase transition which is nearly second-order, showed that in these crystals the second scale is observed as a bulk effect. It follows from the experiments performed with the materials studied that the strong interaction of the elastic

strains and order parameter apparently leads to the appearance of a narrow peak in the critical scattering above the transition temperature. A review of this problem, together with experimental data and possible explanations of this phenomenon, has recently been given in Ref. 8.

In Ref. 9 we established, by measuring simultaneously the small-angle neutron scattering and the depolarization of a transmitted neutron beam, that two length scales of magnetic correlations are present above the Curie point T_c in the Invar alloy $Fe_{75}Ni_{25}$ (with the addition of 0.7% carbon), which possesses fcc structure. It should be noted that the alloys of Fe and Ni with Invar composition are fundamentally disordered systems.[10] The anomalous behavior of the linear thermal expansion coefficient and Young's modulus in the temperature range from 0 K up to the magnetic phase transition temperature T_c shows that the magnetic and volume characteristics of Invar alloys are strongly coupled. Apparently, the appearance of a second magnetic correlation length at temperatures $T>T_c$ is due to the strong interaction of the disordered magnetic subsystem with elastic strains near the transition temperature. In the present work we measured, using small-angle neutron scattering over a wide range of momentum transfer $q\in[2\times10^{-3}-5\times10^{-1}]\text{Å}^{-1}$, the temperature dependence of the two scale lengths of magnetic correlations in an Invar iron–nickel alloy above T_c and we found the critical exponents of both scales. It is also shown that the correlation functions of different scales differ strongly in form and can be described for the short and long scales by an Ornstein–Zernicke expression and the square of such an expression, respectively.

This letter reports measurements of the cross section for small-angle scattering of polarized neutrons by a polycrystalline sample of a fcc carbon-doped (0.1 at. %) iron-nickel alloy $Fe_{70}Ni_{30}$. The sample was produced in an argon atmosphere in an induction furnace. It was homogenized at 1200 °C for 4 h and then quenched in water. The fcc structure of the sample was proved by the method of neutron diffraction on a mini-SFINKS system.[11] The experiments were performed on a SANS-2 small-angle polarized-neutron scattering setup in the FRG-1 reactor at GKSS, Geesthacht, Germany. The system is equipped with a X–Y position-sensitive detector (80×80 cells with dimensions of 7×7 mm), which can be placed at distances ranging from 1.5 to 21.5 m after the sample, thereby making it possible to perform measurements in a wide range of momentum transfer. The scattered neutrons were detected in the range $2\times10^{-3}\leqslant q\leqslant5\times10^{-1}$ Å^{-1} with a step $\Delta q=2\times10^{-4}$ Å^{-1}. The spectrum-averaged wavelength is $\lambda=5.1$ Å ($\delta\lambda/\lambda=0.1$). The instrumental resolution of the apparatus (half width at half maximum) equals 5×10^{-4} Å^{-1}. The magnetic scattering intensity I_s analyzed in the present work was determined as the excess above the nuclear scattering, for which the scattering by the fcc lattice of the alloy in a paramagnetic state at $T_p=400$ K was used:

$$I_s(T,q)=I(T,q)-I(T_p,q). \tag{1}$$

The temperature measurements were performed in a helium-filled furnace in a wide temperature range near the transition temperature T_c ($T\in[290,340]$) with a 5 K step and 0.1 K stabilization.

Figure 1 displays a typical (for the alloy investigated) form of the magnetic differential small-angle scattering cross section $d\sigma/d\Omega$ at $T=313$ K, normalized to the volume of the sample, as a function of the momentum transfer q in double-logarithmic coordi-

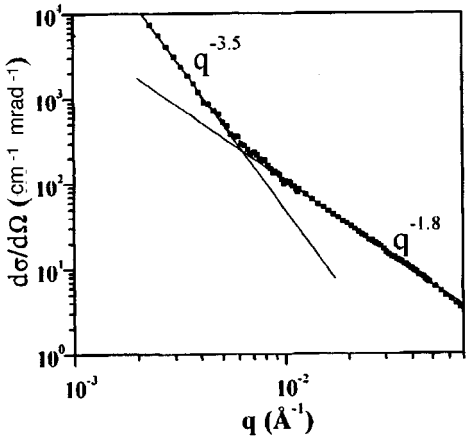

FIG. 1. Small-angle scattering cross section $d\sigma/d\Omega$ as a function of the momentum transfer q at $T=313$ K for $Fe_{70}Ni_{30}$.

nates. It is clearly seen from the figure that there exist two different ranges of q where the small-angle scattering cross section $d\sigma/d\Omega$ is described by different scattering laws q^{-n}. In the region $q \leqslant q_0$ (where $q_0 \approx 10^{-2}$ Å^{-1} is the point of the bend in the q dependence of the cross section) the exponent n of the scattering law is close to 4, while in the region $q \geqslant q_0$ the exponent n is approximately 2. This form of the function $d\sigma/d\Omega$ demonstrates the presence of two magnetic correlation functions of different form which characterize the system near the Curie temperature. Each correlation function dominates in the corresponding range of momentum transfer. This indicates, in turn, a large difference in the correlation lengths. We conjectured that the scattering cross section in the entire range of q values can be described by a sum of the Ornstein–Zernicke expression and a squared Ornstein–Zernicke expression:

$$\left(\frac{d\sigma}{d\Omega}\right)(q) = \frac{A_1}{a_0^2 \cdot (q^2+\kappa_1^2)} + \frac{A_2}{a_0^4 \cdot (q^2+\kappa_2^2)^2}, \tag{2}$$

where $a_0 = 1$ Å is a constant of the order of the interatomic distance, A_1 and A_2 are scattering amplitudes with dimensions of a differential scattering cross section, and $\kappa_1 = R_{c1}^{-1}$ and $\kappa_2 = R_{c2}^{-1}$ are the reciprocals of the short and long correlation lengths. A χ^2 fit of the data, taking account of the resolution function, gives with good reliability ($\chi^2 \approx 1$) the values of the parameters A_1, A_2, κ_1, and κ_2 and their temperature dependences. The results are displayed in Figs. 2 and 3.

The amplitudes A_1 and A_2 increase with decreasing temperature, and their absolute values differ by two to three orders of magnitude. The quantities κ_1^2 and κ_2^2 decrease with temperature. At $T=295$ K the value of κ_2^2 becomes close to 0 to within the resolution limits of the apparatus, and κ_1^2 at this temperature is the same as the value measured at $T=303$ K. In our opinion, the second-order phase transition is disrupted in this temperature range.

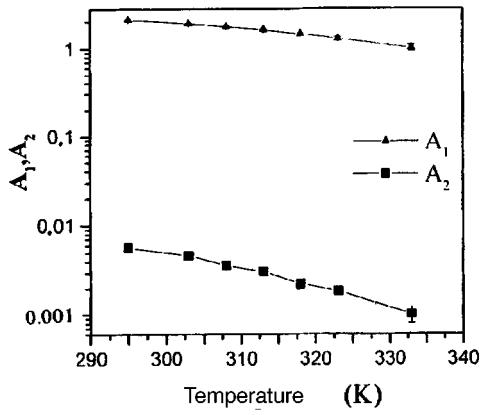

FIG. 2. Temperature dependence of the scattering amplitudes A_1 and A_2.

Assuming that both correlation lengths are normalized to the same temperature T_c, we can write

$$\kappa_{1c}^2 = \kappa_{01}^2 \tau^{2\nu_1}, \quad \kappa_{2c}^2 = \kappa_{02}^2 \tau^{2\nu_2}, \tag{3}$$

where $\nu_{1,2}$ are the critical exponents and $\tau = (T - T_c)/T_c$ is the reduced temperature. Taking the logarithms of both equations, and expressing $\ln(\tau)$ from one equation, substituting the expression obtained into the other equation, we obtain a linear relation $\ln \kappa_{2c}^2 = (\nu_2/\nu_1) \ln \kappa_{1c}^2 + \text{const}$. The slope of the straight-line plot of $\ln \kappa_{2c}^2$ versus $\ln \kappa_{1c}^2$ equals the ratio of the exponents ν_2/ν_1. Figure 4 displays $\ln \kappa_{2c}^2$ versus $\ln \kappa_{1c}^2$ and the line $(\nu_2/\nu_1) = 1.95 \pm 0.04$. In other words, the critical exponent ν_1 of the short correlation length R_{c1} is half the critical exponent ν_2 of the long correlation length R_{c2}.

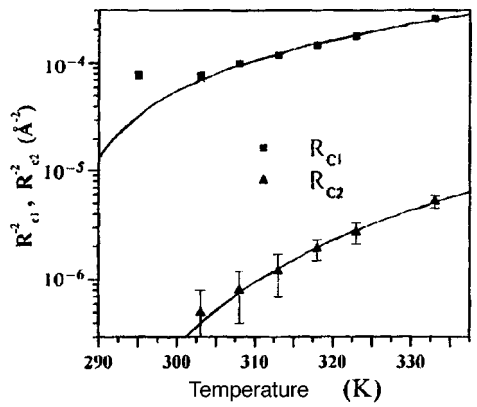

FIG. 3. Squared reciprocals κ_1^2 and κ_2^2 of the correlation lengths existing in the system versus temperature T. The solid curves show the computed dependences with the parameters obtained from a χ^2 fit.

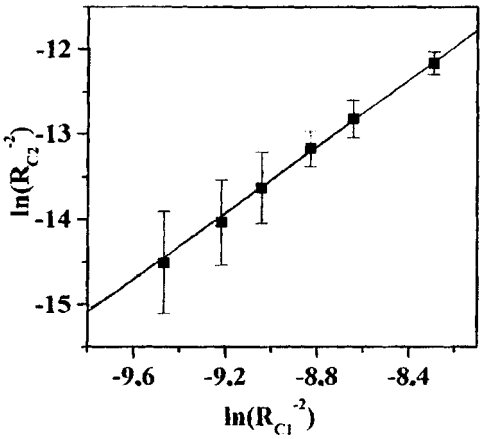

FIG. 4. $\ln \kappa_{2c}^2$ versus $\ln \kappa_{1c}^2$. The slope of the straight line corresponds to the ratio ν_2/ν_1 of the critical exponents of different scale lengths and equals 1.95 ± 0.04.

Similar arguments can be made for the amplitudes A_1 and A_2. A plot of $\ln A_2$ versus $\ln A_1$ is displayed in Fig. 5. A clear linear dependence is observed, and the slope of the straight line obtained from the curve equals 2.5 ± 0.1.

The experimental temperature dependences $\kappa_{c(1,2)}^2(T)$ were analyzed by fitting the power law (3) with $T_c = 285$ K. The following values were obtained for the parameters: $\kappa_{01}^2 = 0.0024 \pm 0.0003$ Å^{-2}, $\kappa_{02}^2 = 0.0005 \pm 0.0001$ Å^{-2}, $\nu_1 = 0.64 \pm 0.03$, and $\nu_2 = 1.3 \pm 0.1$. The computed dependences $\kappa_{c(1,2)}^2(T)$ with the least-squares parameters are displayed in Fig. 3 (solid curves).

We plan to continue the investigations of the two magnetic correlation lengths above

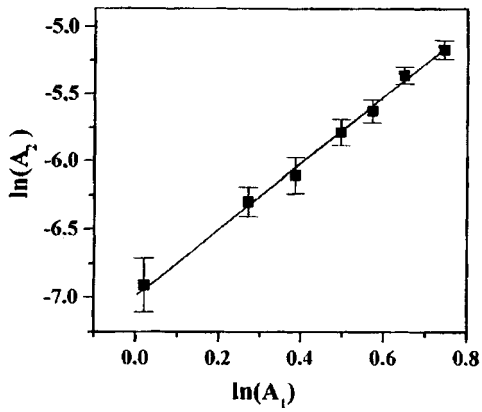

FIG. 5. $\ln A_2$ versus $\ln A_1$. The slope of the straight line corresponds to the ratio of the critical exponents of the scattering amplitudes of different length scales and equals 2.5 ± 0.1.

T_c in an Invar alloy with the classical composition $Fe_{65}Ni_{35}$. However, we can already say now that in order to understand the experimental data presented in this letter additional efforts from theorists are required.

This work was supported by the Russian Fund for Fundamental Research (Project L-EN-96-15-96775) and the State Science and Technology Program ''Neutron Investigations of Condensed Media.''

[a)]e-mail: grigor@rvv.lnpi.spb.su

[1] S. R. Andrews, J. Phys. C **19**, 3712 (1986).
[2] G. Shirane, R. A. Cowley, M. Matsuda *et al.*, Phys. Rev. B **48**, 15595 (1993).
[3] T. R. Tharston, G. Helgensen, D. Gibbs *et al.*, Phys. Rev. Lett. **70**, 3151 (1993).
[4] T. W. Ryan, R. J. Nelmes, K. A. Cowley *et al.*, Phys. Rev. Lett. **56**, 2704 (1986).
[5] U. J. Nicholls and R. A. Cowley, J. Phys. C **20**, 3417 (1987).
[6] K. Hirota, G. Shirane, P. M. Gehring *et al.*, Phys. Rev. B **49**, 11967 (1994).
[7] N. Sato, N. Aso, K. Hirota *et al.*, Phys. Rev. B **53**, 14043 (1996).
[8] R. A. Cowley, Phys. Scr. **66**, 24 (1996).
[9] S. V. Grigor'ev, A. I. Okorokov, and V. V. Runov, Preprint PIYaF-2112 [in Russian], St. Petersburg Institute of Nuclear Physics, Gatchina (1996).
[10] V. L. Sedov, *Antiferromagnetism of γ-Iron. The Invar Problem* [in Russian], Nauka, Moscow, 1987.
[11] O. K. Antson, A. P. Bulkin, P. E. Hiismaki *et al.*, Physica B **156–157**, 567 (1989).

Translated by M. E. Alferieff

Laser acceleration of electrons in a thin metal film

A. V. Zinov'ev[a)] and A. V. Lugovskoĭ
Akadempribor Scientific and Production Association, 700143 Tashkent, Uzbekistan

(Submitted 12 May 1997)
Pis'ma Zh. Éksp. Teor. Fiz. **66,** No. 1, 8–12 (10 July 1997)

A mechanism acceleration of electrons to relativistic velocities in a thin metal film irradiated with ultrashort ($\tau_L \leqslant 1$ ps) high-power ($I > 10^{16}$ W/cm^2) laser pulses is proposed. The acceleration is due to a resonance action of the nonuniform field on a portion of the electrons, viz., those which oscillate in the direction transverse to the film with a frequency close to the frequency of the field. © *1997 American Institute of Physics.* [S1063-7761(97)00213-8]

PACS numbers: 52.40.Nk, 73.61.At

The possibility of producing electromagnetic fields with relativistic intensities under experimental conditions permits posing the problem of the efficient acceleration of electrons by an electromagnetic field and the construction of compact laser electron accelerators based on such an acceleration. A number of methods for solving this problem have now been proposed. A discussion of the possibilities and drawbacks of these methods, as well as citations to the original works, can be found in Ref. 1. This letter examines a new laser acceleration scheme based on the characteristic features of radiation absorption in an ultradense laser plasma — the rapid decay of the field in the direction into the plasma and the collisionless character of the electron motion when the energy of an electron is of the order of or higher than the rest energy mc^2.

Let two laser pulses differing in phase by π be incident on the two sides of a metal film (of thickness 2δ) in the direction normal to the film (Fig. 1). Let the x axis be directed along the electric field vector, parallel to the surface, and let the y axis be directed perpendicular to the surface. In the general case, the dependence of the intensity $E(y,t)$ of the total field in the film on the coordinate y is determined by solving a self-consistent problem for the electron gas in the film and for the electromagnetic field (as done, for example, in Refs. 2 and 3). However, it follows from the symmetry of the problem that the intensity $E(y,t)$ of the total field in the film is an odd function of y. The qualitative form of this dependence is displayed in Fig. 1. If the film is thin ($\delta \ll \lambda$, where λ is the wavelength of the radiation and, moreover, δ is somewhat less than the depth l_s of the skin layer), then the total intensity $E(y,t)$ can be written as

$$E(y,t) = E_0 g(y) f(t) \sin \omega t, \tag{1}$$

where

$$g(y) \approx g_1(y+\delta) - g_1(\delta - y) \approx 2y l_s, \quad -\delta \leqslant y \leqslant \delta, \tag{2}$$

$g_1(y)$ describes the damping of a single laser pulse in the direction into the plasma, E_0 is the amplitude of the electric field of the wave, and $f(t)$ is the envelope of the pulse.

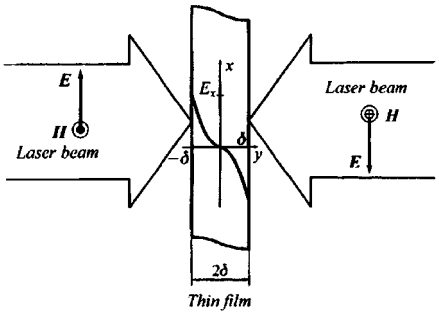

FIG. 1. Diagram of an experiment on the laser acceleration of electrons in a thin film. The qualitative form of the dependence of the intensity of the total electric field of the beams on the coordinate y is shown.

We shall assume that the pulse duration does not exceed several hundred femtoseconds and the radiation power density is of the order of or greater than 10^{16} W/cm^2. When a film is irradiated with laser pulses with such intensity, the lattice atoms in the irradiation zone are completely ionized within a time of the order of several femtoseconds.[4] The delocalized-electron density n_e can reach values of $\sim 10^{24}$ cm^{-3}. Furthermore, there is no doubt that at such high intensities the film in the irradiation zone is completely destroyed. However, in view of the finite rate of energy exchange between the electronic subsystem of the metal and the lattice, it can be assumed that the crystal lattice of the metal remains in an ordered state over times of the order of 100 fs. Without going into the details of the physics of the interaction of ultrashort laser pulses with matter (a detailed discussion of which can be found in the review in Ref. 4), we note that the destruction of the film, accompanied by the formation of an expanding plasma cloud, will start after the laser pulse ends and will not influence the character of the processes discussed in the model proposed here.

Since the Coulomb cross section decreases rapidly with increasing velocity of the colliding particles, for the laser radiation intensities considered here the radiation is absorbed in the anomalous skin-effect regime.[5] The depth of the skin layer is determined not only by the frequency but also by the intensity of the radiation, and in order to find the skin depth it is necessary to solve a self-consistent problem for the electrons and the field. In studying the present model we shall nonetheless assume that l_s remains unchanged during the entire duration of the pulse and, as follows from Refs. 2 and 3, is of the order of 10^{-7}–10^{-6} cm.

In a relatively weak field, when the magnetic field of the wave can be neglected, the radiation acts only on the motion of an electron parallel to the surface in the direction of the electric field vector. The field does not change the character of the electron motion in the direction normal to the surface. An electron, reflecting from the film boundaries (the reflection is assumed to be specular), oscillates with period $T_{\rm osc}=4\delta/v_y$, where v_y is the magnitude of the normal component of the electron velocity, in the direction normal to the surface and executes a translational motion with velocity v_x in a direction parallel to the surface.

If the frequency $\omega_{\rm osc}$ and phase of the oscillations of an electron are close to the

frequency and phase of the field, then the electron will be continuously accelerated. Otherwise, in the case when the synchronism condition

$$\omega_{\mathrm{osc}} = \omega \tag{3}$$

does not hold, the phases of acceleration and retardation of the electron by the field will compensate each other, and there will be no appreciable velocity increment.

This acceleration mechanism is based on the same principle as that of Wideröe linear accelerators[6] — at the moment when the field direction reverses, the action of the field on the electron is screened. In the present case the screening is achieved not by metal cylinders but rather by the damping of the field in the direction into the film. Another close analogy to the laser acceleration effect in a thin film is cyclotron resonance.[7]

In contrast to the case of a linear accelerator, in describing the behavior of the electron gas in a thin film one must take scattering into account. Electron collisions will disrupt phase matching and thereby prevent the electrons in the field from continuously accumulating energy. At the same time, the electron collision frequency decreases rapidly as the electron energy increases. For example, at a velocity $v \sim 0.15c$ the electron–ion collision frequency $\nu_{e-i} = 2\pi Z n_e e^4 \Lambda / m^2 v^3$ is already $\sim 10^{-13}$ s^{-1} (Z is the nuclear charge of a lattice atom and Λ is the Coulomb logarithm), so that an electron with such a velocity does not undergo any collisions during a 100 fs pulse. Electron–electron collisions can also be neglected, since their frequency is Z times less than ν_{e-i}. Therefore, for the relativistic field intensities assumed here, scattering in the film can be neglected[5] and the relativistic equations of motion[8] can be used to estimate the acceleration effect:

$$\frac{dv_x}{dt} = \frac{e}{m}\sqrt{1-\frac{v^2}{c^2}}\left\{E(y(t),t) + \frac{v_y}{c}H(y(t),t) - \frac{v_x^2}{c^2}E(y(t),t)\right\}, \tag{4}$$

$$\frac{dv_y}{dt} = -\frac{e}{m}\sqrt{1-\frac{v^2}{c^2}}\left\{\frac{v_x}{c}H(y(t),t) + \frac{v_x v_y}{c^2}E(y(t),t)\right\} + F(y). \tag{5}$$

The term $F(y)$ on the right-hand side of Eq. (5) permits taking account of electron reflection from the inner surfaces of the film. Reflection will occur if the normal component v_y of the electron velocity does not exceed $v_{\mathrm{cr}} = \sqrt{2U_0/m}$ (U_0 is the height of the potential barrier at the film–vacuum boundary). However, if $v_y > v_{\mathrm{cr}}$, then the electron leaves the film. In the absence of a field, U_0 is equal in order of magnitude to 10 eV, which corresponds to $v_{\mathrm{cr}} \sim 2 \times 10^8$ cm/s. It should be noted that the height U_0 of the potential barrier can be different under irradiation. This could happen because of excess positive charge produced in the film as a result of electron emission, which is unavoidable at such high field intensities.

For relativistic velocities, in the general case, the action of the magnetic field on the motion of an electron can be comparable to that of the electric field, even when $v_y \ll c$. However, since the magnetic and electric fields of the wave are shifted by a quarter

period relative to one another and the field decays in the direction into the film, it can be expected that even in the relativistic case a magnetic field will have very little effect on electrons moving in phase with the electric field.

To estimate the acceleration effect, we assume, without loss of generality, that

$$y(t)=\delta \sin \omega t, \quad \nu_y=\delta\omega \cos \omega t. \tag{6}$$

Averaging expression (4) over one period of the field with the use of expressions (6), we arrive at the equation

$$\frac{d\nu_x}{dt}=\frac{eE_0\delta}{ml_s}\left(1-\frac{\nu^2}{c^2}\right)^{1/2}\left(1-\frac{\nu_x^2}{c^2}\right)f(t),$$

which can be easily solved after separating variables:

$$\nu_x(t)=\frac{A(t)}{\sqrt{1+A^2(t)}}\sqrt{c^2-\nu_y^2}, \quad A(t)=\frac{c}{\nu_y}\tan\left(\frac{\nu_y}{c}\frac{eE_0\delta}{mcl_s}\int_{-\infty}^{t} f(\tau)d\tau\right). \tag{7}$$

Hence we obtain finally $A(\infty)\approx c\nu_y^{-1}\tan(eE_0\nu_y\tau_L\delta/ml_sc^2)$. Expression (7) is applicable if the transverse-velocity increment $\Delta\nu_y$ due to the magnetic field is small ($\Delta\nu_y<\nu_{\rm cr}$). The restriction on the effect of a magnetic field stems not only from the fact that an increase in the transverse velocity can result in emission of the accelerated electrons, but also, and most importantly, from the need to maintain the synchronism conditions. The following estimate for the increment $\Delta\nu_y$ can be obtained from Eq. (5):

$$\Delta\nu_y(t')=\int_{t'}^{t'+T_{\rm osc}/4} d\nu_y \approx \frac{eE_0\delta}{m\omega l_s}f(t')\frac{\nu_x(t')}{c}\left(1-\left(\frac{\nu_x(t')}{c}\right)^2\right)^{1/2}, \quad t'=2\pi n/\omega,$$

$$n\in Z. \tag{8}$$

It can also be shown that the increment to the transverse velocity over the next quarter period, with the corresponding orientation of the H vector, is approximately equal to $-\Delta\nu_y$, and therefore the average change in the transverse velocity over one oscillation is very small. The function $\Delta\nu_y(t)$, calculated from Eq. (8) with expressions (7), is plotted in Fig. 2. It follows from this figure that for power density $I=10^{16}$ W$\cdot$cm^{-2} and pulse duration $\tau_L=500$ fs the maximum increment to the transverse velocity does not exceed $0.3\nu_y$. The maximum possible longitudinal velocity of an electron equals $0.9994c$.

It can be shown, taking account of the initial phase of the electron oscillations, that the fraction of electrons accelerated is of the order of $\Delta\nu/2\nu_y$. We shall estimate the velocity interval $\Delta\nu$ where acceleration is possible, assuming that the disruption of the electron phase over the duration of the pulse does not exceed $\pi/2$. Since the frequency of the electron oscillations equals $\omega_{\rm osc}=\pi\nu_y/2\delta$, we obtain $\Delta\nu\cdot\tau_L\leqslant\delta$. Therefore for $\delta\approx 1.5\times10^{-7}$ cm, $\nu_y\approx 2\times10^8$ cm/s, and $\tau_L\approx 500$ fs a high-end estimate of the fraction of accelerated electrons is $\delta/2\nu_y\tau_L\approx 7\times10^{-3}$.

In summary, when a thin metal film is irradiated with powerful ultrashort laser pulses, a portion of the electrons in the film can be efficiently accelerated to relativistic velocities. Certain difficulties could arise in the practical implementation of this method. From the synchronism condition and the restriction on the transverse velocity, it follows

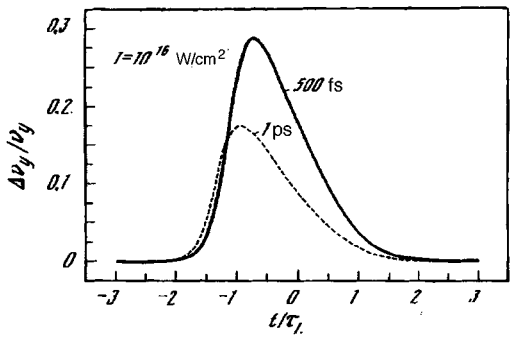

FIG. 2. A plot of the increment to the transverse velocity of an electron in one-fourth of the field period versus the time ($\omega=2\times10^{-15}$ s^{-1}, $\delta=1.5\times10^{-7}$ cm).

that the thickness of the film should be very small ($\sim$30–40 Å). The electron reflection from the film surface should be specular, which imposes stringent requirements on film quality. Furthermore, such a film is actually transparent at low field intensities, when ionization of the atoms in the irradiation zone has not occurred and the electron density is relatively low. Under the conditions of the proposed two-beam geometry, the transparency of the film makes it possible to relax somewhat the requirements on the contrast of the laser pulses. However, this question also remains important, since at a power density $\sim10^{16}$ W/cm^2 and contrast $\sim10^{-5}$, the amplitude of the prepulse is $\sim10^{10}$ W/cm^2, and the fraction of the power density absorbed remains very high even with attenuation by a factor of $I_s/\delta\sim10$.

Some of the problems described above can be eliminated if the resonance condition is met for thicker films ($\delta>l_s$). Since the film thickness is chosen so that $2\delta=\pi v_y/\omega$, an increase in film thickness can be achieved by decreasing the radiation frequency. We also note that the acceleration effect can be obtained by using films of thickness $2(n+1)\delta$, where $n+1$ is the number of field oscillations occurring within one electron oscillation. However, in this case the acceleration efficiency will be lower by a factor of $2n$.

[a)]e-mail: zinoviev@acpr.silk.org

[1] M. V. Fedorov, *Electrons in a Strong Light Field* [in Russian], Nauka, Moscow, 1991.
[2] E. G. Gamaliy and R. Dragila, Phys. Rev. A **42**, 929 (1990).
[3] W. Rozmus and V. T. Tikhonchuk, Phys. Rev. A **42**, 7401 (1990).
[4] B. Luther-Davis, E. G. Gamaliĭ, and Yanzhi Vang *et al.*, Kvantovaya Élektron. (Moscow) **19,** 317 (1992) [Sov. J. Quantum Electron. **22**, 289 (1992)].
[5] E. G. Gamaliĭ and V. T. Tikhonenko, JETP Lett. **48**, 453 (1986).
[6] R. Fernow, *Introduction to Experimental Particle Physics*, Cambridge University Press, New York, 1989.
[7] A. A. Abrikosov, *Fundamentals of the Theory of Metals*, North-Holland, Amsterdam, 1988 [Russian original, Nauka, Moscow, 1987].
[8] L. D. Landau and E. M. Lifshitz, *The Classical Theory of Fields*, Pergamon Press, New York, 1975 [Russian original, Nauka, Moscow, 1988].

Translated by M. E. Alferieff

Quantum-nondemolition measurement of the number of photons in a microcavity

Yu. P. Malakyan and D. M. Petrosyan
Institute of Physical Studies, Armenian National Academy of Sciences, 378410 Ashtarak-2, Armenia

(Submitted 23 May 1997)
Pis'ma Zh. Éksp. Teor. Fiz. **66**, No. 1, 58–63 (10 July 1997)

A new scheme for quantum-nondemolition measurement of the number and statistics of photons in a microwave cavity on the basis of interferometry of strongly-controlled V atoms which interact by a dispersion interaction with a cavity mode at a different transition is proposed.
 [S1063-7761(97)01313-9]

PACS numbers: 42.50.Ar, 42.55.Sq

1. This letter proposes a new scheme for quantum-nondemolition measurement of the number of photons in a microcavity. The scheme is based on interferometry of V atoms which interact by a dispersion interaction with a cavity mode at the transition $1\rightarrow 3$ (Fig. 1) and are controlled by a coherent field at a neighboring transition $1\rightarrow 2$. We show that inside the cavity the dressed states of the system ''atom + coherent field'' undergo different phase shifts which are induced by the quantum field and therefore depend on the number of photons n in the cavity. When the appropriate conditions are satisfied, n remains unchanged over the transit time of the atoms through the cavity. At the same time, the phase shifts lead to observable effects in the distribution of atoms which leave the cavity in the states 1 and 2; this makes it possible to measure the number of photons of the cavity field without changing its value. The dependence of the populations of the atomic levels on the phase shifts arises on account of the nonadiabatic switching on and off of the control field at the entrance and exit of the cavity; this results in a strong mixing of the dressed states or Ramsey interference. Nondemolition measurement of a small number of photons in a cavity has been discussed in Refs. 1–3. In Refs. 1 and 2, a Ramsey interferometry scheme in separated oscillatory fields was considered for observing the dispersion phase shift of nonresonant Rydberg atoms. In our case, throughout its entire flight through the cavity an atom interacts simultaneously with both a cavity mode and the Ramsey field; this is close to the experimental situation in microcavities.[4] We note that Ramsey-type interference, which is produced by nonadiabatic mixing of the upper and lower states of a two-level Rydberg atom, was observed in these experiments.

2. Let us consider the interaction of a V atom with the field of a single-mode cavity at frequency ω_c detuned from the frequency of the atomic transition $1\rightarrow 3$ by the amount $\Delta_c=\omega_{31}-\omega_c\neq 0$. The atom is controlled by an external classical field E at the frequency $\omega_1=\omega_{21}$ (Fig. 1a), whose intracavity Rabi frequency equals $\Omega_0=g_0E/\delta_c$ (Refs. 5 and 6), where g_0 is the coupling constant between the atom and the electromagnetic field at the transition $1\rightarrow 2$ and $\delta_c=\omega_c-\omega_1$ is the detuning of the field E from the cavity. Cavities

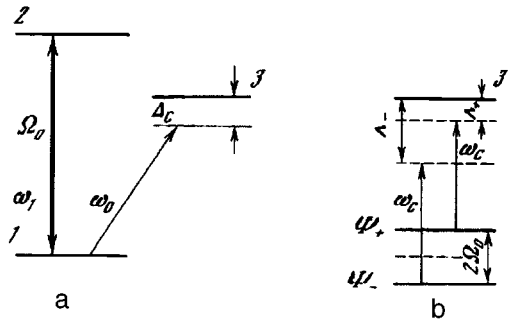

FIG. 1. Configuration of the levels of a V atom in the basis of bare (a) and dressed (b) states of the system. Ω_0 is the Rabi frequency of the control field.

with three openings for entrance and exit of atoms and for injection of an external field were recently used in experiments in Ref. 7.

Let us assume first that the cavity mode is in a Fock state with n photons. It is obvious that the interaction with the atom does not change n, provided that both the detunings Δ_c and δ_c are so large that as the atom passes through the cavity the photon absorption on both transitions $1\rightarrow 2$ and $1\rightarrow 3$ can be neglected. A pair of dressed states of the system ''atom + classical field'' $|\Psi_{\pm}\rangle = (1/\sqrt{2})\,(|1\rangle \pm |2\rangle)$, which are split by an amount equal to the Stark splitting $2\Omega_0$ (Fig. 1b), is formed inside the cavity. In Ref. 6 it was shown that the transition rates of an atom from $|\Psi_{\pm}\rangle$ into the level 3 with the absorption of one cavity photon are equal to, respectively,

$$\Gamma_{\pm} = \frac{g_1^2 kn}{k^2 + \Lambda_{\pm}^2}. \tag{1}$$

Here g_1 is the coupling constant between the atom and the electromagnetic field at the transition $1\rightarrow 3$ and k is the rate of decay of the number of photons in the cavity: $k \ll \Omega_0$ and $\Lambda_{\pm} = \pm\Omega_0 - \Delta_c$. If the transit time of the atom through the cavity equals T, then the condition for a dispersion interaction at the transition $1\rightarrow 3$ has the form $\Gamma_{\pm} T \ll 1$, which in the case of large detuning $\Delta_c \gg \Omega_0 \gg k$ reduces to

$$g_1^2 nkT/\Delta_c^2 \ll 1 \tag{2}$$

or

$$\Delta_c \gg \Delta_{\text{th}} = g_1 (nkT)^{1/2}. \tag{3}$$

The restriction on δ_c is stronger and follows from the obvious condition $\omega_{23} \gg 2\Omega_0$, which gives $\delta_c = \omega_{23} + \Delta_c \gg \Omega_0$.

Let us now consider the evolution of the atomic wave functions under the conditions described. In the experiment, the atoms are prepared and detected outside the cavity. For this reason, regions where both fields are switched on and off are present at the entrance and exit from the cavity, and therefore the coupling constants g_0 and g_1 for a monokinetic beam of atoms are functions of time, they are constant inside the cavity and vary

continuously in the cavity openings. However, if on account of a large detuning Δ_c the interaction with the cavity mode with moderate atom velocities is adiabatic everywhere, then the switching on and off of a classical field which is in exact resonance with the atom is always of a nonadiabatic character. Let us represent the Rabi frequency $\Omega(t)$ in the form

$$\Omega(t)=\begin{cases}\Omega_0=g_0E/\delta_c, & 0\leqslant t\leqslant T\\ \Omega_0\times f_1(t), & -\infty<t\leqslant 0,\\ \Omega_0\times f_2(t), & T\leqslant t\leqslant\infty\end{cases} \tag{4}$$

where $f_{1,2}(t)$ are normalized so that $f_1(0)=f_2(T)=1$ and $f_1(-\infty)=f_2(\infty)=0$. Then the atom, initially prepared in state 1 and passing through the region where the control field is switched on, is in a superposition state

$$|\Phi\rangle=a_1(0)|1\rangle+a_2(0)|2\rangle, \tag{5}$$

where

$$a_1(t)=\cos\ \eta_1(t), \quad a_2(t)=-i\ \sin\ \eta_1(t) \tag{6}$$

$$\eta_1(t)=\int_{-\infty}^{t}\Omega(\tau)d\tau=\Omega_0,$$

$t\leqslant 0$, is the area of the the field envelope in this region. The equation (5) describes the Ramsey interference due to nonadiabatic interaction of the atoms with the field E. Inside the cavity it is convenient to switch to a basis of dressed states, representing $|\Phi\rangle$ in the form

$$|\Phi\rangle=b_+(0)|\Psi_+\rangle+b_-(0)|\Psi_-\rangle, \tag{7}$$

where

$$b_\pm(t)=\frac{1}{\sqrt{2}}[a_1(t)\pm a_2(t)], \quad 0\leqslant t\leqslant T. \tag{8}$$

Using the Hamiltonian describing the interaction of the atom with the quantum field of the cavity in a basis of dressed states[6] and also Eq. (6) as initial conditions, we easily find the amplitudes $b_\pm(T)$:

$$b_\pm(T)=b_\pm(0)\,\delta_\mp(T)+i\frac{r}{\varphi}\ \exp(irT)\sin(\varphi T)b_\mp(0), \tag{9}$$

where $r=g_1^2n/(2\Delta_c)$, $\varphi=\sqrt{r^2+\Omega_0^2}$, and

$$\delta_\pm(T)=\left[\cos(\varphi T)\pm i\ \frac{r}{\varphi}\sin(\varphi T)\right]\exp(irT).$$

We note that in Eq. (9) the cavity-field-induced phase shifts of the states $|\Psi_\pm\rangle$ are taken into account to all orders. It is also easy to verify that

$$|b_+(T)|^2+|b_-(T)|^2=|b_+(0)|^2+|b_-(0)|^2=1,$$

i.e., the level 3 is not excited by absorption of a photon from the cavity field and therefore the number of photons n is conserved.

The amplitudes $a_{1,2}(T)$ of the bare states are obtained by an inverse transformation from Eq. (8). Using them as initial conditions for the Schrödinger equation in the region $t \geqslant T$, we find the solution for these amplitudes at the detector, i.e., in the limit $t \to \infty$:

$$a_{1,2}(\infty) = a_{1,2}(T)\cos\eta_2(\infty) - i a_{2,1}(T)\sin\eta_2(\infty), \tag{10}$$

where

$$\eta_2(t) = \Omega_0 \int_T^t f_2(\tau)\, d\tau,$$

$t \leqslant T$, is the area of the envelope of the control field in the region where the field is switched off. The secondary Ramsey interference at the exit from the cavity makes it possible to preserve information about the phase shifts in the populations of the atomic levels $P_i(\infty) = |a_i(\infty)|^2$, $i = 1, 2$, which are measured in the experiment as a function of the number n of photons, the detuning Δ_c, and the transit time T of the atoms. If the cavity field is not in a Fock state, then the probability of counting atoms as a function of Δ_c is measured in the experiment as an average over the photon distribution $p(n)$:

$$P_i(\Delta_c, t) = \sum_n p(n) P_i(\infty, n, \Delta_c, T). \tag{11}$$

In a real experiment, however, we deal with a thermal beam of Rydberg atoms, and therefore $P_i(\Delta_c, T)$ must also be averaged over the velocities of the atoms or over the transit times $T = L/v$, where L is the cavity length and v is the velocity of the atoms. It must be kept in mind, however, that the dependence of P_i on the photon statistics vanishes under such averaging, if the temporal distribution has a width greater than r^{-1} or if the width of the velocity distribution of the atoms is greater than $\Delta v = v_0^2 (Lr)^{-1}$, where v_0 is the most probable velocity of the atoms. We shall estimate Δv on the basis of the following considerations. It is known that random electromagnetic fields localized in cavity openings result in uncontrollable Ramsey interference for incoming and outgoing atoms.[4] This effect is absent for slow atoms, whose interaction with random fields can be assumed to be adiabatic. Under the conditions of the experiment performed in Ref. 4, the time of flight of these atoms is of the order of 8×10^{-5} s, which with $L \cong 2.5$ cm corresponds to velocities $v_0 \cong 300$ m/s. In further estimates, for reliability, we take $T \geqslant 4 \times 10^{-4}$ s. Since the coupling constant g_1 for Rydberg atoms is ordinarily equal to 10^5 s^{-1}, for $n \cong 10$, $\Delta_c \cong 200$ kHz, and correspondingly $r \cong 2 \times 10^5$ s^{-1}, we find that the ratio $\Delta v / v_0$ equals several percent (see also Ref. 8). Then velocity averaging has virtually no effect on the final results. Therefore, fixing v_0, we can choose Ω_0 so that $\eta_1(0) = \eta_2(\infty) = \pi/2$. As a result, we obtain simple expressions for the populations of the atoms. Specifically, in the case of a cavity mode in a Fock state we have for P_i

$$P_2 = \frac{\Omega_0^2}{\varphi^2} \sin^2\left(\varphi \frac{L}{v_0}\right), \quad P_1 = 1 - P_2. \tag{12}$$

For $\omega_c \cong 20 - 50$ GHz and cavity $Q \cong 10^9$, which corresponds to damping $k \cong 10 - 25$ Hz, we find from Eq. (3) with $n = 10$ that $\Delta_{\text{th}} \cong 20 - 30$ kHz. In Fig. 2 we display P_2 (11) and

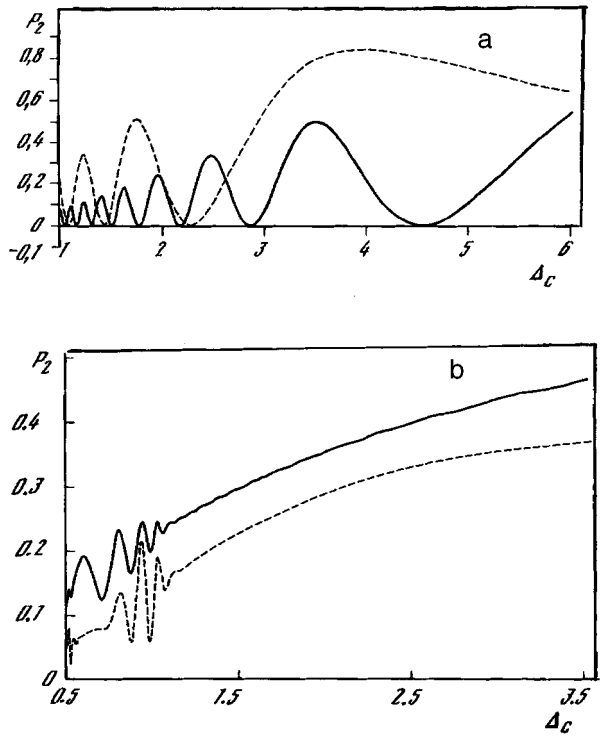

FIG. 2. Population of the upper level 2 of a monokinetic atomic beam at the exit from the cavity as a function of the detuning Δ_c (in units of $4\Omega_0$, $\Omega_0=50$ kHz): a — Cavity field in a Fock state: $n=10$ (dashed curve) and $n=25$ (solid curve); b — coherent field (dashed curve) and thermal field (solid curve). The average number of photons in the last two cases is $\langle n\rangle=10$.

(12) versus the detuning Δ_c for $\Delta_c\geqslant 100$ Hz and three states of the cavity field. One can see that in all cases the oscillations in P_2 vanish with increasing Δ_c in the region where $r<\Omega_0$, i.e., when the frequency of the oscillations of the dipole moment which are induced by the cavity field become less than the frequency of the oscillations of the dipole moment of the dressed states. As follows from Fig. 2b, the coherent and thermal distributions are manifested completely differently. This makes it possible to distinguish these two states of the field easily.

We now note that since every measurement changes the quantum state of the field, even though it leaves unchanged the number n of photons a measurement of the photon statistics on the basis of the mechanism presented above presumes that the previous distribution of the photons is restored after each separate atom is detected. However, if this is not done, then the proposed scheme makes it possible to stimulate a Fock state in a manner similar to Refs. 2 and 3. Figure 3 displays the results of numerical calculations for the collapse of the initial coherent photon distribution with $\langle n\rangle=7$ into a Fock state with $n=4$. To simulate the measurements we used the parameters $g_1=6\times 10^4$ s^{-1}, $\Omega_0=100$ kHz, and $T=5\times 10^{-4}$ s^{-1}. After the field in the cavity is found to be in a state

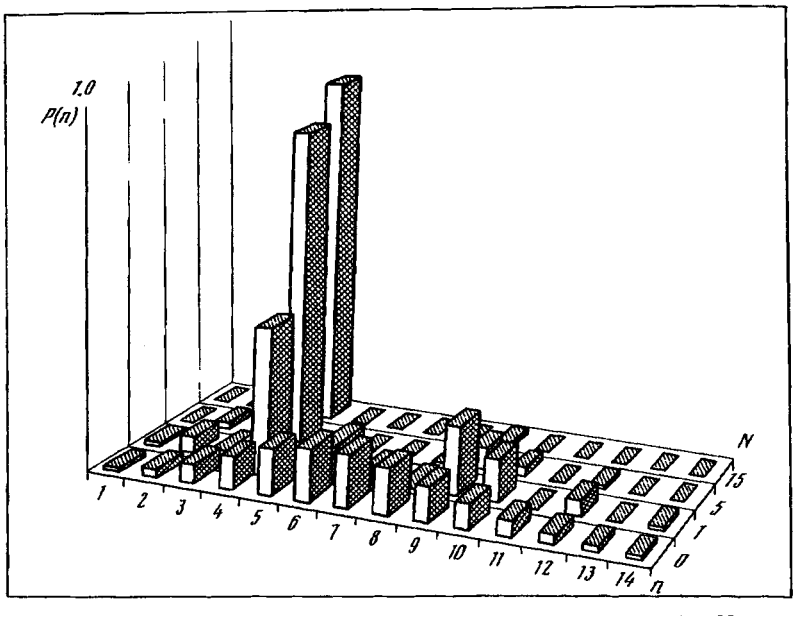

FIG. 3. Distribution $P(n)$ of the number of photons in the cavity, showing the collapse of the initial coherent cavity field with $\langle n\rangle = 7$ into a Fock state with $n = 4$ after successive detection of $N = 1$, 5, and 15 atoms.

with a fixed number of photons, repeated atomic measurements during a time longer than the decay time in the cavity should reveal quantum jumps in the state of the field. These questions will be discussed in detail elsewhere.

[1] M. Brune, S. Haroche, V. Lefevre *et al.*, Phys. Rev. Lett. **65**, 976 (1990).
[2] M. Brune, S. Haroche, J. M. Raimond *et al.*, Phys. Rev. A **45**, 5193 (1992).
[3] M. J. Holland, D. F. Walls, and P. Zoller, Phys. Rev. Lett. **67**, 1716 (1991).
[4] H. Walther, Usp. Fiz. Nauk **166,** 777 (1996).
[5] G. S. Agarwal, W. Lange, and H. Walther, Phys. Rev. A **48**, 4555 (1993).
[6] Yu. P. Malakyan, J. Mod. Opt. **43**, 1621 (1996).
[7] W. Lange and H. Walther, Phys. Rev. A **48**, 4551 (1993); Acta Phys. Pol. A **86**, 7 (1994).
[8] L. Davidovich, M. Brune, J. M. Raimond, and S. Haroche, Phys. Rev. A **53**, 1295 (1996).

Translated by M. E. Alferieff

Quantum cryptography based on homodyne detection (vacuum-state cryptosystem)

S. N. Molotkov and S. S. Nazin
Institute of Solid-State Physics, Russian Academy of Sciences, 142432 Chernogolovka, Moscow Region, Russia

(Submitted 3 June 1997)
Pis'ma Zh. Éksp. Teor. Fiz. **66**, No. 1, 64–68 (10 July 1997)

A new protocol is proposed for quantum cryptography. The protocol is based on the use of a set of measurements which make it possible to reconstruct completely the density matrix — the information carrier — of a physical system. Such a protocol can be implemented by means of homodyne detection (well known in quantum optics) of an electromagnetic field. An example is given of a quantum cryptosystem in which the vacuum state of the photon field is used as one of two information states.
[S1063-7761(97)01413-3]

PACS numbers: 42.50.−p

The information carriers in quantum cryptography are quantum states. Information is extracted as a result of measurements performed on these states. The logical 0 and 1 correspond to transmissions of the density matrices $\hat{\rho}_0=|\psi_0\rangle\langle\psi_0|$ and $\hat{\rho}_1=|\psi_1\rangle\langle\psi_1|$ (in what follows we confine our attention to pure states only), respectively, from user **A** to user **B** along a quantum communication channel. Secrecy in quantum cryptography is based on the fact that for a pair of nonorthogonal states it is impossible to obtain any information without perturbing the states.[1,2] To be more precise, if it is unknown in advance which of two nonorthogonal states is subjected to a measurement, then it is impossible to make a positive (with probability 1) assertion about the state. Any pair of nonorthogonal states can be used as information carriers.[2] The operators

$$\overline{P_0}=1-|\psi_0\rangle\langle\psi_0|=1-\hat{\rho}_0, \quad \overline{P_1}=1-|\psi_1\rangle\langle\psi_1|=1-\hat{\rho}_1 \tag{1}$$

were used in the initial key generation protocol[2] in a noise-free channel. These projectors possess the obvious properties

$$\mathrm{Tr}\{\hat{\rho}_0\overline{P_0}\}\equiv 0, \quad \mathrm{Tr}\{\hat{\rho}_1\overline{P_1}\}\equiv 0. \tag{2}$$

To generate the key users **A** and **B** employ, besides a quantum communication channel, an auxiliary open (accessible to all) channel along which user **A** reports to user **B** the content of a portion of the transmissions. A comparison made by user **B** of the transmitted states and the measurement results makes it possible to discover eavesdropping attempts. For example, if user **A** transmitted a state $\hat{\rho}_0$ and an eavesdropper interpreted this state as $\hat{\rho}_1$ (because of the impossibility of reliably distinguishing $\hat{\rho}_0$ from $\hat{\rho}_1$) and

retransmitted $\hat{\rho}_1$ to user **B**, then a measurement of an observable corresponding to the projector $\overline{P_0}$ performed on this state can give a nonzero result with probability

$$\mathrm{Tr}\{\hat{\rho}_0\overline{P_1}\}=1-|\langle\psi_0|\psi_1\rangle|^2\neq 0. \tag{3}$$

This result is statistical in the sense that a nonzero result is guaranteed for a sufficiently long series of measurements, though a zero result can also be obtained in each individual measurement. In a noise-free channel the first nonzero result is sufficient for discovering eavesdropping. However, this ''first'' nonzero outcome may not occur in the first measurement.

So far, the information carriers used in real quantum cryptosystems have been photon states. For them, the implementation of an experimental measurement procedure corresponding to the projectors $\overline{P_{0,1}}$ is a nontrivial problem. Our idea is to not use the projectors (1) for measurements but to use instead a set of measurements M_θ which make it possible to reconstruct completely the state of the quantum system from the results of a large number of measurements with different values of θ. For example, in the method of homodyne detection of an electromagnetic field, which is based on the measurement of the quadrature component of the field, the following identity for the density matrix of the field is used:[3–5]

$$\hat{\rho}\equiv\int\frac{d^2\alpha}{\pi}\,\mathrm{Tr}\{\hat{\rho}\hat{D}^+(\alpha)\}\hat{D}(\alpha), \tag{4}$$

where $\hat{D}(\alpha)=\exp(-\alpha a^+ +\alpha^* a)$ and a^+ and a are creation and annihilation operators for the corresponding mode of the field. Changing to polar coordinates $\alpha=(i/2)\,k\,\exp(i\theta)$, one can rewrite Eq. (4) in the form

$$\hat{\rho}=\int_0^\pi\frac{d\theta}{\pi}\int_{-\infty}^{\infty}\frac{dk|k|}{4}\int_{-\infty}^{\infty}dx\;p(x,\theta)\exp(-ik(\hat{x}(\theta)-x)), \tag{5}$$

where $\hat{x}(\theta)=(a^+\exp(i\theta)+a\exp(-i\theta))/2$ is a quadrature variable for the photon field and the angle θ is the phase of the test field, which is set by the measuring apparatus. The trace in Eq. (4) is calculated in a basis of eigenstates of the quadrature variable $\{|x\rangle_\theta\}$, and $p(x,\theta)={}_\theta\langle x|\hat{\rho}|x\rangle_\theta$. The probability density $p(x,\theta)$ of the quadrature component is an experimentally measured quantity in the method of homodyne tomography.[6] Therefore the quantity $p(x,\theta)$ completely determines the initial density matrix.

In the proposed cryptosystem the protocol is as follows. Let user **A** transmit the state $\hat{\rho}_0$ or $\hat{\rho}_1$ (0 or 1). User **B** randomly selects a value of θ and performs a measurement M_θ. In so doing he obtains the result x (for simplicity, we assume that for all measurements M_θ the spaces of the results are identical to the set of real numbers). After a series of measurements has been performed, user **A** reports for some of the measurements (for example, half) to user **B** along an open channel the number of measurements in which the state $\hat{\rho}_0$ was transmitted. User **B** arranges his data in two arrays. Data for the numbers of measurements in which the state $\hat{\rho}_0$ was transmitted are present in one array and data for measurements referring to the state $\hat{\rho}_1$ are present in the other array. Then a sufficiently long series of measurements will give user **B** an estimate for the distribution functions

$p_{0,1}(x,\theta)$ for fixed θ in the states $\hat{\rho}_0$ and $\hat{\rho}_1$. The accuracy of this estimate will be higher the longer the series of measurements and can be obtained from the law of large numbers.

Let us now consider the measurements performed by user **B** on the state $\hat{\rho}_0$. The results x obtained by user **B** in this case for fixed θ are described by the random variable ξ with probability density $p_0(x,\theta)$ and the corresponding distribution function

$$P(x,\theta) = \Pr\{\xi \leqslant x\} = \int_{-\infty}^{x} p(\xi,\theta)\,d\xi.$$

The pair (ξ,x) fixes a discrete random quantity ζ which takes on the values 1 or 0 depending on whether or not the inequality $\xi \leqslant x$ is satisfied. In real experiments the number of measurements is always finite. Therefore user **B** has available a set of N identical independent random quantities ξ_i $(i=1\ldots N)$ with fixed θ. A series of N measurements gives the random quantity $P_N^*(x,\theta)=(1/N)\Sigma_{i=1}^{N}\zeta_i$ with the distribution

$$\Pr\left\{P_N^*(x,\theta)=\frac{k}{N}\right\}=\binom{N}{k}P(x,\theta)^k[1-P(x,\theta)]^{N-k}. \tag{6}$$

If the distribution function $P(x,\theta)$ is continuous, then Kolmogorov's theorem[7,8] gives a measure of the deviation of the empirical distribution function from the true function

$$\lim_{N\to\infty}\Pr\{\sqrt{N}\delta_N^{+}\leqslant z\}=\lim_{N\to\infty}\Pr\{\sqrt{N}\delta_N^{-}\leqslant z\}=1-\exp(-2z^2) \tag{7}$$

for any z, and

$$\delta_N^{\pm}=\pm\sup_{-\infty<x<\infty}[P_N^*(x,\theta)-P(x,\theta)].$$

Therefore Kolmogorov's theorem makes it possible to give the limits within which the distribution function $P_N^*(x,\theta)$ lies with probability as close to 1 as desired immediately for all values of the argument. If it has been observed for the open part of the measurements that one of the inequalities $\sqrt{N}\delta_N^{+}\leqslant z\,\sqrt{N}\delta_N^{-}\leqslant z$ is violated for some values of N and z, then this indicates the presence of eavesdropping (the converse is not true).

We note that even in the protocol of Ref. 2 the hypothesis that there is no eavesdropping must also be accepted according to some statistical criterion. Indeed, let us assume that after a discussion through an open channel user **B** distinguished a group of N_0 test measurements in which user **A** transmitted the state $\hat{\rho}_0$ and user **B** measured the observable $\overline{P_0}$. If there was no eavesdropping, then a zero result should be obtained in all N_0 measurements. However, if a zero result was obtained in all measurements, then this does not at all mean that there is no eavesdropping, since there is a nonzero, though small, probability that the eavesdropper correctly guessed the state transmitted by user **A** in all test transmissions.

Let us now consider the secrecy of the proposed protocol. To prove secrecy it is necessary to show that there do not exist measurements which an eavesdropper can perform and, based on the results, transmit to user **B** instead of the intercepted states other density matrices selected so that their mixture on the state $\hat{\rho}_0$ $(\hat{\rho}_1)$ equals $\hat{\rho}_0$ $(\hat{\rho}_1)$. In our case the impossibility of the existence of such measurements is obvious, since the

pure states $\hat{\rho}_0$ and $\hat{\rho}_1$ are extreme points of a convex space of states of a quantum system, i.e., they cannot be represented in the form of a convex linear combination of any other density matrices.

After the absence of eavesdropping has been established, the remaining undisclosed portion of the measurements can serve for key generation. User **B** can proceed as follows. First, he must choose a decision function $F_\theta^{\rho_0,\rho_1}(x)$ which fixes his strategy for interpreting the measurement results: If a measurement described by the parameter θ yields a result x, then user **B** chooses a logical 1 with probability $F_\theta^{\rho_0,\rho_1}(x)$ and a logical 0 with probability $1-F_\theta^{\rho_0,\rho_1}(x)$. Let $p_i(x,\theta)$ be the probability of obtaining a result x in a measurement described by the parameter θ under the condition that the state ρ_i was transmitted. Note that if user **A** transmits the states ρ_0 and ρ_1 with equal probability, then the result x will be observed $p_1(x,\theta)/p_0(x,\theta)$ times more often in the case when the state ρ_1 was transmitted than in the case when the state ρ_0 was transmitted. For this reason, it is natural to choose as the function $F_\theta^{\rho_0,\rho_1}(x)$ a quantity proportional to $p_1(x,\theta)$, i.e.,

$$F_\theta^{\rho_0,\rho_1}(x)=\frac{p_1(x,\theta)}{p_0(x,\theta)+p_1(x,\theta)}.$$

To calculate the mutual information of the channel it is necessary to find the probability $P(1,1)$ that in the case when user **A** transmits a state ρ_1 user **B** perceives the measured result as a logical 1, and the corresponding probability $P(0,0)$. It is obvious that

$$P(1,1)=\int d\theta\Pi(\theta)\int dxF_\theta^{\rho_0,\rho_1}(x)p_1(x,\theta),$$

$$P(0,0)=\int d\theta\Pi(\theta)\int dx(1-F_\theta^{\rho_0,\rho_1}(x))p_0(x,\theta),$$

where $\Pi(\theta)$ is the probability that user **B** chooses a measurement described by the parameter θ. It is easily verified that $P(0,0)=P(1,1)$, i.e., the channel obtained in this manner is symmetric. Therefore, introducing the notation $q=P(1,1)=P(0,0)$ (so that $P(0,1)=P(1,0)=1-q$), we obtain for the desired mutual information

$$I=1+q\log_2 q+(1-q)\log_2(1-q).$$

According to Shannon's theorem, I determines the information that can be transmitted reliably in a single message by means of an appropriate block code.[9,10]

Let us now consider the possibility of the practical implementation of the cryptosystem proposed above. Here we can employ the above-mentioned homodyne detection (used in quantum optics) of an electromagnetic field, making it possible to reconstruct completely the density matrix of the field from the results of a set of measurements parameterized by an angle θ representing the phase of the test field.[11] In this case it is possible to construct a quantum cryptosystem on two nonorthogonal states, one of which is the vacuum state of the electromagnetic field $\hat{\rho}_0=|0\rangle\langle 0|$ and the other is a coherent state of the field arising at the output of an ideal laser: $\hat{\rho}_1=|\alpha\rangle\langle\alpha|$. To transmit a logical

0 user **A** does not transmit anything into the communication line and to transmit a logical 1 user **A** transmits the coherent state $|\alpha\rangle$. The coherent state contains the vacuum component

$$|\alpha\rangle = \exp(-|\alpha|^2/2)\sum_{n=0}^{\infty}\frac{\alpha^n}{\sqrt{n!}}|n\rangle,$$

so that $\langle\alpha|0\rangle = \exp(-|\alpha|^2/2) \neq 0$; the states are increasingly nonorthogonal the smaller the value of α (the intensity of coherent radiation). The possibility of reconstructing the density matrix for vacuum and squeezed states of a radiation field has been demonstrated experimentally.[11] Therefore a quantum cryptosystem employing a vacuum state is entirely realistic. Moreover, it may even be simpler to implement, since homodyne detection does not require the use of interference effects at large distances, as is necessary in existing cryptosystems based on long-baseline interferometry (the so-called time division interferometer[12]).

This work was supported by the Russian Fund for Fundamental Research (Project No. 96-02-19396).

[1] W. K. Wootters and W. H. Zurek, Nature **299**, 802 (1982).
[2] C. H. Bennett, Phys. Rev. Lett. **68**, 3132 (1992); C. H. Bennett, G. Brassard, and N. D. Mermin, Phys. Rev. Lett. **68**, 557 (1992).
[3] K. E. Cahill and R. J. Glauber, Phys. Rev. **177**, 1882 (1969).
[4] K. Vogel and H. Risken, Phys. Rev. A **40**, 2847 (1989).
[5] G. M. D'Ariano, http://xxx. lanl. gov/quant-ph/9701011.
[6] H. P. Yuen and J. H. Shapiro, IEEE Trans. Inf. Theory **IT–26**, 78 (1980); H. P. Yuen and V. W. S. Chan, Opt. Lett. **8**, 177 (1983).
[7] A. N. Kolmogorov, Giornale dell'Instituto degli Attuari **4**, 83 (1933).
[8] L. Takács, *Combinatorial Methods in the Theory of Stochastic Processes*, Wiley, New York, 1967.
[9] C. E. Shannon, ''Mathematical theory of communications,'' Bell Syst. Tech. J. **27**, 379; 623 (1948).
[10] I. Csiszár and J. Körner, *Information Theory: Coding Theorems for Discrete Memoryless Systems*, Kiado–Budapest: Akademiai, 1981.
[11] D. T. Smithey, M. Beck, M. G. Raymer, and A. Faridani, Phys. Rev. Lett. **70**, 1244 (1993).
[12] C. Marand and P. D. Townsend, Opt. Lett. **20**, 1695 (1995).

Translated by M. E. Alferieff

Instructions for authors

The journal ''Pis'ma Zh. Éksp. Teor. Fiz.'' publishes short articles which require rapid publication and are of general interest for a wide range of physicists. Rapid publication is for first observations of new physical phenomena and theoretical works containing fundamentally new results.

The complete text should not exceed 20 kB of TeX, allowing 1 kB for each figure. If there are no figures, this is approximately eight or nine double-spaced typewritten pages, including the abstract and references. As a rule, tables are not published.

The first page of the manuscript should look like this:

Title

Initials and last names of authors.

Institutional affiliation of the authors (including city and postal code;

it is recommended that the e-mail address of one author be given).

Abstract

PACS: ...

The main text follows after skipping one line.

The last names of foreign authors are written in Russian transcription, but the original spelling must be indicated in a footnote. The names of foreign institutions are written in English.

PACS is the classification scheme of the American Institute of Physics. It is published in Pis'ma Zh. Éksp. Teor. Fiz. **58**, Nos. 7 and 9.

We call to the attention of Russian authors the fact that the transliteration of last names from Russian into English is done according to strict rules (see Pis'ma Zh. Éksp. Teor. Fiz. **58**, No. 8, p. 699). If for some reason the authors desire a different transcription of the last name, they must indicate it on a separate sheet of paper.

Since abstracts are now also disseminated separately from the articles (data bases, on-line systems, etc.), the text of the abstract must be self-contained: There should be no citations to the references, the notation should be understandable, and there should be no abbreviations.

Uppercase letters (with no periods) should be used for the common abbreviations and their combinations and each abbreviation should be explained the first time it appears. Footnotes should be numbered sequentially throughout the entire article.

The references should be listed at the end of the article and numbered in the text, for example, Ref. [1]. The references are listed in the order in which they appear in the text. For journal articles, first the initials and then the last names of the authors, the title of the journal, the number of the volume (underlined), the page, and the year in parentheses are given. If there are more than four authors, then only the first three are listed. For example:

1. A. B. Ivanov, V. G. Petrov, I. M. Sergeev *et al.*, Pis'ma Zh. Éksp. Fiz. **92**, 290 (1990).

 0021-3640/97/010073-02$10.00

In the case of books the initials and last names of the authors, the complete title of the book, and the year and location of publication are given (if the book is a translation, then the information for the original must be indicated in parentheses).

Since no proofreading will be done, the manuscripts must be prepared extremely carefully. When possible, cumbersome notation should be avoided and the composition of the formulas should be simplified (for example, by using exp). *Russian letters should not be used in designations and indices*. For example, P_{opt} should be used instead of $P_{\mathrm{опт}}$.

Vectors should be underlined with a thick blue line (overarrows should not be used).

We request that authors who use computer graphics for preparing the figures adhere to the following recommendations: plots should be framed; the scale marks on the axes should be directed inwards; the Ariel type font should be used, if possible; the height of the numbers and in-line letters and numbers on the axes should be 3–4% of the maximum size (height or width) of a figure; units of measurement on the axes should be enclosed in parentheses.

Manuscripts with figures should be submitted in two copies, one of which must be signed by all authors. Gray-scale figures should be submitted in three copies. (Publication could be accelerated by submitting in addition diskettes with the text in TeX or LaTeX.) In addition, for countries in the Commonwealth of Independent States the institution that is to appear in the title of the article as the principal institution should be indicated.

The exact address with the postal code, the last name, the full first name, and the patronymic and the telephone number at work and at home of the author to whom correspondence should be addressed should be attached to the manuscript.

The editorial office mails out (to Muscovites gives out) reprints of articles (25 copies of the Russian version and 15 copies of the English translation).

Reprints are kept in the editorial offices for not more than three months from the day of publication. The classification is published in Pis'ma Zh. Éksp. Teor. Fiz. **58**, Nos. 7 and 9.

Pis'ma Zh. Éksp. Teor. Fiz. also accepts articles in English. Therefore the journal is bilingual. Authors desiring to publish their article in English must submit two copies of the English text, three copies of the figures with the English designations, on a separate sheet of paper the title of the article and the last names of the authors in Russian, and a diskette with the text prepared using the TeX or LaTeX programs.

The editorial staff will not engage in editing the language. However, the editorial staff reserves the right to reject an article if there are any doubts concerning the correctness of the English. In this case a Russian version of the article can be resubmitted.

The editorial office accepts articles submitted by e-mail to the address letters@kapitsa.res.ru (REVTex or LaTeX format). Figures can be submitted by fax to (095)1377589 or in PS format as well as in the form of Origin files.

Translated by M. E. Alferieff